INVESTIGATIONS INTO THE STORAGE AND USE OF HYDROGEN AS AN AUTOMOTIVE FUEL

by

WILLIAM LLEWELLYN RICHARDS

A DOCTORAL THESIS

Submitted in partial fulfilment of the requirements
for the award of
Doctor of Philosophy of the Loughborough University of Technology
August 1982

Supervisor: Dr G G LUCAS
Department of Transport Technology

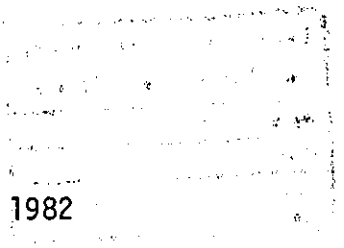


TRANSPORT TECHNOLOGY
HYDROGEN/PETROL VEHICLE
RJU 685W

SYNOPSIS

This thesis describes an investigation into the use of hydrogen as a fuel for automotive use. Due to problems of backflash into the engine intake when hydrogen is used as the sole fuel, a dual-fuel system using petrol and hydrogen together was studied. Using this system, a spark-ignited engine has been run at all speeds with a wide-open throttle, and the specific fuel consumption and BTE figures indicate a greater part load efficiency than those from a throttled engine. The performance and emissions curves of the engine are presented, both at the standard compression ratio of 8.9:1 and at a higher compression ratio of 11.7:1. Emissions data indicate reduced levels of CO, and NO_x at part load due to the very lean mixtures used. No problem of backfiring was experienced since the concentration of hydrogen was very low.

A vehicle was modified to run on such a dual-fuel system, and details of this modification are also presented.

A major problem with using hydrogen as an automotive fuel is its on-board storage. This is discussed in some detail, with particular reference to the use of metal hydrides as storage media. Metal hydride tanks are now commercially available, and a detailed mathematical model of such a tank has been developed to describe its behaviour under both hydriding and dehydriding conditions. In contrast to other hydride models previously reported in the literature, this model simulates an actual, commercially available containment vessel, rather than that of an abstract ideal situation. Thus the model provides a convenient means of predicting the time taken to release or absorb given amounts of hydrogen. These are calculated from the heat transfer characteristics and diffusion properties of particular metal alloys. Comparisons are given between the actual operating characteristics and those simulated by the model.

A brief discussion of the reaction kinetics of hydriding certain metal alloys is also included.

ACKNOWLEDGEMENTS

The author wishes to acknowledge the co-operation and assistance he has received from many quarters, and in particular is indebted to his supervisor, Dr G G Lucas. Dr Lucas' help, advice and encouragement greatly aided in the completion of this thesis. The author also wishes to extend his thanks to Professor F D Hales for his advice and assistance with the development of the mathematical model. Thanks must also go to Mr A Broster and Mr D M Harkis for their considerable help in technical matters. The author wishes to express his gratitude to the Science and Engineering Research Council, for providing the financial support for the study. Thanks must also go to both the Ford Motor Company and to BL Cars Limited for providing the test engines and vehicle used in this study. The help and advice of the MPD Technology Corporation is also much appreciated. Finally thanks must go to Christine Slivinski for the typing of this thesis.

August 1982 W L Richards

CONTENTS

APPENDICES

LIST OF TABLES

LIST OF SYMBOLS

a	Air Fuel Ratio
B	Temperature Independent Coefficient, Constant
C	Constant
C_p	Heat Capacity, Specific Heat at Constant Pressure
C_v	Specific Heat at Constant Volume
D	Diffusion Coefficient
Do	Constant
Ea	Activation Energy
Eo	Electrolysis Cell Voltage
δo	Arbitrary Fraction
ΔH	Pressure Differential
ΔH_H	Relative Partial Molar Enthalpy
I	Current (amps)
J	Hydrogen Diffusion Flux
K	Constant
k_s	Thermal Conductivity
ℓ	Jump Distance of Protons
N_{BI}	Biot Modulus
P	Pressure
Peq	Equilibrium Pressure
Po	Absolute Pressure
R,r	Radius, Specific Gas Constant
R_G	Rate of Hydrogen Generation
r_v	Compression Ratio
t	Time
T	Temperature

To	Absolute Temperature
ΔT	Temperature Difference
W	Indicated Load
α	Thermal Diffusivity (thermal conductivity/thermal capacity)
γ	Ratio of Specific Heats
λ	Separation Constant
ϕ	Equivalence Ratio (stoichiometric air requirement/actual air present)
ρ_f	Density of Fuel
ρ_p	Density of Powder

Abbreviations

(aq)	Aqueous
B.M.E.P.	Brake Mean Effective Pressure
E.G.R.	Exhaust Gas Recirculation
(g)	Gas
(l)	Liquid
M.B.T.	Minimum Spark Advance for Best Torque
(s)	Solid
S.P.E.	Solid Polymer Electrolyte
T.D.C.	Top Dead Centre

CHAPTER 1

INTRODUCTION

CHAPTER 1

1.1 GENERAL

Since the energy crisis of 1973, the price of petroleum products has risen sharply. It has also become clear that the amount of oil available in the world is limited. There are several means whereby petroleum products can be made to last longer, thereby maintaining the extensive infrastructure of the oil industry. The two which have received most attention are supplementation of petrol with methanol, and using petrol derived from coal. However, there are drawbacks with both of these ideas.

The major problem with using methanol-petrol mixtures is one of phase separation. If water condenses inside a tank to the extent that it constitutes one percent or more of the total fuel, then the methanol will separate out from the fuel mixture into the water. This will happen whatever alcohol is used. It should be noted[1]* also that the improvements shown on fuel economy and exhaust emissions, using methanol-petrol blends, are directly related to methanol's leaning effect on carburation, and are only significant in older, rich-operating cars.

The manufacture of oil products from coal is very expensive, and necessitates the large-scale hydrogenation of the coal to increase the hydrogen/carbon ratio (the Fischer-Tropsch process). Since the

* Numbers in parentheses designate References at the end of this thesis.

calorific value of hydrogen is nearly three times that of petrol, it is a logical conclusion that the hydrogen should be used directly. Another problem with using petrol as a fuel, apart from its rising costs and diminishing reserves, is that of atmospheric pollution. Awareness of this problem has increased in recent years, and legislation has become steadily harsher in an attempt to reduce the emission of noxious exhaust gases.

Hence it appears an alternative fuel to petrol must be found in the near future for motor vehicles. A considerable amount of work has been done recently[2] on battery design for electric vehicles. Although these have proved useful in certain applications, such as urban delivery vehicles, their major problem is that of the low power to weight ratio of the batteries. Lead/acid batteries have energy densities up to 50 watt-hours per kilogram, and even solium/sulphur batteries have energy densities of only 130 watt-hours per kilogram, whereas the energy density of petrol is approximately 12180 watt-hours per kilogram. Allowing for electrical conversion efficiencies of 75 percent and petrol conversion efficiencies of 25-30 percent, the penalty of electric vehicles is still apparent. Purpose built electric cars today have ranges of the order of fifty miles, with cruising speeds of approximately forty miles per hour. It must also be remembered that a standard three kilowatt outlet would have to be connected for eight hours to charge a battery for only 30-50 miles range.

A second alternative, which has received far less attention than electric vehicles, is that of using hydrogen as a fuel for internal combustion engines - thereby making minimal changes to the current concept of motor cars.

1.2 HYDROGEN AS A FUEL

There are many advantages in using hydrogen as an automotive fuel. It is "clean" burning (the major combustion product being water, from which hydrogen is obtained), is easily ignited, and has wide flammability limits (4-75% by volume in air at ambient temperature and pressure)[3]. Using a gaseous fuel such as hydrogen, rather than a liquid, avoids such problems as fuel atomization and evaporation during cold start and warm up, uneven distribution of the fuel to different cylinders arising from the existence of a liquid film on the walls of the intake manifold and unwanted variations in air-fuel ratio during transient conditions such as acceleration and deceleration.

However, there are some major problems using hydrogen as a fuel for general vehicle use; in particular the on-board storage of hydrogen, and serious back-firing into the engine intake. Hence, in this thesis I have investigated means of overcoming both these problems.

In the next chapter I have also discussed various means of economically producing and distributing hydrogen as a general purpose automotive fuel.

As the most feasible method of storing hydrogen on board vehicles appears to be using thermally decomposable metal hydrides, these are discussed in some detail, and a mathematical model has been developed to simulate both the charging and discharging behaviour of metal hydrides.

Engine back-firing appears to be a fundamental problem when hydrogen is used as a fuel, and several theories have been proposed

regarding its cause. What is known is that back-firing is predominant at rich operating conditions under load. Possible causes of back-firing are discussed in the next chapter. However, the bulk of this investigation has centred around the use of dual-fuel mixtures of hydrogen and petrol, thus avoiding the problem of back-firing into the engine intake, and simultaneously reducing the problem of storing hydrogen on-board the vehicle. The investigation was initially carried out using an engine and dynamometer on a test bed. However, the results obtained indicated vehicle modification using such a system was feasible. The modifications to the vehicle are also presented here.

1.3 OBJECTIVES OF THIS STUDY

The objectives of this study were as follows:

(a) To determine theoretically which method of storing hydrogen is most suitable for general automotive applications, and to determine the requirements of implementing such a storage system on a vehicle. As a result of the storage method decided, a means of predicting the rate of hydrogen absorption and desorption was required. Thus a secondary objective was to develop a model to simulate the rate of heat transfer in a hydride bed, and to predict the hydride rate kinetics.

(b) Having developed a mathematical model, to compare other workers' hydriding and dehydriding data with those predicted by the model. As a further development of this, to predict the effect of changing hydride bed dimensions, and to determine the most

satisfactory hydride for a given set of operating parameters.

(c) To investigate the effect of wide-open throttle operation using a dual-fuel mixture of hydrogen and petrol, both on brake thermal efficiency, and on exhaust emissions.

(d) To modify a vehicle to operate using such a dual-fuel system, and to develop a suitable control system for satisfactory "drive-ability". No detailed measurements of fuel consumption or emissions data were possible due to lack of access to a chassis dynamometer.

CHAPTER 2

REVIEW OF PREVIOUS WORK

CHAPTER TWO

There are four major requirements for an automotive fuel. These are:

i) It must be readily available, or cheap to produce;
ii) It must be distributed nationwide economically;
iii) It must be easily stored on-board any vehicle;
iv) It must perform satisfactorily as an engine fuel.

The only fuel which meets all these requirements today is petrol. However, in certain applications there is already a recognised role for hydrogen as an automotive fuel (for operation in mines, and for vehicles used indoors) and in some areas, fleet vehicles have been converted to run on hydrogen[4], or are in the process of being converted. In this survey, each of the above four areas will be considered in detail.

2.1 PRODUCTION OF HYDROGEN

At present, there are three methods used for large scale production of hydrogen[5]. These are:

i) Electrolysis.
ii) From hydrocarbons (such as methane).
iii) From coke.

It is also possible that in an era of cheap nuclear power, the heat energy of the nuclear source could be used directly to split the water molecule into its constituent elements. A variety of thermo-

chemical cycles are being investigated to find a practical means of doing so. Each method of production is discussed below.

2.1.1 Electrolysis

As a by-product, hydrogen is formed in substantial quantities during the electrolytic preparations of chlorine and of sodium hydroxide from brine. Using a moving mercury cathode, the sodium produced forms an amalgam with the mercury. When this amalgam makes contact with water, the mercury precipitates as the pure metal, and the sodium reacts with the water to form sodium hydroxide and hydrogen:

$$2Na_{(s)} + 2H_2O_{(l)} \rightarrow 2NaOH_{(aq)} + H_{2(g)}$$

Hydrogen is also produced by the direct electrolysis of water. However, water electrolysis has not been used extensively for hydrogen production because of the high cost of electrical energy compared to natural gas or coke. Only where substantial amounts of low-cost hydroelectric power or off-peak nuclear power are available have economics favoured electrolytic hydrogen. Electrolysis can directly produce 99.9% pure hydrogen. All large scale water electrolysis plants are built following a multi-module concept. Each module has a power rating of 1-2 MW.

Electrolysis of water occurs when a direct electric current is passed between two electrodes immersed in an aqueous electrolyte. For water to decompose, the voltage across the two electrodes must

be greater than that corresponding to the free energy of formation (decomposition) of water, plus the voltage needed to overcome electrode and ohmic polarizations.

With water electrolysis cells using an alkaline or acid electrolyte, hydroxyl (alkaline) ions or hydronium (acid) ions are required for the water to conduct. In alkaline electrolytes the reactions associated with electrolysis are:

$$\text{cathode} \quad 4e^- + 2H_2O \rightarrow 2H_2 + 4OH^-$$

$$\text{anode} \quad 4OH^- \rightarrow O_2 + 2H_2O + 4e^-$$

$$\text{net reaction} \quad 2H_2O \rightarrow 2H_2 + O_2$$

With acid electrolysis, the reactions occurring are:

$$\text{cathode} \quad 4e^- + 4H^+ \rightarrow 2H_2$$

$$\text{anode} \quad 2H_2O \rightarrow O_2 + 4H^+ + 4e^-$$

$$\text{net reaction} \quad 2H_2O \rightarrow 2H_2 + O_2$$

Both the cathode and anode must be corrosion resistant in the electrolyte at the potentials used. They must also be good electronic conductors, and catalyze the evolution of hydrogen and oxygen. All large scale electrolysis units in use today have iron cathodes, and nickel (or nickel-plated iron) anodes.

The electrolyte must not produce any impurities during the electrolysis reaction, and must be stable at the voltages used. It must also provide a sufficient concentration of hydroxyl or hydronium ions for good electrolytic (ionic) conductivity. All systems presently in use have an aqueous solution of 20% - 30% potassium hydroxide.

The electrolytic cell must also have a diaphragm to separate the hydrogen and oxygen, both as gases, and dissolved in the electrolyte. It must also have ionic conductivity, or absorb the electrolyte to have adequate ionic conduction. In all cells the diaphragm is made of asbestos.

For electrolysis to occur at practical rates, the voltage (V) applied to the cell must exceed the reversible cell voltage (Eo). The difference V - Eo, is needed to overcome the resistances (electric and polarization) associated with the electrolysis process. The corresponding energy is eventually dissipated within the cell as irreversible heat. The minimum electrolysis voltage (Eo) decreases substantially with increasing temperature, at $25^{o}C$, Eo = 1.229 V, whereas at $150^{o}C$, Eo = 1.11 V[6].

Most commercial electrolyzers operate between $70^{o}C$ and $90^{o}C$. As the temperature is raised above this level, corrosion problems begin to limit life. In addition, it becomes necessary to pressurise the system to reduce water loss through evaporation. These complications limit the temperature capability of present technology.

The rate of hydrogen generation is proportional to the current that passes through an electrolysis cell according to:

$$R_G = 4.4 \times 10^{-4} I$$

where R_G is the rate of hydrogen generation, m^3/hour (assuming no recombination within the cell), and I is the current in amps.

Over the past five years, a considerable effort, in terms of labour and finance, has been invested in an attempt to make more efficient use of electrolytic manufacture of hydrogen. The two main areas of improvement have been in advanced alkaline electrolyzers and the use of solid polymer electrolytes.

2.1.1.1 Advanced Alkaline Electrolyzers

By increasing the temperature of alkaline electrolysis from 80°C to 150°C, the reversible cell voltage is reduced, and the activation over-voltage is almost negligible at this temperature[7], so the overall efficiency of the process is increased. By using high temperature alkaline electrolysis, in conjunction with improved cathodes and anodes, cell efficiencies can be increased from 67% up to 78%.[8]

The major problem in using temperatures above 100°C is that asbestos, which is used as a diaphragm in the electrolytic cell, is attacked by the caustic solution. However, the addition of dissolved silicates to the electrolyte to shift

the equilibrium of asbestos dissolution reduces corrosion[7]. Also, new chemically resistant ion exchange membranes are being used. Of these potassium titanate looks promising[9].

2.1.1.2 Solid Polymer Electrolytes

The use of solid polymer electrolytes can give system efficiencies of 85% - 90%[10]. The solid polymer electrolyte (SPE) is a thin sheet (5 - 10 mm thickness) of a sulphonated fluoropolymer. It is a plastic material which serves as the sole electrolyte (there are no acid or caustic liquids in the system), and also forms a barrier between the hydrogen and oxygen chambers. The electrodes are thin catalyst layers bonded to the surfaces of the plastic sheet, which serves as the H_3O^+ conducting electrolyte. However, the SPE is highly acidic and severely corrosive to materials which are in direct contact with it[7], resulting in expensive current collector and electrode materials. Noble metals (platinum, iridium and rhodium) are required as catalysts, and acid-resistant metals are required as current collectors. Although the noble metal catalysts are expensive because of their high dispersion, only small quantities (eg - 10 to 40 g/m^2) are required to achieve high cell performance. Current collectors are made from titanium, tantalum, or niobium; the selection depends on temperature, pressure and current density[6]. The advantage of SPE systems is their high current density capability (over 30 kA/m^2) at high temperatures (150^oC) and high pressures

(up to 600 psi), all of which contribute to high energy efficiencies. There is also an extensive research interest into cheaper electrode catalysts with better performance[11].

Table 2.1 gives a comparison of present day and predicted costs for various types of electrolysis units.

2.1.2 Hydrogen from Hydrocarbons

The cracking of hydrocarbons thermally is an important part of petroleum refining and produces much hydrogen. Methane, from natural gas, may also be thermally decomposed to hydrogen and carbon:

$$CH_4 \rightleftarrows C_{(s)} + 2H_2$$

Temperatures of the order of 850°C, and a catalyst are required in this process. The carbon deposits on the catalyst surface leave a gaseous product of hydrogen and unconverted methane. It is possible to directly produce 95% pure hydrogen using this process. The catalyst is continually circulated from the reactor to the regenerator, where air is used to burn the coke formed on the catalyst surface. This reaction simultaneously cleans the catalyst surface and reheats it to the reaction temperature.

The process consists of a fluidized bed reactor which contains a 7% nickel on alumina catalyst and a fluidized bed regenerator. The temperature in the regenerator is approximately 1200°C, while

TABLE 2.1 - ECONOMICS OF ELECTROLYSIS

	Conventional Electrolysis	Solid Polymer Electrolysis	Advanced High Temperature Electrolysis
1980	$18/MBTU	$14/MBTU	-
Predicted ($1980)	$16/MBTU	$11/MBTU	$14/MBTU (Approx)

NB 1 MJ ≡ 947.8 BTU

1 kgH_2 ≡ 119.96 MJ

the temperature in the reactor is 850°C. Because the decomposition reaction is endothermic, the circulating solids function as a method of supplying heat to the reactor, as well as a catalyst for the reaction.

However, the two fluidized beds, and the solids-circulation system are expensive. In addition, the replacement of the catalyst to make up for attrition is an important cost. Thus the reaction of steam with methane at 1100°C is preferable:

$$CH_4 + H_2O \rightarrow CO + 3H_2$$

The objective of steam reforming is to convert as much of the steam and hydrocarbon as possible into a mixture of carbon monoxide and hydrogen. The carbon monoxide is converted in a subsequent water-gas step to carbon dioxide and more hydrogen using an iron or cobalt catalyst at 400°C:

$$CO + H_2O \rightarrow CO_2 + H_2$$

A steam reformer is a furnace operating at one atmosphere pressure which encloses packed catalyst tubes operating at 300 psi or less, and has a heat exchanger to recover the heat located in the flue[12].

The cost of producing hydrogen by this process ranges from $1.50/MBTU to $6.30/MBTU depending on the cost of the natural gas feed (50 cents per thousand cubic feed - $3.00 per thousand cubic feet). The hydrogen produced in this manner can be up to 95% pure.

2.1.3 Hydrogen from Coke

There are two gasification processes to produce hydrogen from coal or coke. The first is the water gas reaction where steam is passed over coke at temperatures above 1000°C:

$$C_{(s)} + H_2O_{(g)} \rightleftarrows CO + H_2$$

This reaction is endothermic, and is generally run in alternation with the passage of air to heat the coke to the correct temperature. Steam is then passed through the bed of hot coke. However, the cyclic nature of this process makes the economics unfavourable.

In the second process, steam plus air (or oxygen) is reacted with coke to produce a synthesis gas, containing hydrogen plus several other gases, including nitrogen and carbon dioxide. The carbon monoxide is converted to carbon dioxide using the water gas process mentioned earlier. The carbon dioxide is removed by washing with water under pressure, and nitrogen is removed by cooling with liquid air. Coke oven gas has also been processed to yield hydrogen by fractional liquefaction.

The cost of hydrogen produced by gasification of coal is dependent primarily on the cost of the coal, and ranges from $2.80/MBTU to $5.20/MBTU with the cost of coal ranging from $10/ton up to $30/ton. Like the steam reforming of methane, the hydrogen produced is 95% pure.

2.1.4 Thermochemical Production of Hydrogen

A thermochemical hydrogen production process is one which requires only water as a material input and mainly thermal energy, or heat, as

an energy input. The output of the process is hydrogen and oxygen, and perhaps some waste heat. The process itself comprises a series of chemical reactions which sum to water decomposition, and the products of each reaction must be separated and either recycled or sent to the next reaction.

Interest in thermochemical processes arose from the potential they offer for lower capital and/or operating costs and higher overall thermal efficiency than water electrolysis.

2.1.4.1 Single-Stage Decomposition

For the direct decomposition reaction

$$2H_2O \rightleftharpoons 2H_2 + O_2$$

equilibrium composition does not shift in favour of H_2 rapidly enough with increasing temperature to suggest that a single-step thermal decomposition process offers great promise in the near future[13]. At 2000 K and 1 atm, the equilibrium mixture contains only 3.6% hydrogen by volume. High-temperature-gas-cooled reactors provide heat in the range of 1200-1300 K. In any real system using this process, there will be severe practical problems related to the very high temperatures required.

2.1.4.2 Multi-Stage Decomposition

One of the earliest decomposition processes studied was that using vanadium and chlorine[14] in the reactions:

$$2\,VCl_2 + 2\,HCl \rightarrow 2\,VCl_3 + H_2$$

$$4\,VCl_3 \rightarrow 2\,VCl_4 + 2\,VCl_2$$

$$2\,VCl_4 \rightarrow 2\,VCl_3 + Cl_2$$

$$Cl_2 + H_2O \rightarrow 2\,HCl + \tfrac{1}{2}O_2$$

The efficiency of this process was approximately 18% when using temperatures of the order of 1360 K. The most advanced process under investigation is the hybrid "bromine-sulphur" cycle[15], where the first step is electrochemical:

$$2H_2O + Br_2 + SO_2 \rightarrow H_2SO_4 + 2HBr \text{ (electrochemical)}$$

$$H_2SO_4 \rightarrow H_2O + SO_2 + \tfrac{1}{2}O_2$$

$$2HBr \rightarrow H_2 + Br_2$$

One of the major problems with this particular process is the thermal decomposition of concentrated sulphuric acid at 1000 K. Thus it is unlikely to be used to produce hydrogen on a large scale.

Due to practical difficulties in maintaining thermochemical cycles, these show less promise as a means of hydrogen production, especially when recent advances in electrolytic production of hydrogen are considered.

2.2 DISTRIBUTION OF HYDROGEN

One of the crucial issues regarding the use of hydrogen as a fuel is its nationwide transmission. The introduction of synthetic petrol before the widespread use of hydrogen as an automotive fuel will probably be due to the existing infrastructure of the oil industry.

There are two methods by which hydrogen can be transported in bulk, using a gas pipeline system, or by surface transport of liquid hydrogen.

2.2.1 Gas Pipelines

An experimental study conducted with contemporary gas distribution equipment (ie - for natural gas) in hydrogen service indicated no incompatibilities in service[16]. It was concluded that existing in-place components and piping, with the possible exception of meters, should be adequate for hydrogen delivery.

Since the calorific value of hydrogen is approximately one third that of natural gas, it appears that the energy capacity of the pipeline will be far lower for hydrogen. However, since the mass flow rate of gas inside a pipe depends upon the square root of the density of the gas[17], and because the density of hydrogen is about one ninth that of natural gas, there is a compensating factor of one third that results in the given pipe having essentially the same energy-carrying capacity for natural gas as for hydrogen.

In practice, it has been found[16] that if piping and operating pressures are not changed, hydrogen energy delivery will be about eighty to ninety percent of natural gas energy delivery under turbulent flow conditions, but may be only forty percent of natural gas delivery under laminar flow conditions.

The major hazard associated with pipeline transmission of hydrogen gas is leakage, followed by combustion. Due to its small molecular size, hydrogen is more likely to leak than any other gas. When hydrogen was transmitted in natural gas pipelines, the observed overall hydrogen-to-natural gas leak ratio was about 3.25[16], and the overall energy loss ratio was about 1.04.

An explosion of hydrogen-air mixtures is very unlikely to occur as a result of a pipeline leak. Detonation limits of hydrogen-air mixtures range from eighteen to fifty-nine percent by volume[17]. Since the hydrogen molecule has a very low mass, it would rise rapidly in air, and unless a leak occurred in a confined region, it is unlikely the lower detonation limit would be reached.

An existing hydrogen pipeline in Germany[18] was extended to a total length of about 130 miles in 1954. This transmits fairly pure (greater than ninety-five percent pure) hydrogen at pressures of 15 atm (225 psi). Pipe diameters range from 6 to 12 inches, and are buried one metre deep. During the last thirty years, there have been some fires, but no explosions or any problems with hydrogen embrittlement, indicating there are no severe technical problems to be overcome.

2.2.2 Liquid Hydrogen Transmission

Hydrogen exists in the liquid state at temperatures below 20.3 K. As a liquid, it has a very low density (70 g/l) compared to petrol (733 g/l) or water (1000 g/l), resulting in nearly four times the volume for the same energy content as petrol. The theoretical energy requirement for the liquefaction of hydrogen is 14.1 MJ/kg, which is more than ten percent of the calorific value of hydrogen (119.96 MJ/kg). The low temperature requirement can cause significant thermal contraction (0.3% in steels), as well as change the mechanical properties of structural materials (eg - tensile strength). To maintain temperatures below 20.3 K, it is necessary to provide sophisticated insulation systems as well as pressure relief and venting systems. All these factors result in much higher costs than for gaseous hydrogen.

However, long-distance transporation of liquid hydrogen is fairly common in the United States, although it is not widespread in Europe. In America, transport is by road, rail and by barges at sea[19]. Road transport is made in 48,000 litre and 52,000 litre trailer-mounted Dewars. All these vehicles are fitted with multilayer insulation, with typical boil-off losses amounting to approximately ¼% per day.

Rail cars for the transport of liquid hydrogen are horizontal cylindrical Dewars with a storage capacity of 100,000 litres. Barge-mounted Dewars have been built for the US National Aeronautical and Space Administration and have a capacity of one million litres. These

very large Dewars have loss rates as low as 0.1% per day.

The two most commonly used insulation systems are evacuated perlite and evacuated multilayer insulation[19]. The largest vessels used for stationary storage are almost spherical in shape. Since the heat input is largely a function of the surface to volume ratio, the boil-off rate (as a percentage) decreases as the size becomes larger.

2.3 STORAGE OF HYDROGEN

There are three basic methods for storing hydrogen on board a vehicle:

i) As a compressed gas;
ii) As a liquid;
iii) As a chemical compound - eg, a metal hydride.

In terms of ease of operation and cost, storage using compressed gas at 17MPa (2500 psi) would appear the answer. However, using comparisons based on the energy equivalent of 15 imperial gallons of petrol (68.2 litres or 50.0 kg), it is found that 18.2 kg of hydrogen at 17 MPa would occupy more than 1.2 cubic metres - ie, too large for the average vehicle. The storage vessel would weigh nearly 1.5 tonnes.

The same amount of liquid hydrogen (18.2 kg) would occupy a volume of 260 litres, and using data from liquid hydrogen vehicles in use[20], this would require a total tank volume of 485 litres, and an empty container weight of 156 kg.

The liquid hydrogen containers in use are of conventional double-walled vacuum-jacket construction fabricated of welded aluminium alloy components. Aluminium foil/fibreglass layers are used as radiation shields in the main vacuum space. This construction is necessary to keep the temperature below 20.3 K. The tanks in use today[21] have boiloff rates of ten percent/day. When no hydrogen is being taken from the tank, the heat leaking into the liquid hydrogen causes some of it to evaporate. If the tank is closed (unvented) the pressure increases at about 3 psi/hr for a nearly full Dewar or about 6.6 psi/hr for a nearly empty Dewar until the relief valve is activated (at 65 psi). This happens after 10 to 21 hours, depending on the liquid level in the Dewar. After the valve opens, or if the tank is left in a vented condition, liquid hydrogen will be lost at the rate of 0.77 kg/day. This means a full tank of liquid hydrogen would evaporate completely in less than 2 weeks, thus causing potential safety problems, particularly in vehicles used on an intermittent basis. The cost factor and energy required for liquefaction and storage of liquid hydrogen must also be considered. It should be noted however, that liquid hydrogen may well prove to be a viable fuel for particular forms of transport - eg, aircraft. Economic and technical surveys on the prospects for liquid hydrogen fuelled aircraft have already been completed[22].

Hydrogen can also be stored as a chemical compound - either as a metallic (or saline) hydride, or encapsulated in a molecular sieve zeolite. As yet, no hydride or other material has been found entirely satisfactory for automotive applications, either for reasons of weight,

cost, or operating conditions which are difficult to maintain on a vehicle. However, these show the most promise of all storage media, since hydrogen can be stored at a greater density than as liquid hydrogen.

2.3.1 Molecular Sieve Zeolites

Fraenkel and Shabtai[23] have investigated the feasibility of using zeolite molecular sieves as hydrogen storage media by intracrystalline encapsulation. The hydrogen is stored as compressed gas in a "bulk container" of zeolite cages. A simplified model for the hydrogen encapsulate of Cs_3Na_9-A type zeolite is shown in figure 1.

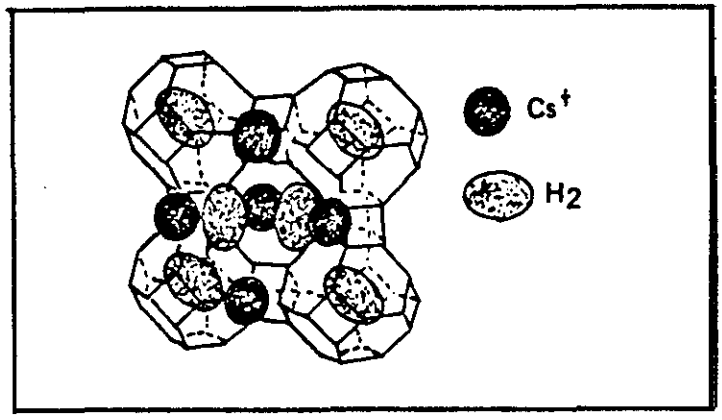

FIGURE 1 - Proposed model for the hydrogen encapsulate of Cs_3Na_9A - type zeolite.

The major factors affecting the storage efficiency of zeolites are the aluminosilicate structure of the zeolite and the charge, size and content of the exchangeable cation. Of the types so far examined[24]

the best zeolite is the Linde A-type, and the highest efficiency was obtained with an exchangeable cation mixture containing 2.6 Cs^+ and 9.4 Na^+ ions per unit cell. At a temperature of 200°C and a pressure of 60 MPa (8700 psi) this system could encapsulate 85 cm^3/g (STP) of hydrogen, corresponding to 0.76% by weight. Extrapolation to higher pressures suggests that some zeolite systems are capable of storing one percent by weight of hydrogen.

Hydrogen encapsulation in zeolites appears to be a better form of storage than hydrogen as a compressed gas (at 17 MPa or 2500 psi) due to the ability to store the gas at pressures which are an order of magnitude higher, without the need of heavy tanks, and under much safer conditions. The hydrogen capacity of zeolite encapsulants is comparable with that of alloys such as lanthanum nickel or iron titanium, yet zeolites are potentially much cheaper and large-scale zeolite production technologies are well known. However, zeolite encapsulants suffer from inconvenient volume capacity for hydrogen because of their relatively low densities, and their loading requires very high hydrogen pressures. This suggests molecular sieve zeolites will be limited to stationary hydrogen storage.

2.3.2 Hydrogen Storage Using Hydrides

There are three basic types of hydride compounds: saline (or ionic); metallic; and covalent. This classification is based predominantly on the character of the hydrogen bond. However, in terms of hydrogen storage they can be reclassified into two groups - those which release hydrogen by the addition of water to the hydride, and

those which are thermally unstable, and will decompose to evolve hydrogen when moderate amounts of heat are supplied. Metallic hydrides, and some saline hydrides fit into the latter category, whereas the hydrides of the alkaline earth metals will evolve hydrogen when water is added. The reaction of hydrides with water is discussed in the next chapter.

2.3.3 Thermal Decomposition of Hydrides

The absorption of hydrogen by a metal to form a hydride is an exothermic reaction, and as the reaction is generally reversible, hydrogen can be recovered by raising the temperature above, or lowering the pressure below, the temperature and pressure required for the absorption process. At any one temperature, the hydride is in equilibrium with a particular pressure of hydrogen - namely its decomposition pressure. If the hydrogen is consumed, resulting in a pressure drop, decomposition occurs until the evolved hydrogen has built up to the decomposition pressure again. Since the formation of hydrides is exothermic, energy must be supplied for their decomposition. This can be obtained from the waste heat of the internal combustion engine. Thus a balance is required between the heat produced, and that required, both as to quantity and temperature. Hence the hydride must have an appreciable decomposition pressure (preferably at least one atmosphere) at the temperature of operation of the hydrogen producing device.

The equation for the formation of hydrides which undergo thermal decomposition is as follows:

$$M + \frac{n}{2} H_2 \rightleftharpoons MH_n$$

and this reaction, when proceeding to the right, is normally exothermic. The behaviour of a metal-hydrogen system is frequently represented by a pressure-composition - temperature diagram, an example of which is shown in figure 2.

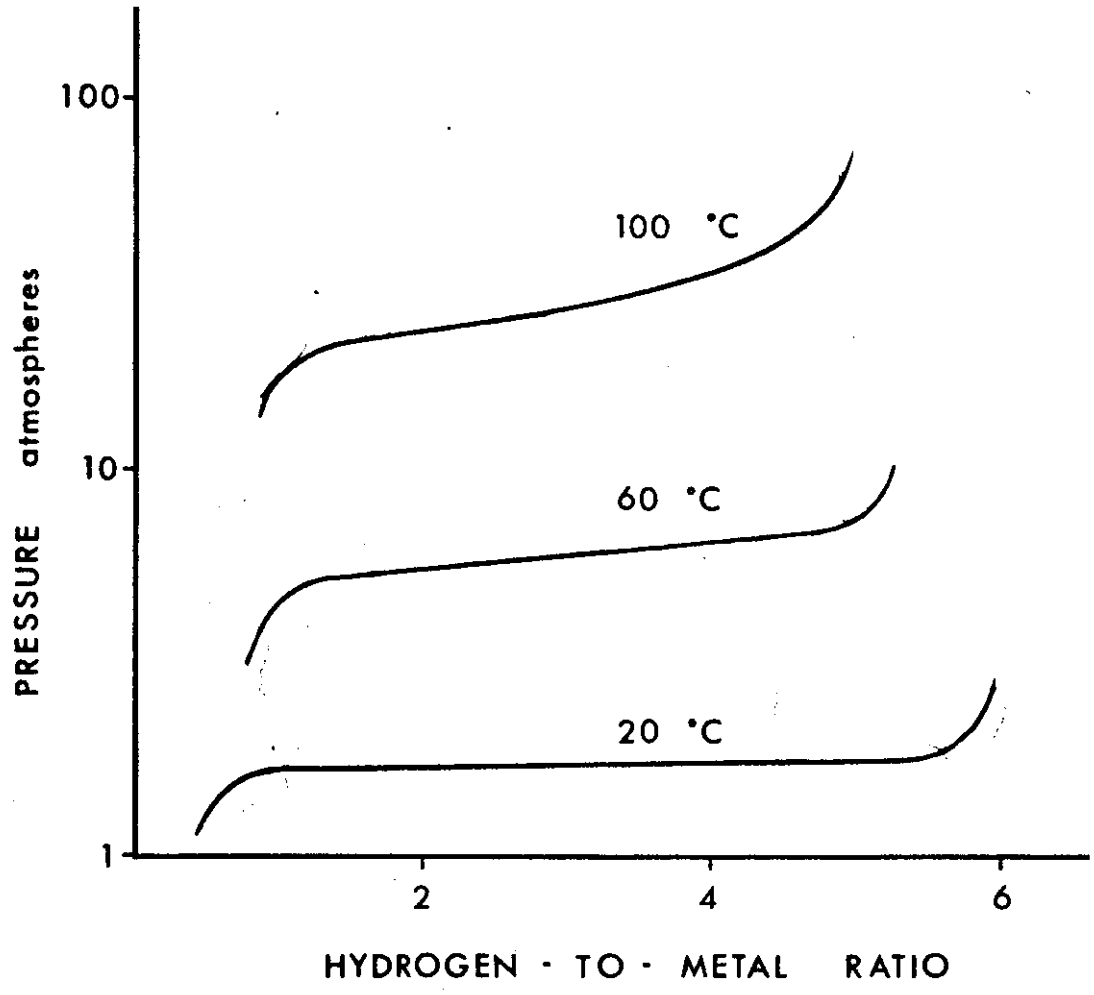

FIGURE 2 - Pressure-temperature-composition diagram for $LaNi_5$-H showing the equilibrium hydrogen dissociation pressure vs the hydrogen concentration in the metal.

At any particular temperature, hydrogen will dissolve in the metal phase as the pressure increases. The beginning of the "plateau region" indicates the appearance of a distinct metal hydride. Since the solubility of hydrogen in many metals can be appreciable, metal hydrides are often non-stoichiometric. Upon the appearance of this hydride phase, the hydrogen pressure remains almost constant until all the solid attains this composition. Above this "plateau region", any further adsorption of hydrogen requires a large increase in pressure. The effect of increasing temperature is shown by the higher temperature isotherms. As the temperature rises, the miscibility gap tends to narrow, accompanied by a consequent reduction in the plateau length, until at some critical temperature the miscibility gap and the pressure plateau disappear.

Many hydrogen-metal systems depart from ideal behaviour by exhibiting a pressure hysteresis effect in the region of the pressure plateau, an effect which is particularly noticeable in the unstable hydrides (those with a plateau dissociation pressure of 101.4 kPa - ie, one atmosphere - at 300^{o}C, or less). This hysteresis is thought[25] to be a consequence of the large volume change which occurs upon hydriding, and is illustrated for the case of iron titanium in figure 3. In general, the equilibrium pressure at any given temperature is the dissociation equilibrium pressure, unless specifically stated otherwise.

The idea of using metal hydrides as hydrogen storage media for automobiles was first proposed by Hoffman et al[26] in 1969. The

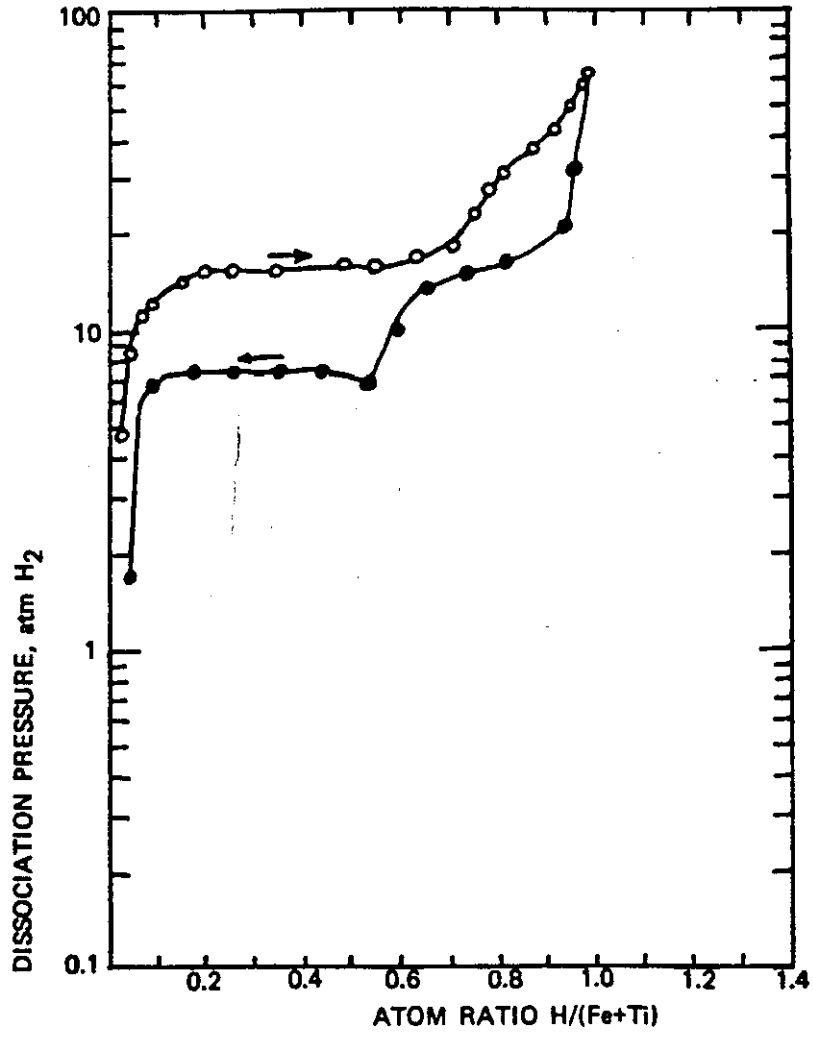

FIGURE 3 - Hysteresis in the FeTi-H System (40°C)
(C H Waide, J J Reilly, R H Wiswall 1974)

hydride suggested was catalyzed MgH_2, which is very attractive in terms of the weight of the hydrogen stored. Several different types of hydride material are now available for automotive applications, and a summary of their properties is given in table 2.2.

TABLE 2.2 - PROPERTIES OF METAL HYDRIDES

Hydride	Density of Metal Alloy g/c.c.	$\%H_2$ (wt.)	N_{H_2} *	Temp. ^oC Peq=1**	Standard Enthalpy of Formation ΔH_f	Cost £/kg (1980)
MgH_2(10%Ni)	1.4	6.94	6.6	287	-78.3	≈12.00
$Mg_{2.4}NiH_4$	2.6	3.84	≈6.2	253	-64.4	14.10
FeTi	5.47	1.75	6.01	-11.4	-28.0	12.50
$LaNi_5$	8.25	1.43	5.4	12	-31.0	30.80
$MMNi_5$	8.1	1.41	3.4	-7.9	-20.9	15.6
V	4.5	1.98	10.3	27	-25.1	-
$CaNi_5$	6.65	1.39	2.2	41	-31.8	13.00
LiAl	0.91	8	7.6	≈100	-28.4	≈90.00
Liquid H_2	0.071	100	4.2	-253	-	-

* $N_{H_2} \times 10^{22}$ = No. of H atoms per cubic centimetre

** Temperature (^oC) at which equilibrium dissociation pressure = 1 atm.

2.3.3.1 Magnesium Hydride

The direct sythesis of magnesium hydride (MgH_2) from magnesium and hydrogen can only be carried out with difficulty, and the uncatalyzed conversion of pure magnesium to magnesium hydride is incomplete, even at temperatures above 400°C and pressures up to 300 atmospheres[27]. However, by alloying small amounts (5-10%) of certain metals with magnesium, intermetallic phases are formed which catalyze the magnesium-hydrogen reaction.

Such catalysts are permanently incorporated into the system and are effective over many hydriding-dehydriding cycles. Copper, nickel and aluminium can all be used to catalyze the Mg-H reaction, but nickel appears to be the most promising. This is due to the formation of the intermetallic compound, Mg_2Ni, which reacts rapidly with hydrogen to form the ternary hydride, Mg_2NiH_4[28] according to the reaction:

$$Mg_2Ni + 2H_2 \rightleftarrows Mg_2NiH_4$$

This hydride appears to have a definite stoichiometric composition, indicated by the abrupt termination of the pressure-composition isotherm at a composition corresponding to Mg_2NiH_4[29]. The hydride is a rust coloured fine powder, stable in air at 20°C for short periods, but slowly oxidizes over a period of months. A slight reaction occurs with water although it reacts vigorously when immersed in mineral acids.

The decomposition of magnesium nickel hydride occurs rapidly (in approximately four minutes at 240°C[29]) and the back reaction is negligible provided the final pressure of the system is less than 25% of the equilibrium dissociation pressure. However, since the amount of hydrogen (by weight percent) in Mg_2NiH_4 is less than half that in MgH_2, the magnesium nickel hydride is not as useful as a hydrogen storage medium.

The major problem in using magnesium hydride (catalyzed with ten percent nickel) as a hydrogen storage medium is the high temperature required for dissociation (nearly 300°C to give an equilibrium decomposition pressure of one atmosphere). Magnesium nickel hydride has an equilibrium pressure of one atmosphere at approximately 250°C. Thus, the commercially available magnesium-nickel storage system is a mixture of Mg_2Ni and Mg, resulting in a hydrogen capacity of 3.84% by weight[30].

Another magnesium alloy system which has been studied is the Mg-Cu system, since Mg_2Cu reacts with hydrogen as follows[31]:

$$2Mg_2Cu + 3H_2 \rightleftarrows 3Mg_2H_2 + MgCu_2$$

This occurs at temperatures above 200°C, and the hydride has an equilibrium dissociation pressure of one atmosphere at approximately 240°C. However, this system has a hydrogen content of approximately 2.7% by weight, which is a significant drop in hydrogen capacity for only a marginal drop in stability.

Both the magnesium-nickel and magnesium copper alloys are rapidly deactivated in the presence of air due to the rapid formation of a surface oxide layer. To maintain a high capacity of the storage system, it is thus important that only high purity hydrogen is used.

2.3.3.2 Iron-Titanium Hydrides

At present the iron-titanium and other similar systems appear to be the most favourable for hydrogen storage since they have high dissociation pressures at low temperatures, as shown in the isotherms in figure 4[32].

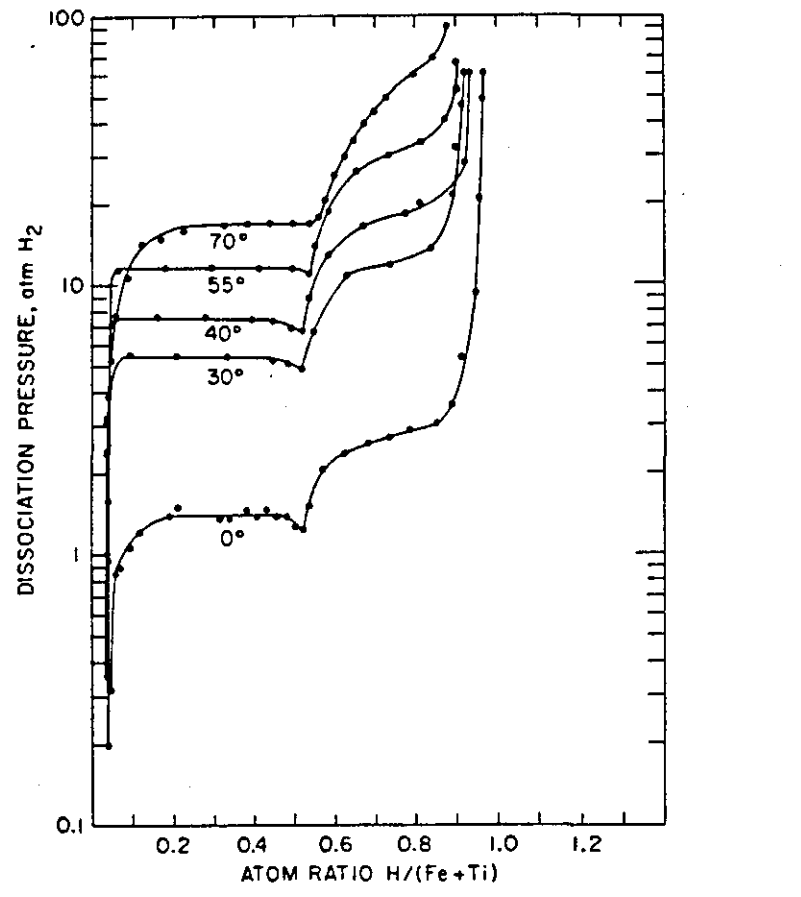

FIGURE 4 - Pressure-temperature-composition diagram for the FeTi-H system. Reilly 1977

The starting materials also have the advantage of high abundance and low cost. The important intermetallic compound in terms of hydrogen storage is FeTi, which reacts directly and reversibly with hydrogen to form two ternary hydrides. The reactions occurring are:

$$2.13\ FeTiH_{0.1} + H_2 \rightleftarrows 2.13\ FeTiH_{1.04}$$

and

$$2.20\ FeTiH_{1.04} + H_2 \rightleftarrows 2.20\ FeTiH_{1.95}$$

Exposure of these hydrides to air results in deactivation, and although both hydrides have dissociation pressures well above one atmosphere at 25°C, they will decompose only very slowly in air at room temperature. This can be a severe problem, since minute quantities of oxygen will substantially reduce the storage capacity of iron-titanium, and practical systems in some cases have only half the theoretical hydrogen capacity. Thus very high purity hydrogen (>99.99995% pure) must be used, leading to greatly increased fuel costs[33].

Iron-titanium hydrides are already in use as automotive hydrogen storage media[34][4]. However, due to the relatively small capacity (1.75% by weight) compared with magnesium alloys, the weight of the hydride plus container is considerable. The actual capacity of iron-titanium hydride may be much smaller

than the theoretical hydrogen capacity due to the formation of iron oxides and can be as low as one percent by weight. Daimler Benz[34] have a 2.4 ton minibus (with a 2.3 litre engine) running on hydrogen, where iron-titanium is used as the storage medium. The storage unit occupies a volume of 65 litres and contains 200 kg of iron-titanium hydride, or 3.6 kg of hydrogen. This amount was enough to keep the engine running at a constant 1700 rpm for nearly three hours, and gave the vehicle a range of approximately 130 km. The energy content of this amount of hydrogen is equivalent to nearly 10 kg of petrol (approximately 13 litres). After running the engine, the temperature of the hydride bed was found to be 76^{o}C, so it had to be cooled considerably using external cooling water before it could be recharged. After cooling, up to 75% of the total hydrogen capacity was absorbed during the first ten minutes, although to fully recharge the hydride took 45 minutes, due to the evolution of heat during the recharging process.

2.3.3.3 Hydrides of the Lanthanide Series

Many of the rare earth containing intermetallic compound systems have the ability to store large quantities of hydrogen. Lanthanum nickel hydride ($LaNi_5H_6$) has a 30% higher density of hydrogen in the hydride than that of liquid hydrogen[35]. However the density of lanthanum nickel is fairly high (8.25 g/cc), resulting in a hydrogen capacity of only 1.4% by weight. However, the reaction kinetics for this hydride are very fast, even at room temperature, and lanthanum nickel is less susceptible to poisoning than the other hydrides.

During the formation of lanthanum nickel hydride, the alloy expands volumetrically by a factor of approximately 25%[36]. While expanding, the brittle material breaks up into finer particles and thus a large uncontaminated and highly active surface is formed. The composition of the hydride is dependent on the temperature and pressure of the system. The heat of reaction is about 30.2 kJ/gram mole H_2, which gives rise to a large increase in temperature when the $LaNi_5$ powder is reloaded (which takes place in a few seconds at a pressure of 3MPa (435 psi) hydrogen).

The major disadvantage of using lanthanum nickel as a hydrogen storage media is its high cost, although this has reduced markedly during the last five years.. However, Lunden and Lynch[37] have investigated a rare earth alloy known as mischmetal which has the composition 50% cerium, 25% lanthanum, 18% neodymium, Praseodymium 5%, and other rare earths 2%. This is available at a cheaper cost than lanthanum, and when alloyed with nickel has similar hydrogen storage properties as $LaNi_5$. Mischmetal nickel, $MMNi_5$, also has very fast kinetics for absorption and desorption of hydrogen, but suffers from a small decrease in hydrogen capacity. This is possibly due to the presence of cerium, since $CeNi_5$ does not form a reversible hydride[36].

2.3.3.4 Vanadium Dihydride

Vanadium, niobium and tantalum all react with hydrogen to form a stable monohydride. However, vanadium and niobium

monohydrides will react further at room temperature to form an unstable dihydride as follows:

$$1.92\ VH_{0.95} + H_2 \rightleftarrows 1.92\ VH_2$$

The rate of decomposition of vanadium dihydride to the monohydride is extremely rapid at 40°C. It has also been found that the presence of impurities in commercial grade vanadium, or the doping of pure vanadium with silicon, substantially increases the rate constant[38]. Of all the unstable hydrides, VH_2 has the highest weight percent of available hydrogen (1.98%). The major problem with using vanadium hydride as a storage material is its high cost.

2.3.3.5 Calcium-Nickel Hydride

Calcium-nickel hydride, $CaNi_5H_6$, appears to be another promising hydrogen storage system in that the metals are relatively cheap and abundant, and the temperatures required for dissociation pressures of one atmosphere or more are low. However, the density of the stored hydrogen is relatively low (1.39% by weight) and like magnesium and iron titanium systems, the hydride is easily deactivated in the presence of oxygen[39].

Another hydride system which has been investigated, and which gives higher hydrogen dissociation pressures is the calcium-nickel-mischmetal alloy, where mischmetal replaces some of the calcium in the original alloy[40]. Although there is a slight increase

in density compared to the pure $CaNi_5$ alloy, this is offset by a slightly lower density of hydrogen.

2.3.3.6 Complex Aluminohydrides

The complex aluminohydrides are salts of the alanate ion, AlH_4^-, of which lithium aluminium hydride, $LiAlH_4$, is the most widespread today. This hydride contains 8% by weight available hydrogen, and decomposes at 100°C[41] according to the reaction:

$$2LiAlH_4 \rightarrow 2LiH + 2Al + 3H_2$$

The major problem using this hydride is one of reprocessing, since the above reaction is not reversible. However, according to Ashby et al[42], lithium hydride reacts with aluminium and hydrogen at a temperature of 140°C and a hydrogen pressure of 34.5 MPa (5000 psi), although the reaction will only occur in tetrahydrofuran or a hydrocarbon solvent and takes at least five hours. The reaction occurring is as follows:

$$LiH + Al + 1\tfrac{1}{2}H_2 \rightarrow LiAlH_4$$

Other similar hydrides with relatively high capacities of hydrogen are sodium aluminium hydride, $NaAlH_4$, and magnesium aluminium hydride, $Mg(AlH_4)_2$. Certain properties of the hydrides discussed are summarised in Table 2.2. As can be seen from the heats of formation, it does appear that the thermal decomposition of lithium aluminium hydride could become reversible in the

presence of an appropriate catalyst, thus reacting in a similar manner to magnesium in the presence of nickel.

2.3.4 Rate Kinetics of Thermal Decomposition of Metal Hydrides

There are three different types of reaction which can occur in a metal-alloy bed. These are:

(a) The previously unreacted metal reacting with hydrogen to form a metal hydride.

(b) The metal hydride dissociating to form the metal, and evolving hydrogen.

(c) The previously reacted metal (ie - a solid solution of hydrogen in the metal) reacting with hydrogen to form a metal hydride.

In each of these three reactions, a different process may be rate-controlling, and for a given reaction, different mechanisms could be involved for different metal alloys.

For both magnesium and iron-titanium systems, surface oxides and adsorbed gases will inhibit the initial hydriding reaction and will also inhibit the dehydriding reaction. However, other alloys, such as lanthanum-nickel, will have a longer useful life as hydrogen storage media due to their resistance to poisoning.

Since the addition of nickel or copper to magnesium catalyzes the hydriding reaction, it seems likely[43] that Mg_2Cu and Mg_2Ni minimize oxide inhibition by providing a clean unoxidized external surface through which the hydrogen gas readily adsorbs, dissociates,

and diffuses into the interior of the alloy where bulk diffusion occurs. However, it was also found that this surface reaction in hydriding magnesium alloys is not the rate controlling factor. The kinetics are rate-limited by the diffusion of hydrogen through the growing hydride layer, and the dehydriding kinetics are rate limited by the diffusion of hydrogen through the growing metal layer.

The adsorption and desorption mechanism of hydrogen in iron-titanium is also thought to be rate-limiting[44], although diffusion occurs more rapidly than in magnesium systems. Although the diffusion constant is surprisingly low[44], the hydriding time is relatively short. This is thought to be due to the very fast diffusion of hydrogen along the boundaries of the metal grains by cracking the metal particles. The hydrogen can then penetrate into the grains and bulk diffusion can take place.

Van Vucht et al[36] found the hydriding/dehydriding reactions of rare-earth alloys of the type $LnTm_5$ (where Tm is either Co or Ni) were rate-limited by the diffusion of hydrogen into the bulk of the metal, whereas Raichlen and Doremus[45] found the desorption of $SmCo_5H_{2.6}$ was limited by the rate of transformation of the hydride to the alloy $SmCo_5$. This transformation is similar to allotropic transformations in pure materials, since it involves a structural rearrangement of the atoms from a hexagonal to an orthorhombic phase. It is unusual for such a change to be rate limiting, since the movement of atoms to form the new structure is slight. It may be that the strain energy involved in incorporating the hydrogen slows the transformation.

The velocity of the hydride-metal interface in such transformations is dependent on the difference, ΔT, between the measurement temperature and the temperature T_1 at which the hydride and alloy co-exist at one atmosphere pressure. A general equation for the interface velocity is

$$v = B.\Delta T.e^{-Ea/RT}$$

where B is a temperature-independent coefficient and Ea is the activation energy for the atomic motion involved. A value of Ea = 50.4 kJ/mole was found for $SmCo_5$[45]. This is much lower than the usual activation energy for diffusion of atoms in metals or for vacancy motion in metals, indicating that allotropic transformation probably does not require full atomic or vacancy jumps.

Van Vucht[36] also found in X-ray measurements that certain regions which are completely hydrogenated may exist in equilibrium with regions having a much smaller hydrogen content. It was concluded that hydrogen does not fill gradually and randomly the available interstices and that there is a positive interaction between hydrogen atoms, possibly by means of a strain that accompanies the filling of an interstitial hole. A hydrogen atom may thus induce another atom to occupy a neighbouring site. This case of rate limitation by hydride-metal transformation is incorporated into the model discussed in chapter four.

2.3.4.1 Diffusion of Hydrogen

The diffusivity of hydrogen into a metal is extremely high, 10^{15} - 10^{20} times higher than that of oxygen or nitrogen[46].

Several techniques may be used to monitor the diffusion of hydrogen, either by detecting a change in the expansion of the lattice, or by measuring a narrowing of the resonance line width according to proton magnetic resonance theory, or by using quasi-elastic neutron scattering techniques. The main advantage of these methods over macroscopic methods (for example permeation experiments) is that the diffusing process is observed over a microscopic range of some Å. The "microscopic" diffusion constant determined in this way has to be distinguished from the diffusion constant for macroscopic bulk diffusion, as determined by lattice expansion, or permeation measurements, which are influenced by interaction effects of hydrogen atoms with one another, by surface effects, and pipe diffusion effects due to dislocations and grain boundaries.

The temperature dependence of the diffusion coefficient is normally given by an Arrhenius equation:

$$D = Do\, e^{-Ea/kT}$$

where Do is a constant and Ea is the activation energy for diffusion of the proton. The measured values[47] for Do and Ea are:

$$Do = (7.2 \pm 3.6) \times 10^{-4}\ cm^2/sec \quad \text{and}$$

$$Ea = 500 \pm 50\ meV \quad (8.0 \pm 0.8) \times 10^{-20} J$$

According to quantum mechanical modified rate theory, the pre-factor Do is a constant, dependent only upon temperature, and should have the same value for all metal-hydrogen systems. It is given by the expression

$$Do = \frac{\ell^2 kT}{12\pi t}$$

where ℓ is the jump distance of the protons. This relationship gives a value for Do of $Do \approx 10^{-3}$ cm^2/sec, and this is in good agreement with previously measured results[47]. In practice, the linear temperature dependence of Do is too weak to be detected in the presence of the exponential temperature dependence of D. These measurements give a value for D at 300 K of $D = 2.9 \times 10^{-11}$ cm^2/sec which compares well with that of Bowman et al[48] of $D \approx 10^{-11}$ cm^2/sec found in a nuclear magnetic resonance study.

Recent work by Nomura et al[49] indicated that the rate determining step of the reaction might be the diffusion of hydrogen through the boundary of the reacted and unreacted portions. The rate equation is

$$\frac{dn}{dt} = k' (P - Peq)/t$$

where $k' = 3.2 \times 10^{-2}$ $((kgf/cm^2)^{-1})$, P is the pressure at time t and Peq is the equilibrium pressure. Hence the probable driving force of the reaction is the difference in concentration of hydrogen between the two parts, which is proportional to (P - Peq).

This result is used later in comparison with the rate of heat transfer in the hydride bed, as determined from a mathematical model of the hydriding/dehydriding processes.[56]

The equilibrium plateau pressure, Peq, is related to the absolute temperature, T, by the van't Hoff equation:

$$\ln Peq = \frac{2}{x}\frac{\Delta H}{RT} + C \equiv \frac{A}{T} + C$$

where x is the hydrogen/metal atom ratio, ΔH is the enthalpy change of the hydriding reaction and C is a constant related to the entropy change of the hydriding reaction.

In order to define the activation energy for hydriding kinetics (as opposed to that for hydrogen diffusion), one must consider the time to reach some arbitrary fixed reacted fraction, ζ_0, (generally 50%) at varying temperatures. Assuming (at constant temperature and pressure) that

$$J \propto \exp\frac{(\Delta H_H - Ea)}{RT}$$

where J is the hydrogen-diffusion flux, and ΔH_H is the relative partial molar enthalpy, determined predominantly by H-metal interactions, then a plot of $\ln t_{\zeta_0}$ vs $\frac{1}{T}$ gives an activation energy for hydriding of $(Ea - \Delta H_H)$. Thus the activation energy for hydriding need not necessarily match that for diffusion. Although

data are not available for the hydriding of magnesium hydride, they are available for the dehydriding[50]. The activation energy for diffusion is 40.2 kJ/mole, whereas the activation energy for dehydriding, when the rate-limiting process is the diffusion of hydrogen through magnesium, is 101.8 kJ/mole. Thus, the activation energy, which defines the temperature dependence of the kinetics, is not given simply by the activation energy for diffusion, but includes also an enthalpy-of-hydrogen-solution term.

2.3.5 Modelling Solid-Hydrogen Storage Beds

In all published mathematical models of hydride beds, numerical solutions to heat transfer equations have been used[51,52,53,54], and idealized hydride containment vessels have been used. In the model of Cummings and Powers[51] it is assumed the hydride bed is a plate-plate heat exchanger, as is illustrated in figure 5.

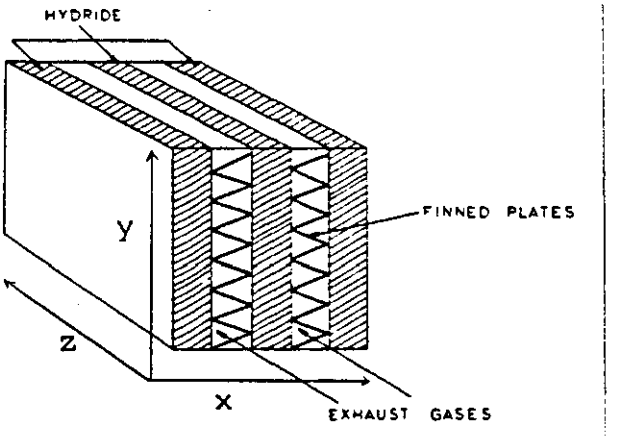

FIGURE 5 - Plate-plate heat exchanger for storing hydride

In practice, this design is not used as a storage system. A model based on this design has temperature gradients in two directions, (since the exhaust gases are flowing through the bed), thus requiring a two-dimensional mathematical model. Since a temperature gradient exists along the length of the bed, end effects must be taken into account, and thus the hydride slabs must be assumed finite. As there are no analytical solutions to the heat transfer equations for a finite slab, the problem must be solved by numerical methods. The method used was that developed by Murray and Landis[55]. Thus the bed is divided into a fixed space network of ten "nodes" across the hydride, and as the reaction front travels through a segment, the temperature of the adjacent node is continuously adjusted. To describe the two-dimensional heat transfer situation in the bed, the one-dimensional problem in the x-direction was solved at a number of locations down the length of the bed.

Yu, Suuberg and Waide[52] discuss two models both based on cylindrical pressure vessel systems. This type of storage vessel is most widely used today. The first model investigated was a convection model, where hot hydrogen gas is heated externally (no mention is made as to how this is done) and is then circulated through a charged hydride bed. No practical systems in use operate on this principle, although the heat content of the hydrogen released from the bed may be a factor influencing further desorption from the hydride.

Because the hydrogen-release reaction is endothermic, and heat is being supplied from one end of the bed, the reaction will travel

from the hot end to the cool end. Whether this reaction zone is broad and covers the entire bed, or is a narrow band moving from one end to another, depends on the relative rates of heat and mass transfer and chemical kinetics. The energy balance equations are given for both the gas phase and the solid phase, but analytical solutions cannot be obtained due to difficulty with the non-linear reaction rate term. Numerical solutions were obtained for magnesium-nickel and iron-titanium hydrides.

The second model of Yu et al[52] was a conduction model. Again this is based on a cylindrical system, and uses a fluid flow through an inner axial passage to provide or release heat during the dehydriding or hydriding process. This model is similar to that developed in chapter four, except the heat conduction is then from the outside of the cylindrical tube, not from an inner passage. If fluid flow through an axial tube is considered, then temperature gradients will exist in both an axial and a radial direction, requiring a two-dimensional solution to the heat conduction equation. This model assumes constant inlet and outlet fluid temperatures, heat transfer from the inner wall only (ie - an insulated outer wall), and that all hydrogen is released at the end of the bed or supplied at the entrance to the bed. A solution to the heat conduction equation was sought by the method of finite differences, but was very time consuming. Since the reaction rate is greater than the heat transfer rate, a simplified scheme was introduced, whereby the rate of hydrogen release is limited by the conduction of heat into the hydride. Thus a numerical solution was obtained for the position of the reaction front versus time.

However, since none of the three models discussed resemble any practical containment vessel, their predicted hydrogen release rates can only be used to compare different hydride materials.

The model of Fisher and Watson[53][54] is based on a cylindrical system with heat transferred to and from the system by water flowing in an annular shell around the test bed. A nodal analysis of the bed is assumed where material within a given volume is assumed to be uniform (having the same temperature and composition as the node). A series of boundary conditions is then developed for each node, along with energy balance equations.

The model is used to predict equilibrium pressure-temperature-composition isotherms at various temperatures for iron-titanium hydride, and it correctly predicts the shape and magnitude of the experimental curves. However, events such as maximum pressure and temperature are predicted to occur at times later than the experimentally observed times[54]. The model has also been developed to predict the behaviour of beds with the same length and containing the same amount of alloy as the previous bed, but with internal cooling tubes (rather than external cooling). It was concluded that the heat transfer surface area is utilized most efficiently when it is distributed throughout the bed - ie, several internal cooling tubes each with the smallest diameter possible. However, from a practical design consideration, such a system would be difficult to fabricate.

2.3.6 Safety of Metal Hydride Systems

One of the major problems in ensuring a safe hyrogen system is to prevent leakage of hydrogen out of the system and to prevent air

(oxygen) entering it. By keeping the storage container and transport lines at positive gauge pressure it is relatively easy to keep out any oxygen. However, there is a problem in keeping hydrogen within the container, since all materials in contact with hydrogen must be chosen to minimise enbrittlement. Aluminium alloys, stable austenitic stainless steels, and copper appear to be unaffected by hydrogen. The presence of small amounts of impurities in the hydrogen, for example methane or other hydrocarbon gases, considerably reduces this tendency for embrittlement.

Data are rather sparse concerning the safety-related behaviour of metal hydrides, although some of the factors known to influence their behaviour are particle size, temperature, surrounding atmosphere, and the inherent nature of the material itself. If one assumes that air is the surrounding atmosphere (as would be the case if the hydride tank had ruptured), then the most important factor affecting a particular hydride's behaviour is the particle size. Gibb and Messer[57] reported that large lumps of lithium hydride can be heated to a red heat without igniting, whereas finely divided lithium hydride will spontaneously ignite at room temperature. Similarly Lundin and Lynch[58] found iron titanium hydride ignited only when the flame of a propane torch was played over the surface of the hydride particles. Such behaviour is attributed to the fact that the hydride is deactivated by air, and even though the dissociation pressure may be more than one atmosphere, no hydrogen gas is evolved until high temperatures ($> 400^{o}C$) are reached.

Thus it does appear that metal hydrides are far less hazardous as fuel storage media than most common volatile fuels currently in use.

2.3.7 On-Board Generation of Hydrogen

In an effort to obtain increased engine efficiency by using hydrogen, yet avoid the problem of on-board storage of hydrogen, an attempt has been made to generate hydrogen on-board the vehicle from the parent fuel. One of the earliest investigations was the Boston reformed fuel car[59]. In this case, petrol was reacted with steam to produce a "reformed" fuel of carbon dioxide and hydrogen upstream of the engine. Initial efforts to develop an engine to burn the mixture revealed a poor starting reliability and carburettor flash-back at high rpm. The basic reaction occurring with steam reformation of petrol is as follows:

$$C_7H_{16} + 14H_2O \rightarrow 7CO_2 + 22H_2 - \text{heat}$$

However, subsidiary reactions are also possible, resulting in the formation of coke or carbon monoxide. The main problem with the reformation process is that a temperature of the order of 1000°C is required, so some of the fuel is burnt in the reformer to achieve this temperature. The steam required for the reaction is condensed from the exhaust, compressed to approximately 800 psi, and then super-heated to near 1000°C. No details concerning thermal efficiency were given.

However, workers at the Jet Propulsion Lab[60] have also developed an on-board hydrogen generator operating on a similar principle. Although engine efficiencies were found to increase by as much as ten percent, overal system efficiencies decreased by ten percent, resulting in a net loss in fuel economy. In this study, a problem of coking the steam reformer was reported. This could only be avoided by the use of a catalyst, which was then found to be subject to poisoning. More recent studies[61] concluded "There appear to be no significant incentives therefore to go to onboard hydrogen generation with gasoline", although it was also mentioned that the picture for methanol is much more favourable.

2.4 HYDROGEN AS A FUEL FOR INTERNAL COMBUSTION ENGINES

Hydrogen has been used as an engine fuel for more than one hundred years, although the first investigation of its effect on the performance of an engine was carried out by Ricardo in 1924[62]. He reported a problem of pre-ignition accompanied by violent firing back into the carburettor, which has proved to be a feature of all engines run on pure hydrogen.

2.4.1 Engine Back-Fire

Engine back-firing, or carburettor flash-back, refers to an extreme condition, in which ignition may take place in the intake system, or in the combustion chamber before the intake valve has closed, resulting in a "firing back" through the intake system. This can result in damage to the fuel/air mixing device, and may also

interrupt or stop engine operation. King et al[63] concluded that this "self-ignition" was due to glowing particles of carbon present in the residual charge. The source of these finely divided carbon nuclei was attributed to pyrolysis of the lubricating oil. They reported being able to eliminate the problem by maintaining all surfaces (cylinder wall, piston face, etc) scrupulously clean. It was later reported[64] that preignition is caused by the presence of any hot spot, including the ceramic core of the spark plug, the exhaust valve, and pyrolysis of the lubricating oil vapour. Other workers[65] have also found hot spots to be a major contributory factor to hydrogen back-firing. The use of cool spark-plugs, and sodium cooled exhaust valves reduced the frequency of intake flash-back[64].

Another mechanism for causing intake flash-back was suggested by Billings et al[66] and is also mentioned by Lynch[67]. The mechanism is preignition caused by an induced voltage in a plug adjacent to the plug which is firing. Thus the intense current pulses from one spark lead were inducing a high enough voltage in an adjacent lead to cause an energy pulse across the plug. Since the ignition energy of hydrogen (1.9×10^{-5} J) is much less than that of petrol (28×10^{-5}J), this induced pulse can be detrimental when operating an engine on hydrogen, and yet is of little significance when operating the same engine on petrol. Separation of the ignition cables from one another was found to decrease the magnitude and frequency of induced sparks[66], and was also found to reduce the frequency of intake flash-back in the present investigation. The use of smaller plug gaps also meant less energy

was required to produce a spark, thus reducing the intensity of any induced voltage.

Watson[68] suggests that intake back-firing (induction ignition) may be caused by residual gas ignition when pre-mixed hydrogen-air is supplied to an engine. To overcome this problem, a specially modified intake valve was used[68][69] to allow air only into the cylinder in the initial charge. This air, by mixing with the unscavenged residual gas reduces the mixture temperature, and thus avoids residual gas ignition of the hydrogen which is admitted somewhat later than the air, as shown schematically in figure 6.

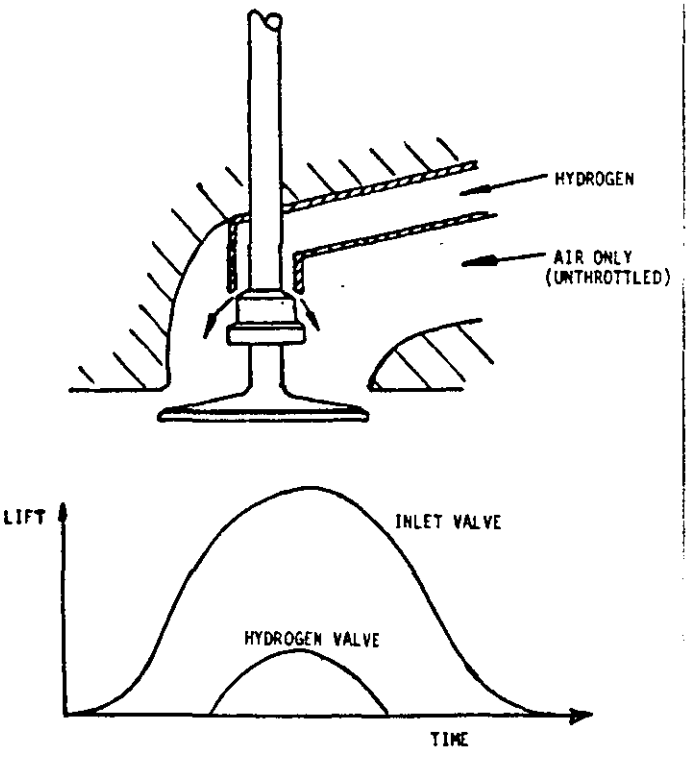

FIGURE 6 - Schematic layout of delayed port admission valve and its timing diagram
(H C Watson, 1979)

This design of intake valve was also suggested by Swain and Adt[70]. However, Watson[66] reports that although this system prevented back-firing with a single-cylinder engine, it still proved to be a re-current problem with a multi-cylinder engine. This was attributed to the presence of lubricating oil in the cylinder, despite applying the best available oil control methods. A point which is not mentioned however is that the minimum ignition temperature of hydrogen/air mixtures is 572°C, whereas that of petrol/air mixtures is ≈ 220°C. Since the combustion temperatures, and hence residual gas temperatures, are similar, if back-firing is caused by residual gas ignition, this should be far more prevalent with engines operating on petrol than on hydrogen. Thus, hot residual gases do not appear to be the fundamental cause of intake flash-back.

Recent studies at Loughborough[65] indicate that although hot-spots and pyrolysis of oil do contribute to the back-fire problem, they are not the fundamental cause. A back-fire cascade effect has been identified where combustion cycles preceding the back-fire cycle progressively diminish in peak pressure. The final cycle before back-fire shows evidence of late burning and a low flame speed, although a lingering flame was not detected in the cycle after the exhaust valve closed, and before the inlet valve opened. The cascade effect suggests some residual property inhibits the next combustion cycle. To create the cascade effect a chemical species is required which would inhibit the bulk hydrogen reaction and, in the process, increase its concentration to further hinder the next cycle. Both NO and HO_2 radicals are known to interrupt the combustion sequence of hydrogen burning in air.

Back-firing can be prevented by injecting the fuel directly into the cylinder[65, 71, 72], although normally rough running and pre-ignition result. Presumably this abnormal combustion includes the back-fire mechanism although the aggressive characteristics are moderated by occurring only in the cylinder. Direct cylinder injection is limited in practical applications due to the possibility of incomplete fuel-air charge mixing in the cylinder resulting in incomplete combustion, which can be responsible for poor thermal efficiency and high nitric oxide emissions[72].

There are two methods generally used at present to suppress intake flash-back. Finegold et al[73] employed exhaust gas recirculation (EGR), recycling up to twenty-five percent of the exhaust, after substantial cooling. This serves as a "thermal diluent", reducing peak combustion temperatures (and consequently NO_x formation) and also lowers the temperature of potential hot spot ignition sources. Nitric oxide concentrations were cut approximately in half, although the maximum power output was also reduced in proportion to the percentage EGR used.

The second method of reducing flash-back is to inject a spray of water vapour into the combustion chamber. This again has the effect of reducing peak combustion temperatures, thus lowering the temperature of hot spots, and reducing nitric oxide concentrations. Such a method has been investigated by several groups[74,75], although a decrease in thermal efficiency is also observed.

Hence, it appears far more basic research on the nature of the ignition of hydrogen is required to identify the back-fire problem rigorously, and, thus, to suggest the ultimate solution.

2.4.2 Performance and Emissions Using Hydrogen

There are two basic methods of operation using hydrogen as an engine fuel. In the first, hydrogen and air can be mixed in the stoichiometric ratio, and power output can be controlled by throttling the intake - ie, varying the flow rate of the total mix whilst keeping it at the stoichiometric condition. However, if this system is used, the power output, when compared to petrol operation, is considerably reduced. The reason being that at stoichiometric mixtures, hydrogen occupies 29.6% of the total fuel/air volume, resulting in a much smaller air-flow into the engine. Petrol only occupies approximately 2% of the fuel/air mixture.

However, since hydrogen has such wide flammability limits (4% to 75% by volume in air)[3], an engine can be operated throughout its load range using a wide open throttle, thus controlling the fuel-air ratio directly. This is termed "quality-governing", and has the advantage of reducing the losses associated with throttling. It also permits operation at the lowest equivalence ratio for a given power output, resulting in lower combustion temperatures, leading in turn to higher thermal efficiencies. Details of this principle are discussed in chapter nine. Several studies have reported this improvement in thermal efficiency. Lucas and Morris[65] found a maximum brake thermal efficiency of 24% using a single cylinder CFR engine

running on hydrogen at 1800 rpm, compared to only 15% with petrol operation. However, the improvement in thermal efficiency is particularly apparent at part-load due to unthrottled operation, and such results are reported by Swain et al[76], with brake thermal efficiencies 90% higher at 35 kPa (5 psi) BMEP at 1800 rpm.

A hydrogen engine is capable of higher reaction temperature (and energy for a given mass of air) and higher flame speeds. Thus, under similar operating conditions a hydrogen engine would be expected to produce more NO_x emissions. This was found to be the case in studies at Loughborough[65], where peak emissions with petrol were 3600 ppm, and with hydrogen were 5550 ppm, both at full throttle at 1800 rpm.

However, as mentioned earlier, both exhaust gas recirculation and water injection reduce combustion temperatures, and hence also reduce nitric oxide formation. Also if a hydrogen engine is being operated using a wide open throttle at all times, combustion temperatures will again be reduced, thus reducing nitric oxide emissions. Finegold and Van Vorst[77] found the total oxides of nitrogen had a maximum value of 420 ppm when an engine was operated using petrol, 30 ppm when the engine was operated on a stoichiometric mixture of hydrogen with water injection, and 10 ppm when the engine was operated on hydrogen with a fully open throttle (with no water injection or EGR).

2.4.3 Dual-Fuel Operation

In order to avoid both the problems of on-board storage of hydrogen, and that of intake flash-back, several workers are now looking at a dual-fuel mixture of hydrogen and petrol[78,79,80,81,82,83,84].

As several different techniques are used, each is discussed individually.

Workers in the USSR reported modifying a car to use a fuel containing five percent by weight of hydrogen[81]. The hydrogen was stored on-board the vehicle in a 180 kg container of iron-titanium hydride, capable of storing up to 1.5 kg of hydrogen. No details are given, however, of actual engine operating conditions, or whether power output is controlled by quality governing of the fuel-air mixture. Exhaust emissions were reduced to levels below legislated values, and petrol consumption was reduced by up to thirty percent.

A later report[80] indicates increases in thermal efficiency of up to one hundred percent at low loads by the use of partial throttling at light loads. This was found to prevent poor combustion, which occurred at equivalence ratios below $\phi \simeq 0.3$. In the present study, audible misfires were found to occur at equivalence ratios below $\phi \simeq 0.4$ when petrol/hydrogen mixtures were used, and partial throttling was again used to prevent this. It is possible that greater combustion chamber turbulence may permit engine operation at weaker mixture strengths.

Work carried out at General Motors in 1974 utilised the idea of hydrogen-supplemented fuel, but mainly in an effort to reduce exhaust emissions[82]. Petrol only was used at mixture strenghs greater than $\phi \simeq 0.8$, and hydrogen was added at weaker mixture strengths. Both hydrocarbon and carbon monoxide emissions were reduced with such operation, but nitrogen oxides were found to have a similar

concentration at comparable mixture strengths. A special carburettor was also developed to maintain a nearly constant hydrogen fraction and stoichiometry for all operating conditions. This gave lower nitrogen oxide emissions, but other workers[80] found such operation greatly reduced power output.

The investigation by Varde[84] was primarily aimed at reducing the fuel consumption of stationary engines, and he found thermal efficiency increased and the lean limit of operation was extended with an increasing hydrogen fraction of the fuel. He also found that flame speed increased by more than ten percent when a hydrogen flow of 10 l/min was added to a slightly weak petrol mixture. However, at very lean operating conditions the flame speed decreased.

It must also be mentioned that other workers[85] are also developing vehicles to run on dual-fuel hydrogen petrol mixtures, although no results have been reported to-date.

CHAPTER 3

THE USE OF SALINE HYDRIDES AS HYDROGEN STORAGE MEDIA

CHAPTER 3

3.1 The saline hydrides are those which have an ionic structure, and include the hydrides of the alkali metals. Metal hydrides evolve any absorbed hydrogen upon thermal decomposition. Saline hydrides however, evolve hydrogen upon their reaction with water. They were first suggested as hydrogen storage media for automotive use by Chatterjee and Som[86], with particular regard to sodium hydride because of its high abundance at low cost. More recently, hydrogen generators operating on this principle have been patented[87]. The reaction occurring when a saline hydride makes contact with water is as follows:-

$$2\,MH + 2H_2O \rightarrow 2MOH + H_2 \qquad \ldots (1)$$

where M = Li,Na,K,Rb or Cs. The alkali metal can be recovered by electrolysis at 310°C, according to the reaction:

$$4NaOH_{(l)} \rightarrow 4Na_{(l)} + O_{2(g)} + 2H_2O \qquad \ldots (2)$$

This involves the use of a β-Al_2O_3 (β-alumina) tube as a diaphragm. Without the use of a diaphragm, there is a high degree of back reaction between anode and cathode products that occurs when NaOH is electrolysed in a non-diaphragmed cell. By using a β-Al_2O_3 tube, molten sodium ends up within the tube since β-Al_2O_3 is a sodium ion (Na^+) conductor. There is no direct contact between the water and sodium produced, thereby eliminating the secondary reaction

$$2Na + 2H_2O \rightarrow 2NaOH + H_2 \qquad \ldots (3)$$

The sodium produced by electrolysis would then require further hydrogen to form the metal hydride again. Chatterjee and Som[86] suggest that electrolysis of the fused sodium hydroxide will produce sodium and hydrogen according to the half cell reaction

$$2NaOH \rightarrow 2Na^{+} + 2H^{+} + O_2 \qquad \ldots (4)$$

However, this reaction cannot occur since any sodium formed will react immediately with the water also produced, as shown in reaction (3).

The initial investigation of the reaction of sodium hydride (and lithium hydride) with water was somewhat cautious, as a large amount of water suddenly released on to a metal hydride can cause a vigorous, and sometimes violent, reaction. This was determined to be due to the initial heat of reaction igniting the hydrogen produced. However, when an inert atmosphere (argon or nitrogen) was maintained above the hydride, no problems were encountered. Both pure sodium hydride and lithium hydride were used, and both proved satisfactory. However, when a 50% oil dispersion of sodium hydride was used, the reaction was too slow to produce a continuous stream of hydrogen.

The apparatus used is illustrated in figure 3.1. A fine spray of water was fed into the brass tube via a fine hypodermic tube. By controlling the pressure above the water in the boiling tube, the flow rate of water to the hydride could be controlled. This is illustrated in figure 3.2. Thus, the flow rate of water, and hence the production rate of hydrogen, could be easily controlled.

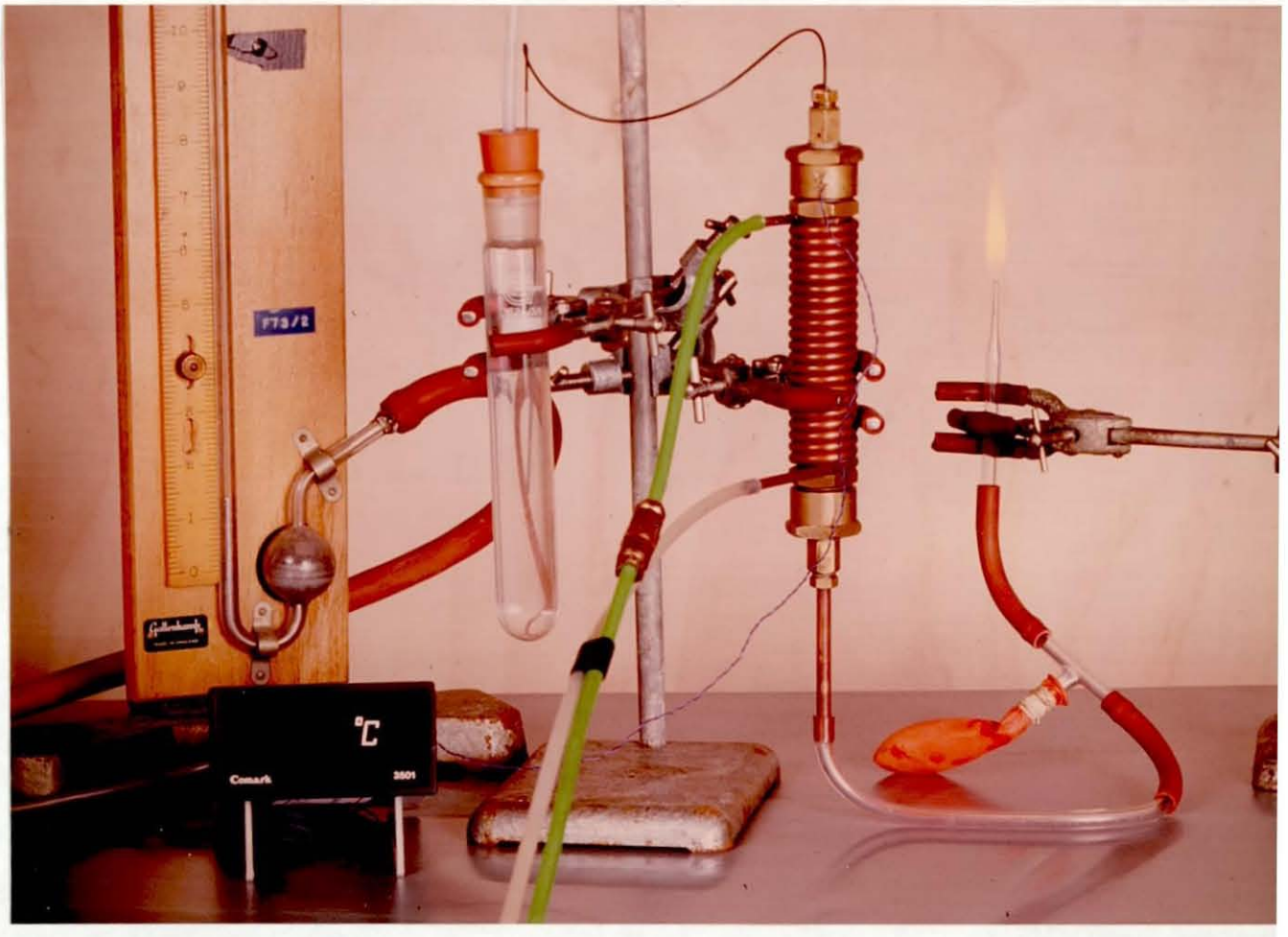

FIGURE 3.1 - Hydrogen Production Using Saline Hydrides

Figure 3.2

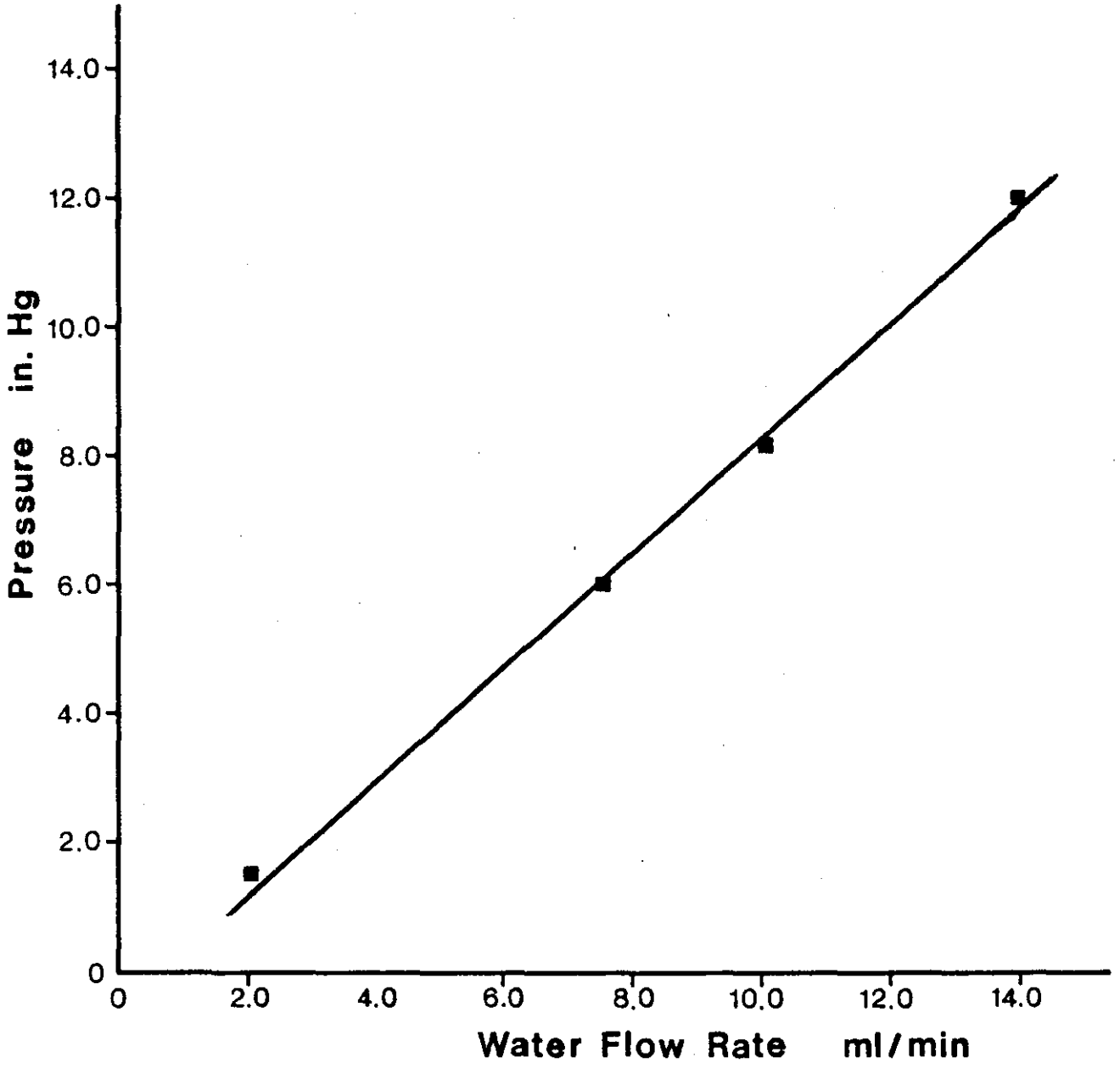

Relationship Between Pump Pressure and Water Flow Rate

The major problem encountered with this method of hydrogen production was one of the produced sodium hydroxide forming a solid cake if the reaction was stopped for more than short periods. This was also reported by Taschek[87]. This meant that large amounts of sodium hydride could remain unreacted if the reaction had been stopped before completion, as would be the case in normal driving cycles. The hard layer so formed prevented the reaction continuing further by creating an impermeable barrier to prevent water reaching the saline hydride.

This problem could be overcome by suitable design considerations. However, since the only means of reprocessing the hydroxide (formed by the reaction) is by electrolysis, the use of saline hydrides as hydrogen storage media was ruled out as being too expensive for automotive use. Working on the equivalent of one gallon of petrol (3.352 kg), 1267g of hydrogen are required to produce the same amount of energy. Calculations show that 15.204 kg of sodium hydride are required to produce 1.267 kg of hydrogen by reaction (1) and this amount of hydride can be produced by 25.34 kg of sodium hydroxide from reaction (2). The electrical energy required to electrolyze this amount of sodium hydroxide is 207.8×10^3 kJ, although another 5.3×10^3 kJ are required for fusion of the hydroxide. Thus a total energy of 213.1×10^3 kJ (98 kWh assuming electrolysis efficiencies of 60%) is required for electrolysis to produce enough sodium hydride to give the equivalent of one imperial gallon of petrol.

CHAPTER 4

DEVELOPMENT OF MATHEMATICAL MODEL OF HYDROGEN STORAGE SYSTEMS

CHAPTER 4

4.1 RATE OF HYDROGEN EVOLUTION

The study of hydriding and dehydriding kinetics in metallic alloys is an example of simultaneous heat and mass transfer with reaction occurring, although in this instance certain properties (eg - the thermal conductivity) also change. Once the hydride-bed has reached thermal equilibrium, any one of a number of factors may be rate-limiting; such as the intrinsic rate of the hydriding/dehydriding reaction, or the diffusion of hydrogen out of the hydride particle, depending on the particular metallic alloy involved. Also, for a given alloy, the rate limiting process for hydriding may not be the same as that for dehydriding. Van Vucht et al[36] found the hydriding of samarium cobalt, $SmCo_5$, was rate limited by the diffusion of hydrogen into the bulk of the alloy (rather than the rate of surface reaction), whereas Raichlen and Doremus[45] found the rate of desorption of hydrogen followed the rate of transformation of the hydride $SmCo_5H_{2.6}$ to the alloy $SmCo_5$.

However, for practical applications, where a hydride bed is used as a hydrogen storage medium (eg - for automotive use), it is most unlikely that the bed will even attain thermal equilibrium. Thus, the primary factor limiting hydrogen release in these cases is the rate of heat transfer to the reaction zone[51][52]. In this investigation, the hydride bed design studied was of the type shown in figure 4.1, produced by M.P.D. Technology Ltd. The aim of the study was to predict the hydrogen release or absorption rate from any metal hydride using a

FIGURE 4.1

Hydride Containment Capsule

manufactured by M.P.D. Technology Ltd

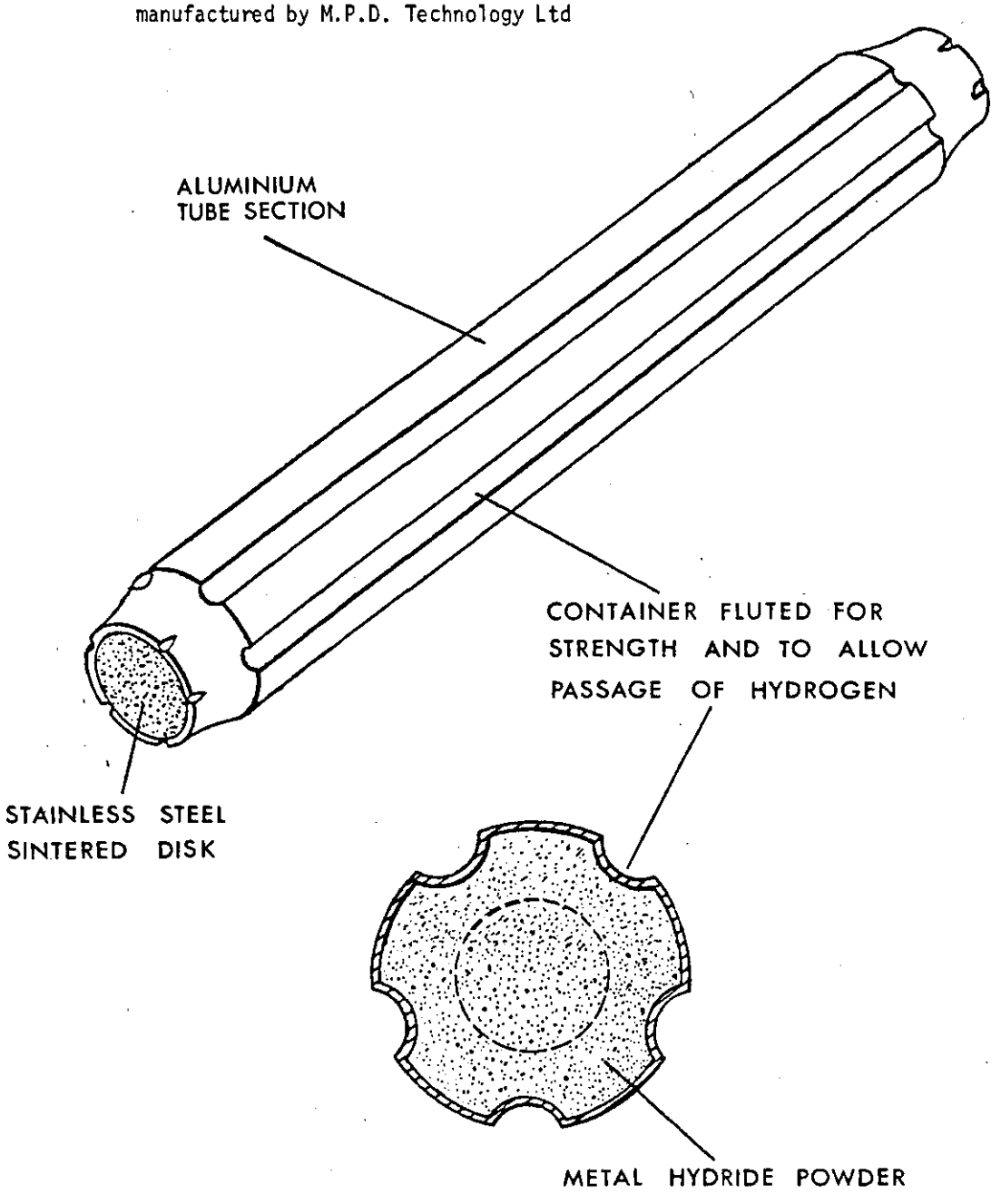

hydrogen storage system of this design.

4.2 HEAT TRANSFER TO REACTION ZONE

For a cylindrical system, such as that shown in figure 4.1, heat is conducted radially. Thus the general conduction equation (with no internal heat generation) is given by

$$\frac{\partial T}{\partial t} = \alpha \left(\frac{\partial^2 T}{\partial r^2} + \frac{1}{r}\frac{\partial T}{\partial r} + \frac{1}{r^2}\frac{\partial^2 T}{\partial \theta^2} + \frac{\partial^2 T}{\partial Z^2}\right) \qquad \ldots (1)$$

where α is the thermal diffusivity (the thermal conductivity divided by the thermal capacity). If the cylinder is assumed to be infinitely long, and that axial symmetry exists, then the heat conduction can be considered to be in a radial direction only. The cylinder can be assumed to be infinitely long provided the heat transfer through the ends of the containment vessels is negligible compared with that in a radial direction. As the cylinders have insulating caps at one end, and a gas space (for hydrogen removal) at the opposite end, this assumption is valid. The heat conduction equation above then reduces to

$$\frac{\partial T}{\partial t} = \alpha \left(\frac{\partial^2 T}{\partial r^2} + \frac{1}{r}\frac{\partial T}{\partial r}\right) \qquad \ldots (2)$$

Seeking a solution of the separable form, ie, $T = R(r).\tau(t)$ where $R(r)$ and $\tau(t)$ are functions only of the indicated variable, then equation (2) becomes

$$\frac{1}{\alpha\tau}\frac{d\tau}{dt} = \frac{1}{R}\left(\frac{d^2R}{dr^2} + \frac{1}{r}\frac{dR}{dr}\right) = -\lambda^2 \qquad \ldots (3)$$

λ^2 is used to represent the separation constant created because each portion of the equation is a function of one of the variables. The separation constant is taken to be negative to obtain a negative exponential solution in t.

The two resulting ordinary differential equations, and their solutions, are

$$\frac{d\tau}{dt} + \lambda^2\alpha\tau = 0 \qquad \tau = B_1 e^{-\lambda^2\alpha t}$$

$$\frac{d^2R}{dr^2} + \frac{1}{r}\frac{dR}{dr} + \lambda^2 R = 0 \qquad R = B_2 Jo(\lambda r) + B_3 Y_o(\lambda r) \qquad \ldots (4)$$

Since the cylinder is solid, and since no undefined solution can occur at r = 0 (the temperature at the centre of the cylinder cannot be infinite), B_3 must be zero, because Y_o is undefined for a zero argument. Thus

$$T = B\, e^{-\lambda^2\alpha t}\, Jo(\lambda r) \qquad \ldots (5)$$

The constants B and λ can then be determined by the initial and boundary conditions.

For the purpose of this model, it is assumed that the hydride vessel is initially at a constant temperature distribution (ambient, T_i) and that its outer surface is suddenly placed in contact with a convecting fluid of constant temperature. The temperature distribution inside the container is given by the solution of the partial differential equation (2). If the temperature at any point inside the cylinder is T', and the temperature of the convecting fluid is T_f, then a temperature difference variable can be defined as $T = T_f - T'$. The boundary conditions are:

$$\text{For } t = 0: \quad T' = T_i \quad \text{or} \quad T = T_f - T_i \qquad \ldots (6)$$

$$\text{For } t \geq 0: \quad \text{at } r = R, \ \frac{\partial T}{\partial r} = -\frac{h}{k}(T_f - T') \quad \text{or} \quad \frac{\partial T}{\partial r} = -\frac{h}{k}T$$

where h is the thermal film coefficient. The second condition of equation (6) leads to

$$Be^{-\lambda^2 \alpha t}[-\lambda J_1(\lambda r)]_{r=R} = -\frac{h}{k}[Be^{-\lambda^2 \alpha t} Jo(\lambda r)]_{r=R}$$

since $$\frac{\partial}{\partial r}[Jo(\lambda r)] = -\lambda J_1(\lambda r)$$

This gives the following defining relation for the λ_n's:

$$\lambda_n R \frac{J_1(\lambda_n R)}{Jo(\lambda_n R)} = \frac{hR}{k} \qquad \ldots (7)$$

Defining the Biot modulus for the cylinder to be $N_{BI} = \frac{hR}{k}$ one finds the λ_n's are the roots of $\lambda_n R \frac{J_1(\lambda_n R)}{Jo(\lambda_n R)} - N_{BI} = 0$.

Then the solution of equation (2) is

$$T = \sum_{n=1}^{\infty} B_n e^{-\lambda^2 n \alpha t} Jo(\lambda_n r) \qquad \ldots (8)$$

Upon application of condition (1) of equation (6)

$$T_f - T_i = \sum_{n=1}^{\infty} B_n Jo(\lambda_n r) \qquad \ldots (9)$$

the B_n's are

$$B_n = \frac{2}{R^2} \frac{(T_f - T_i) \int_o^R r\, Jo(\lambda_n r) dr}{Jo^2(\lambda_n R) + J_1^2(\lambda_n R)} \qquad \ldots (10)$$

Thus the final solution is

$$T = \frac{2(T_f - T_i)}{R^2} \sum_{n=1}^{\infty} e^{-\lambda_n^2 \alpha t} \frac{Jo(\lambda_n R)}{Jo^2(\lambda_n R) + J_1^2(\lambda_n R)} \int_o^R r Jo(\lambda_n r) dr \qquad \ldots (11)$$

which reduces to

$$T = 2(T_f - T_i) \sum_{n=1}^{\infty} \frac{1}{\lambda_n R} e^{-\lambda_n^2 \alpha t} \frac{Jo(\lambda_n r) J_1(\lambda_n R)}{Jo^2(\lambda_n R) + J_1^2(\lambda_n R)} \qquad \ldots (12)$$

since $\int r Jo(\lambda_n r) dr = \frac{r}{\lambda_n} J_1(\lambda_n r)$

A model of the hydride bed was manufactured (figure 4.2) which consisted of an outer copper tube, with an inner aluminium shell, both of commercial purity. The tube was filled with magnesium powder (99.5% pure) and a thermocouple inserted at the centre of the vessel as shown. The vessel was then totally immersed in hot water, and the temperature at the centre of the tube recorded every five seconds. From this temperature record, shown in figure 4.3, the value of the Biot modulus was determined to be 11, using standard heat transfer tables. The first four λ_n values were evaluated using equation (7), and a mathematical model, based on the solution of equation (12), was made to determine the heat transfer for the system. The outer radius of the copper container, shown schematically in figure4.4 is set at 0.01425 m, and is 1.0 mm thick, corresponding to the actual container dimensions. However, these values were altered when comparison was made with other workers[88][89] in measuring hydriding rates. The aluminium vessel is assumed to fit tightly into the copper tube, and is assumed to be 0.5 mm thick. Thus, the following radii are obtained: R_c = 0.01425 m; R_t = 0.01325 m; and R_h = 0.01275 m. An overall value for α (the thermal diffusivity) for the metal container is 1.045×10^{-4} m^2/sec. Using this value in equation (12), and values of λ obtained from the solution of equation (7), it can be seen (figure 4.5) that approximately one minute is required for the inner surface of the hydride container to come to thermal equilibrium with the surrounding fluid.

Due to the large difference in thermal conductivity between a metal hydride and the metal powder, the reaction front is a narrow

FIGURE 4.2 - Model of Hydride Container

Figure 4.3 **Temperature Variation at Centre of Vessel**

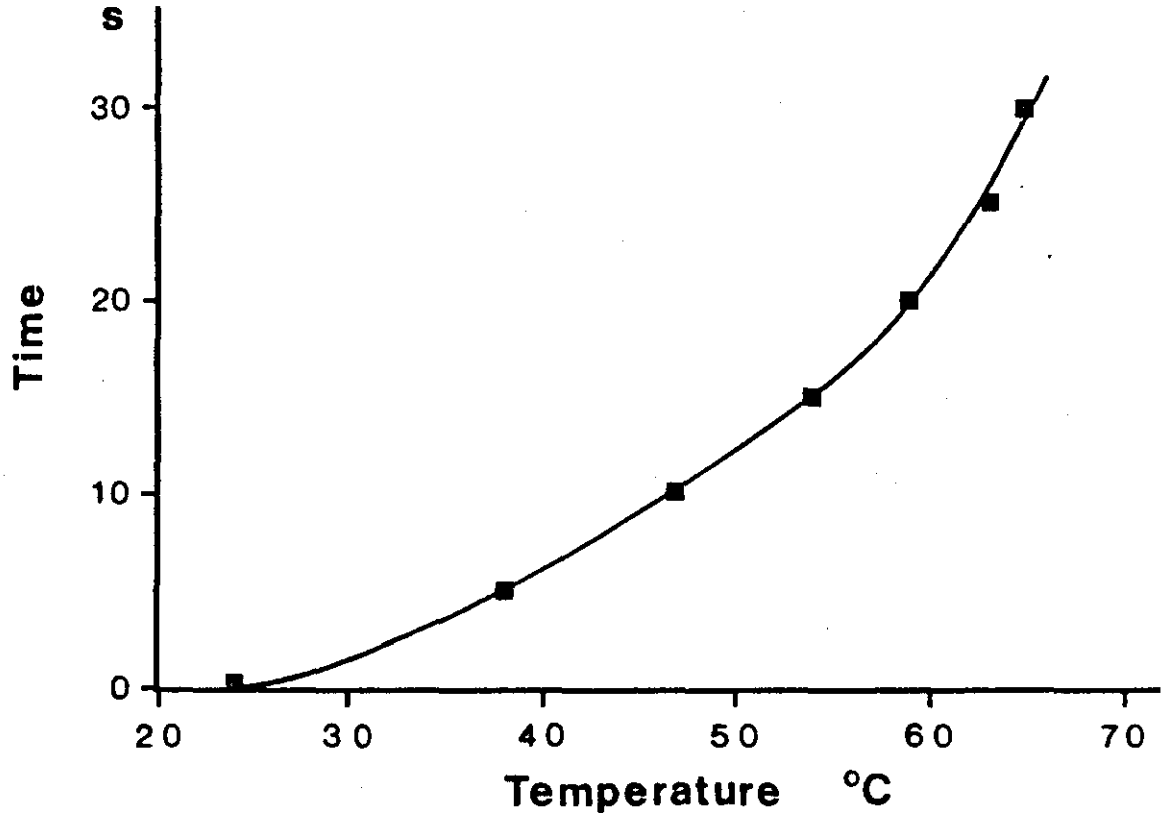

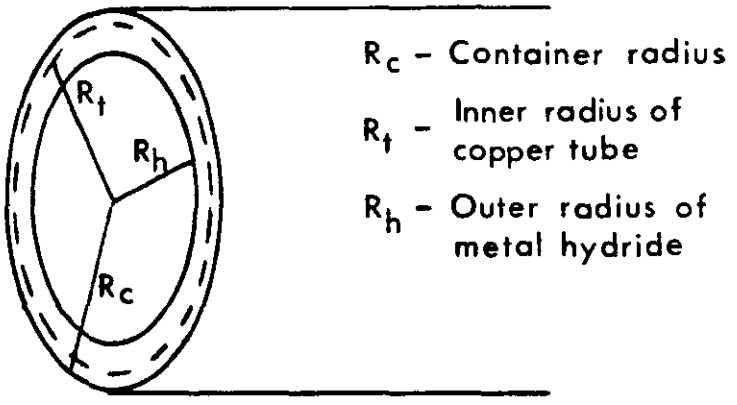

FIGURE 4.4 - Schematic Diagram of Hydride Container

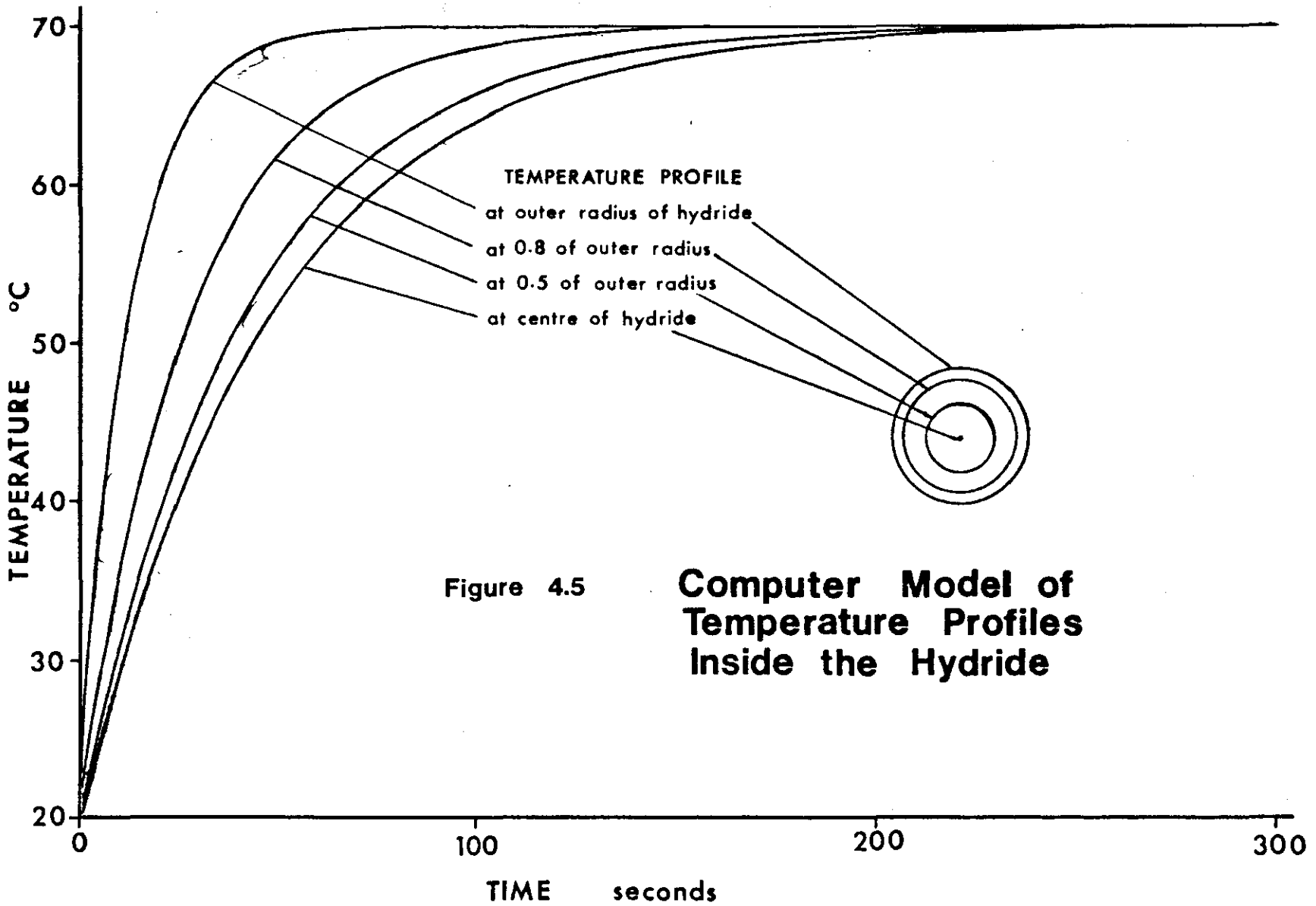

Figure 4.5 **Computer Model of Temperature Profiles Inside the Hydride**

band passing radially through the hydride bed, and for a given alloy the rate of heat transfer is dependent on the temperature difference between the external fluid and the metal alloy, or hydride, inside the bed. For hydriding, the incoming hydrogen reacts with the metal alloy, generating heat, until the temperature inside the bed reaches the equilibrium temperature correspondending to the charging pressure. In practice, this occurs in a matter of seconds, after which internal heat generation ceases. The hydriding reaction then proceeds radially inwards at a rate dependent on the difference between this internal hydride temperatue and the temperature of the external cooling fluid. For the purpose of the model, the time at which the hydriding reaction begins is assumed to be after the bed has reached thermal equilibrium, i.e. the initial heat generation is neglected. Hence there is no internal heat generation term in equations (1) and (2)

For dehydriding, the ambient temperature of the hydride bed is cooler than the temperature of the surrounding fluid, although the rate of heat transfer will again depend on the difference in temperature between the internal temperature of the bed, and that of the external fluid.

In both cases the reaction proceeds radially inwards from the outside of the bed to the centre. Due to the difference in thermal diffusivities between the hydride and the metal alloy, there is a large temperature change across the reaction zone, with effectively the coolant temperature on one size of the zone and the internal temperature of the bed on the other. Thus, for hydriding, the

reaction proceeds radially inwards as heat is rejected to the cooling water, through the hydride layer building up inside the tube. Hence the thermal diffusivity of the hydride powder formed is important. In dehydriding, the reverse is true. In this case, heat is taken from the surrounding fluid, and is conducted through a growing layer of metal powder to the reaction front, and it is the thermal diffusivity of the metal powder which is important. The model developed uses the appropriate value of thermal diffusivity combining the value of the container with the appropriate value for that of the metal or hydride.

Using these data for α and λ_n, a temperature profile vs time was developed in accordance with equation (12). For dehydriding, this depended on the ambient temperature inside the hydride bed, and on the temperature of the heating fluid. For hydriding, the temperature profile depended on the temperature corresponding to the equilibrium hydrogen pressure, and on the temperature of the coolant water. These temperature profiles at various radii inside the bed are shown for dehydriding in figure 4.5, and from these the rate of heat transfer was determined. The time taken to reach a given temperature at known radii gives the heat transfer rate in terms of area reacted per unit time.

4.3 REACTION KINETICS

The work of Nomura et al[49], discussed in Chapter two indicates the rate equation for hydriding is given by

$$\frac{dn}{dt} = k' (P - Peq)/t \qquad \ldots (13)$$

where $k' = 3.2 \times 10^{-2}$ $(kgf/cm^2)^{-1}$, P is the pressure at time t, and Peq is the equilibrium pressure. The equilibrium pressure can be calculated from the Van't Hoff equation:

$$Peq = \exp(TCON/TABS + ENCON) \qquad \ldots (14)$$

where TABS is the absolute temperature of the hydride bed, TCON is a constant depending on the enthalpy change of the hydriding reaction, and ENCON is a constant related to the entropy change. These are tabulated for various hydrides in table 4.1. This equilibrium pressure (in atmospheres), after conversion to kg/cm^2, can then be used in equation (13) to obtain a value for the rate of reaction, taking into account both the reaction kinetics and the rate of diffusion.

By including rate information for diffusion and reaction kinetics with that of heat transfer, an overall rate of reaction can be obtained in terms of the cross-sectional area reacted per unit time. By knowing the length, and total number of hydrogen storage tubes in the containment vessel, the total amount of hydrogen stored can be calculated, and hence the actual rate of hydrogen release can be predicted.

Details of the model, and a listing of the program are included in appendix (vii).

TABLE 4.1 - HYDRIDING REACTION CONSTANTS

	TCON (A)	ENCON (C)
FeTi	-3383	12.76
Mg (6%Ni)	-7736	14.71
$LaNi_5$	-3712	12.96

CHAPTER 5

RESULTS OF MATHEMATICAL MODEL OF HYDROGEN STORAGE SYSTEMS

CHAPTER 5

5.1 INTRODUCTION

In this chapter, the predicted hydriding and dehydriding rates for metal hydride beds are presented for lanthanum pentanickel hydride, and these are compared with the actual results measured by other workers[88][89]. However, the model can also predict hydriding times using different hydrogen pressures and different tube dimensions. Similarly, results can be obtained for different alloys, the thermal properties of which are given in table 5.1.

5.2 DEHYDRIDING - HYDROGEN RELEASE

Figure 5.1 shows the predicted rate of hydrogen release using lanthanum pentanickel hydride, $LaNi_5$-H_x. For the purpose of comparison, the copper tube dimensions have been set at an inside diameter of 2.7 cm, corresponding to the actual dimensions of the hydride bed. The temperature of the heating water was set at $50^{o}C$, corresponding to an equilibrium pressure above the hydride bed of 60 psi (0.41 MPa), and the ambient temperature of the bed set to $20^{o}C$. The value of α (thermal diffusivity) used is $\alpha = 3.73 \times 10^{-5}$ m^2/sec, which is that of the $LaNi_5$ metal hydride, since for dehydriding heat is conducted radially inwards through a growing layer of metal powder to the reaction front. The appropriate constants in the Van't Hoff equation (discussed in the previous chapter) are also included to determine the rate of reaction.

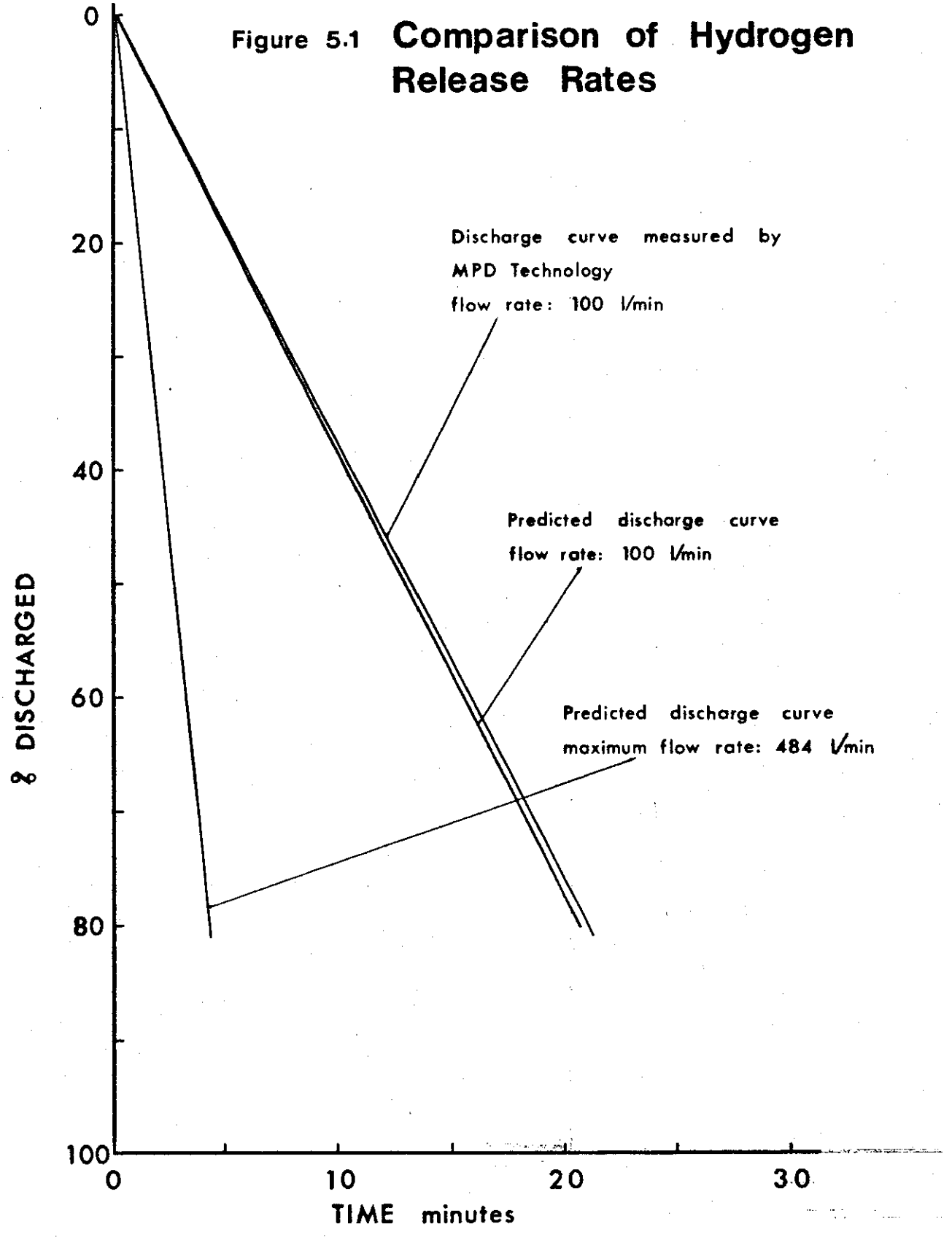
Figure 5.1 Comparison of Hydrogen Release Rates
Discharge curve measured by MPD Technology
flow rate: 100 l/min
Predicted discharge curve
flow rate: 100 l/min
Predicted discharge curve
maximum flow rate: 484 l/min
% DISCHARGED
0
20
40
60
80
100
0
10
20
30
TIME minutes

Two dehydriding curves are illustrated in figure 5.1. One gives a maximum rate of hydrogen release from the bed, assuming no restrictions above the hydride - i.e, the hydrogen is vented into the atmosphere, and the other shows the flow rate of 100 1/min, based on the fact that the maximum discharge rate is a straight line function, so the flow at 100 1/min is simply a constant factor times the predicted maximum flow rate. However, without knowing the partial pressure of hydrogen in the bed with a restricted flow rate, it is not possible to calculate the rate of hydrogen release to correspond to a particular flow rate.

Figure 5.1 also shows the measured rate of hydrogen evolution, as determined by M.P.D. Technology Corp. (88)

Two predicted dehydriding curves are shown in figure 5.1., One gives a maximum rate of hydrogen release from the bed, assuming no restrictions above the hydride - ie. the hydrogen is vented into the atmosphere, and the other gives a restricted flow rate such as might be expected in practical applications.

The hydrogen release rate of 100 l/min is computed from the maximum release rate (484 l/min), which in turn is determined from the total hydrogen capacity of the bed.

Figure 5.1 also shows the measured rate of hydrogen evolution, as determined by M.P.D. Technology Corp.[88]

5.3 HYDRIDING - HYDROGEN ABSORPTION

The results predicted by the computer model for hydrogen absorption are shown in figure 5.2. Again these are for lanthanum pentanickel hydride, $LaNi_5 - H_x$, but for the purpose of comparison, the copper tube dimensions have been set at an internal diameter of 2.0 cm. This corresponds to the tube used by Lynch[89] in the measurements with which these predicted results are compared. Several hydriding curves are presented, each corresponding to a particular hydrogen charging pressure, and hence to a particular equilibrium temperature. In all cases, the temperature of the cooling water is set to $25^{o}C$.

The model can also predict hydriding times using different hydrogen charging pressures and different tube dimensions. Similarly, results can be obtained for different alloys, the thermal properties

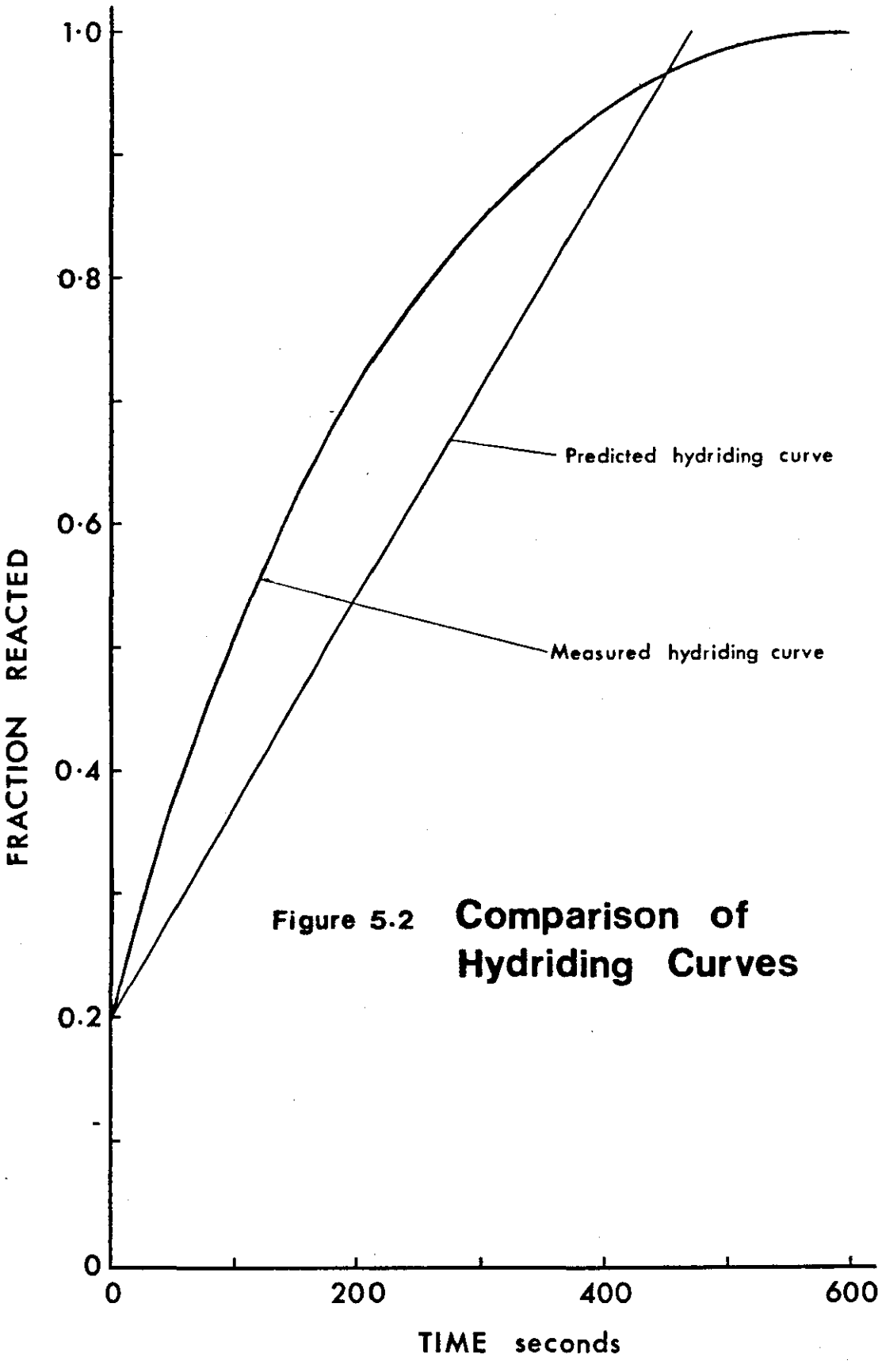

Figure 5.2 Comparison of Hydriding Curves

of which are given in table 5.1. One of the major problems found in this study of modelling hydriding is the lack of published data on thermal conductivities and thermal diffusivities of both the metal alloys and of the hydride powders. The information shown in table 5.1 has been collected from a variety of sources as indicated, or calculated from other information where appropriate, and has not been published collectively. However, if reliable predictions are to be made of the heat transfer in metal hydrides for the purpose of determining rates of hydrogen release, accurate information concerning the thermal properties of the particular hydrides must first be made available. Using the values of thermal diffusivity given in table 5.1, the predicted dehydriding rates of iron-titanium hydride and lanthanum pentanickel hydride are compared in figure 5.3. In both cases, temperature differences and tube dimensions have been chosen to simulate those actually used in a real system. Hence there is a difference between these predicted values and those given in figure 5.1. As can be seen, the predicted hydrogen evolution rate using lanthanum nickel hydride is significantly faster than that using iron-titanium hydride.

Thermal Data of Metal Alloys and Their Hydrides

	Mg*	Mg^*H_x	FeTi	$FeTiH_x$	$LaNi_5$	$LaNi_5H_x$
k_s BTU/(hr-ft-^oF)	99.0	0.8	30.8	0.919	37.8	0.735
J/(m-s-^oK)	171	1.38	53.3	1.59	65.4	1.27
ρ_p lb_m/ft^3	65.4	52.3	236.9	189.5	300.3	240.2
kg/m^3	1048	838.4	3794	3035	4810	3848
C_p BTU/(lb-^oF)	0.242	0.319	0.115	0.152	0.087	0.115
J/(kg-^oK)	1013	1336	480	633	364	481
α ft^2/hr	6.26	4.8×10^{-2}	1.13	3.19×10^{-2}	1.45	2.66×10^{-2}
m^2/sec	1.61×10^{-4}	1.24×10^{-6}	2.92×10^{-5}	8.23×10^{-7}	3.73×10^{-5}	6.86×10^{-7}

TABLE 5.1 - THERMAL PROPERTIES OF METAL HYDRIDES (continued p 89)

* containing 6% nickel by weight

where k_s is the thermal conductivity of the material at $20^{o}C$.

ρ_p is the density of the powder (assuming 40% voids). For the hydride, an expansion factor of 20% is assumed.

C_p is the heat capacity of the powder.

α is the thermal diffusivity, defined by $\alpha = \frac{k}{\rho C_p}$

refs: P D Goodell[90]

D L Cummings and G J Powers[51]

Handbook of Chemistry and Physics[91]

Figure 5.3 **Comparison of Predicted Dehydriding Rates for Different Hydrides**

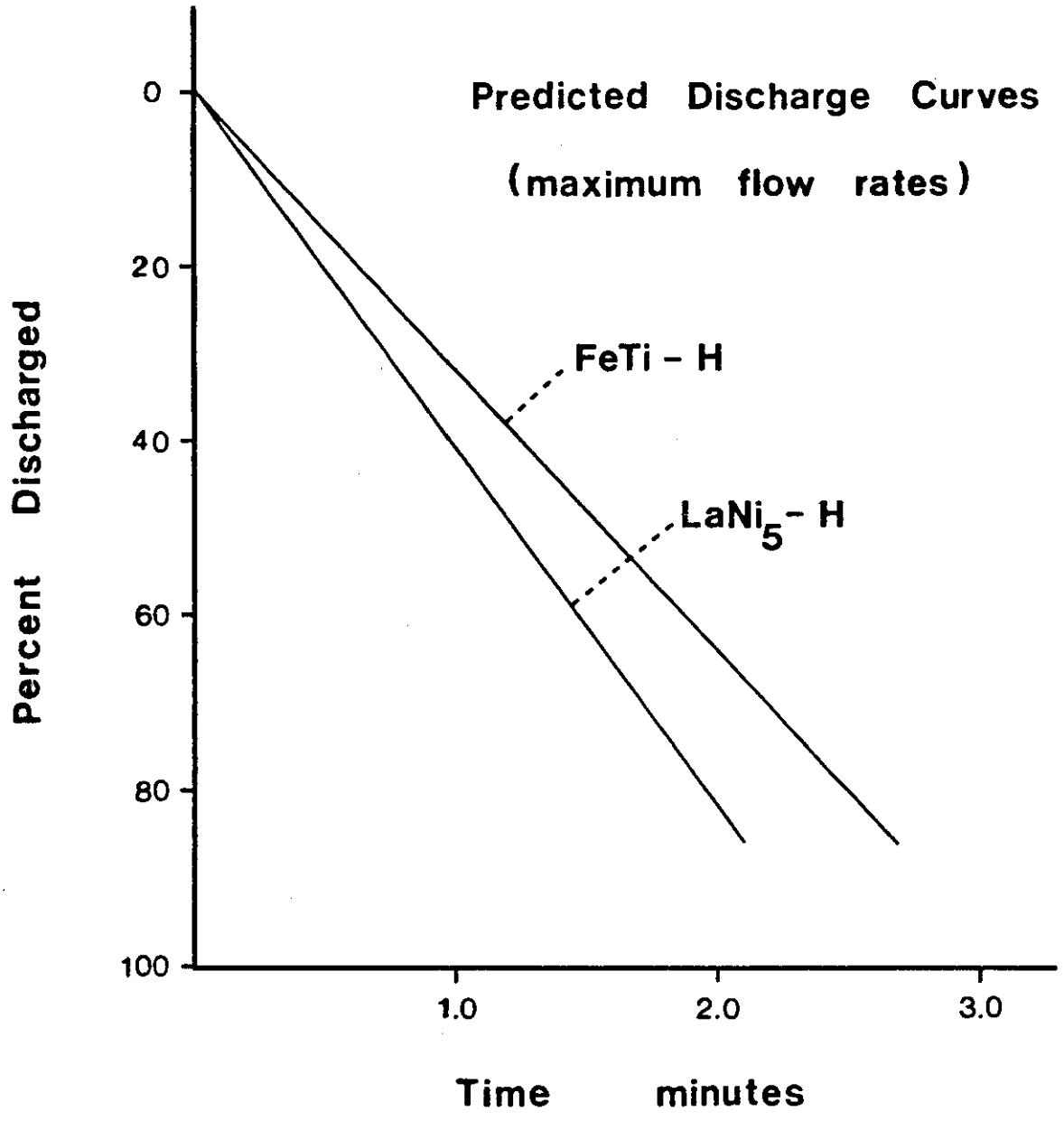

CHAPTER 6

DISCUSSION OF MATHEMATICAL MODEL RESULTS

CHAPTER 6

The rate of heat transfer, which is proportional to hydrogen release, is approximately 0.5×10^{-6} m^2/s (ie - 0.5×10^{-2} cm^2/s) for dehydriding. However, the work of Nomura et al[49] indicates an initial rate of reaction (involving both the instrinsic rate of reaction and the rate of hydrogen diffusion) of 21.3 cm^2/s. Thus for practical storage systems, it is the rate of heat transfer which is the rate-limiting factor, and the fraction reacted is plotted against time in figure 5.1. This gives a maximum rate of hydrogen release from the bed, assuming no restriction above the hydride - ie, the hydrogen is vented into the atmosphere, as well as a restricted flow rate such as might be expected in practical applications.

In figure 5.1 the predicted rate of hydrogen release is compared with that measured by the Ergenics Division of MPD Technology[88]. This indicates a slightly faster predicted rate of hydrogen release than that measured, which could be due to a number of factors. The most likely of these is marginally better heat transfer characteristics in the model illustrated in figure 4.2. However, the hydrogen release rate of 100 litres per minute is computed from the maximum release rate (484 litres per minute), which in turn is determined from the total hydrogen capacity of the bed. If this capacity differs from the 2500 litres quoted, the predicted release rate will also differ. Similarly, any discrepancy in tube dimensions could also be a contributory factor.

The hydriding curve is compared in figure 5.2 with that of Lynch[89]. The difference in shape of these curves with those

measured is possibly due to differences in determining the fraction reacted. In both cases this is done by temperature measurements at given radii throughout the alloy. However, the model predicts the volume fraction reacted. It is not clear if this is the case with Lynch's data. The model does not take into account heat conduction by the hydrogen gas which is relatively insignificant compared to that through the alloy. However, this may be one of the factors influencing the shape of the hydriding curve.

The model can also be used to predict hydriding times using different hydrogen pressures and different tube dimensions. Alternatively, it can be used to predict dehydriding times using different temperatures for the surrounding heating fluid. Similarly results can be obtained for different alloys, the thermal properties of which are given in table 5.1.

Figure 5.3 shows the maximum dehydriding time of both iron-titanium hydride and lanthanum nickel hydride. The rate of hydrogen evolution is significantly faster using lanthanum nickel. This is to be expected since the thermal diffusivity of lanthanum nickel is approximately 28% larger than that of iron-titanium, leading to an increase in the rate of heat transfer.

For dual-fuel operation, the tube dimensions could be much larger (ie - tube diameters of up to 5.0 cm). This would result in a slower heat transfer rate, and a slower rate of hydrogen evolution. However, this would not be a problem as the hydrogen consumption rate is low for dual-fuel operation (approximately 7.0×10^{-5} kg/s). The

advantage of such tube dimensions would be greater hydride/container weight ratios resulting in lighter hydrogen storage units and with larger storage capacities.

One of the major problems found in this study of modelling hydriding and dehydriding processes is the lack of published data on thermal conductivities and thermal diffusivities of both the metal alloys and of the hydride powders. Thus, any predictions of hydrogen absorption or release rates are limited to the alloys whose properties are listed in table 5.1.

CHAPTER 7

EXPERIMENTAL DETAILS

CHAPTER 7

Two engines were used in this investigation. All basic results were obtained with a BL Cars 1275 cc "A series" engine. However, when a vehicle was converted to run on a dual-fuel mixture of hydrogen and petrol, a Ford Transit 2.0 litre O.H.C.engine, identical to that in the vehicle, was also used. The details presented in this chapter concern the BL Cars engine only. Relevant parameters of the Ford Transit engine are presented in Chapter ten.

7.1 THE ENGINE

A BL Cars 1.275 litre "A series" engine was used in this study. This is a four cylinder spark ignition engine with a compression ratio of 8.9:1, details of which are given in table 7.1. No modifications were made to the combustion chamber to enable it to run in a dual-fuel mode. However, the compression ratio was increased to 11.7:1 for some of the results presented in the next chapter. This was achieved by replacing the pistons. The original pistons were dish-shaped (ie - slightly concave), whereas the high-compression pistons were flat, resulting in a smaller combustion volume. Details of combustion chamber dimensions are presented in table 7.2.

The engine was mounted on a test bed and connected to a Heenan and Froude Dynamatic Dynamometer, which was used to load the engine and allow measurement of the power output. A photograph of the engine test rig is shown in figure 7.1.

TABLE 7.1 - DETAILS OF TEST ENGINE

BL Marina 1275 cc Engine

Type	Spark Ignition
Number of Cylinders	4 In-line
Capacity	1275 cc
Bore	70.61 mm
Stroke	81.28 mm
Compression Ratio	8.9:1
Firing Order	1 - 3 - 4 - 2
Ignition Timing (Static)	8^{o} BTDC
Fuel System	SU Carburettor

TABLE 7.2 - COMBUSTION CHAMBER DIMENSIONS

Actual Bore Diameter	7.055 cm
Total Chamber Length	8.202 cm
Clearance Length Above Piston	0.0925 cm
Clearance Volume	3.62 cm^3
Gasket Volume per Cylinder	3.80 cm^3
Head Volume per Cylinder	22.10 cm^3
Total Cylinder Volume	346.52 cm^3
Total Combustion Volume (Compression)	29.52 cm^3
Compression Ratio (High Compression)	346.52/29.52 = 11.7:1
Dish Volume per Piston	10.34 cm^3
Compression Ratio (Standard Compression)	356.86/39.86 = 8.9:1

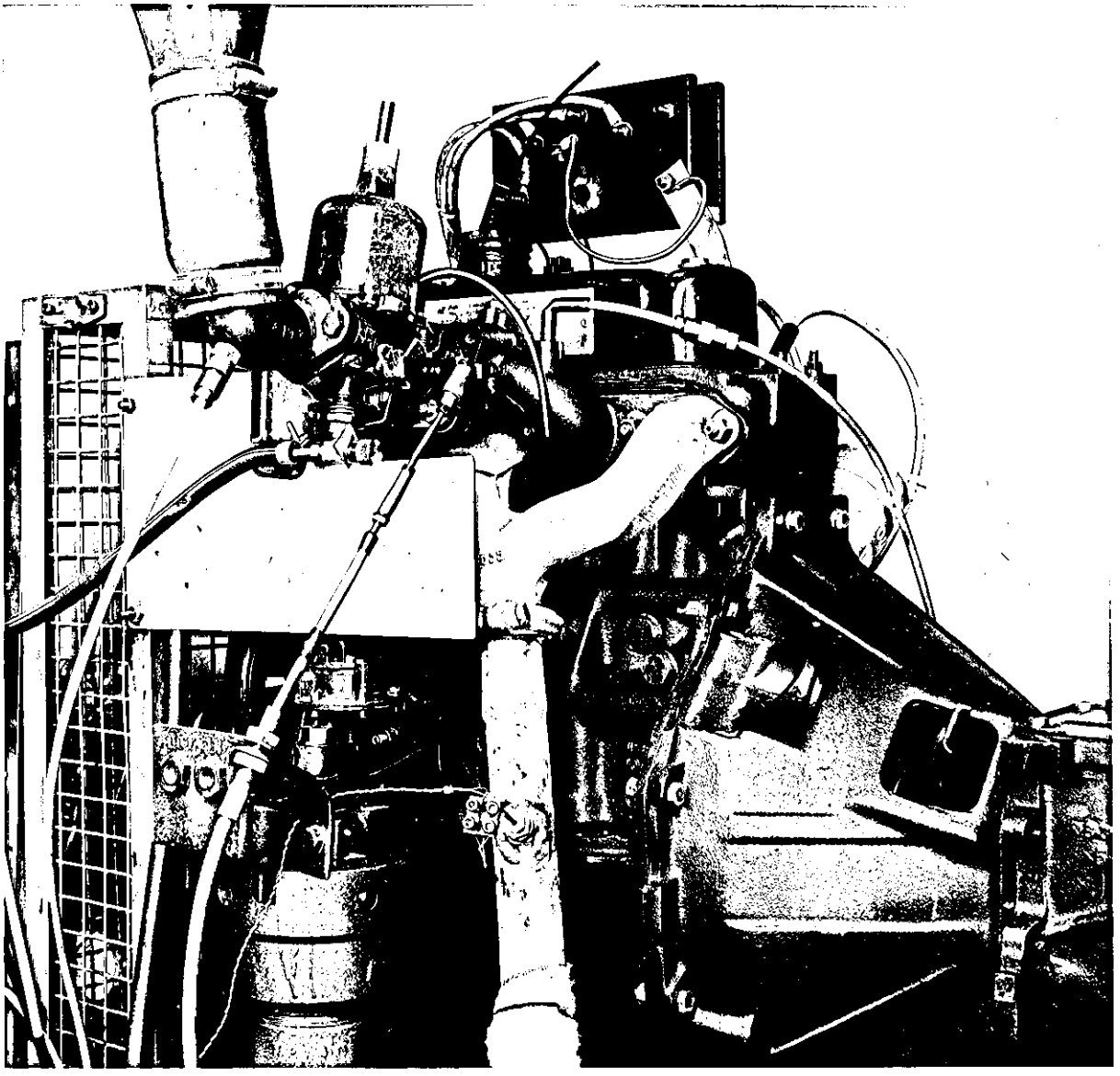

Figure 7.1 Test Engine

7.2 INSTRUMENTATION

The main parameters measured during the work were fuel flow rates of both petrol and hydrogen, and engine load and power output. In addition, exhaust temperature and emissions, air flow rate, coolant flow rate and temperature, inlet manifold depression and ignition timing were also recorded. All the variables (except petrol flow rate and coolant flow rate) were continuously displayed and manually noted during the testing.

The air flow rate was measured using a viscous flowmeter in conjunction with a vertical manometer. An accurate determination of the air flow rate into the engine was required to calculate both the volumetric efficiency of the engine, and the equivalence ratio. Details of viscous flowmeter construction are given by Greene and Lucas[92]. The meter had previously been calibrated against a standard nozzle, the results giving a linear relationship between air flow and the pressure drop across the flowmeter. This relationship is given by

$$\dot{V} = C \times \Delta H$$

where $\dot{V}$ = volume flow rate (l/s)

C = flowmeter constant

ΔH = pressure differential (mm H_2O)

The value of C for the flowmeter used was 0.460 l/s/mm H_2O. The engine results reduction program, discussed in appendix (V) converts

the volume flow rate into the mass flow rate, after correcting for the ambient temperature and pressure.

The petrol flow rate was measured using a 50 ml pipette and 3 way valve arrangement in conjunction with automatic electronic timing. This equipment is also discussed in detail by Green and Lucas[92]. The time for consumption of 50 ml of petrol is recorded, and this is related to the mass flow rate by the following expression:

$$\dot{m} = \frac{50 \times \rho_f}{t \times 10^6} \text{ kg/s}$$

where $\dot{m}$ = mass flow rate of petrol (kg/s)

ρ_f = density of petrol (740 kg/m^3)

t = time for consumption of 50 ml petrol (seconds)

The hydrogen flow rate was measured using a choked sonic nozzle, details of which are given in appendix (i). The mass flow rate is given by:

$$\dot{m} = k \frac{Po}{\sqrt{To}}$$

where $\dot{m}$ = mass flow rate of hydrogen (kg/s)

k = constant, dependent on which nozzle is used

Po = absolute pressure (p.s.i)

To = absolute temperature (K)

The engine speed was measured using a magnetic pick-up from a 60-tooth wheel attached to the dynamometer shaft. The signal obtained was converted to a d.c.voltage, which was then fed to an analogue meter. Calibration checks indicated the speed (in rpm) was correct to within 0.5%.

The engine load was indicated by a balance attached to the load arm on the Heenan and Froude Dynamometer. This dynamometer is of the eddy-current type, which is known for its accuracy of torque measurement. The principle of operation is discussed in detail by Greene and Lucas[92]. One of the major advantages of this type of dynamometer is that engine speed does not change with varying throttle position, thus facilitating constant speed measurements. The load reading can be related directly to torque (and hence brake power) by the followship relationship:

$$\text{Torque} = W \times 17.80 \text{ Nm}$$

where W = indicated load (lbf).

The ignition timing was manually adjusted to give the minimum advance required for best torque (M.B.T.) by rotating the body of the distributor. The centrifugal advance weights were locked into a fixed position at all times, and the vacuum advance mechanism was disconnected. A timing light illuminated a mark engraved on the pulley attached to the crankshaft. This could then be aligned with marks fixed to the engine block, each mark corresponding to five degrees ignition advance. The timing light was disconnected after each adjustment to avoid electrical interference to other instruments.

The exhaust emissions were analysed to determine the concentrations of carbon monoxide, carbon dioxide, nitrogen oxides (as NO) and unburnt hydrocarbons (as hexane) in the exhaust using four non-dispersive infra-red gas analysers manufactured by The Analytical Development Company Ltd. Details of these instruments are given in appendix (ii). The exhaust sample, taken continuously from a tapping approximately 16 cm downstream from the exhaust valves, was cooled, dried and filtered (to remove particulates) before being analyzed. All the analyzers used measure exhaust emissions as percentages by volume. To obtain an output in more useful units (g/BHP-Hr) the readings were converted using the exhaust analysis reduction program discussed in appendix (vi).

The exhaust temperature and coolant temperature were measured using Chromel/Alumel thermocouples in conjunction with Comark Type 1601 electronic thermometers. The exhaust thermocouple was again installed approximately 16 cm downstream from the exhaust valves, and the coolant thermocouple was installed in the coolant pipe approximately 14 cm downstream from the engine.

The coolant flow rate was measured by directing the water flow from the engine into a bucket for sixty seconds, and then weighing the contents. The water supply in this case was taken directly from the mains with no recirculation. The thermostat had previously been removed to ensure steady state conditions.

The depression in the inlet manifold was measured using a mercury manometer. The main purpose of these measurements was to accurately indicate throttle opening at any given speed.

7.3 MODIFICATIONS TO INLET TRACT

Changes were made to the inlet system to accommodate various petrol, hydrogen, and air flow rates. Initially, the flow rate of petrol was controlled by a vacuum pump attached to the float chamber of the carburettor. By regulating the float chamber pressure, the flow of petrol could be maintained at any particular value. However, difficulties were encountered in controlling very small petrol flow rates, resulting in engine surge. This problem was overcome by the use of a high pressure pump and needle valve, shown in figure 7.2. In this case, petrol flow could be accurately controlled by the use of the needle valve located upstream from the carburettor jet. Another modification to the carburettor was a tapping into the top of the piston, so that it could be held fully up during dual-fuel operation. The main cause of the increase in efficiency when the engine uses hydrogen and petrol is that there is no throttling of the air. However, a wide-open throttle does not necessarily ensure that the carburettor piston is fully open, especially at low engine speeds, hence the air-flow could have been restricted.

The hydrogen was fed into the air inlet through a tapping upstream of the carburettor, as illustrated in figure 7.1. The hydrogen was admitted as far upstream as possible to ensure good mixing of the hydrogen/air mixture before entering the combustion chamber.

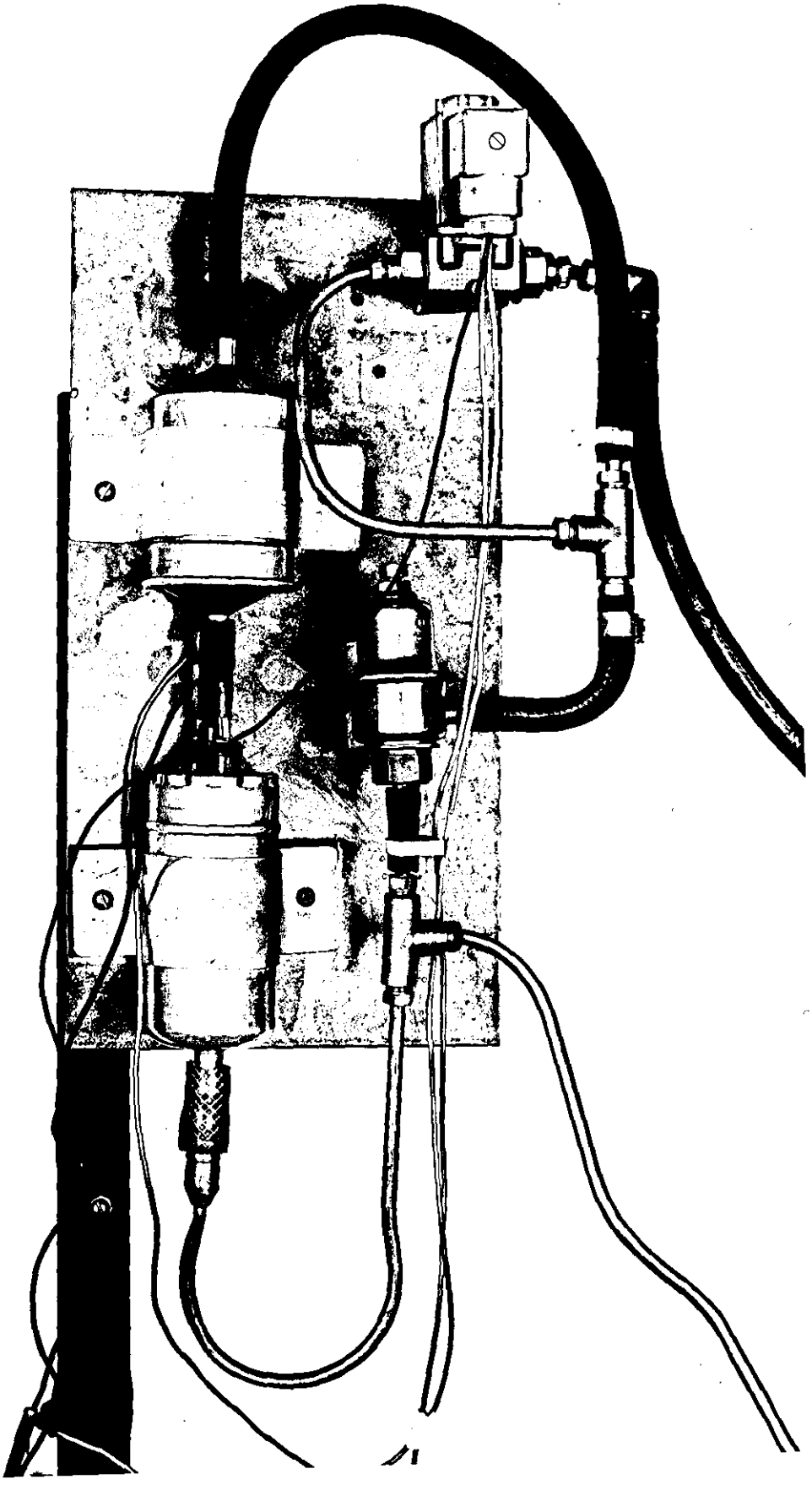

Figure 7.2 Petrol Pump System

CHAPTER 8

ENGINE TEST-BED RESULTS

CHAPTER 8

8.1 INTRODUCTION

The main objective of the engine test-bed investigation was to compare the performance of an engine running on a dual-fuel mixture of hydrogen and petrol at wide open throttle with that of the engine using petrol only. In order to do this, several parameters were measured, as discussed in the previous chapter. Both engines were operated on dual-fuel mixtures, but the results presented are for the BL Cars 1275 cc "A series" engine unless otherwise indicated. The reduction of the actual engine data was achieved using the program listed in appendix (v). The basic performance curves are shown for this engine in figures 8.1-3.

The system investigated was that of an engine, having a wide open throttle, running on hydrogen alone at idle, with the petrol fraction of the fuel increasing from zero with load. As hydrogen has such wide flammability limits, and a high flame speed, it was possible to run the engine using a wide-open throttle at almost all operating conditions, with the exception of low loads. This was due to the lean extinction limit of the hydrogen-petrol mixture having been reached. Wide open throttle operation could be achieved at low loads by increasing the flow rate of hydrogen. Thus the engine efficiency became comparable to that of a diesel engine, as will be shown.

Since the flame speed of hydrogen is much greater than that of petrol (291 cm/sec for hydrogen, 38 cm/sec for petrol[84]*), the dual-fuel mixture burns significantly faster than petrol alone. This is

* No details of the measurement are given in ref.84 but it is assumed these are laminar flame speeds in a tube at ambient temperature and pressure.

indicated by the smaller ignition advance required for best torque, as shown in figure 8.4. Thus the combustion process approaches the constant volume process of the Otto cycle. However, the flame velocity decreases significantly as the mixture ratio decreases from the stoichiometric.

8.2 TORQUE CONSUMPTION LOOPS

To investigate the specific fuel consumption throughout the load range, the engine was initially run on petrol only to provide a set of base figures. The engine was taken throughout its load range, using the throttle and petrol only as its fuel, at a number of fixed engine speeds. At each throttle setting, the petrol flow was adjusted to give a mixture slightly weaker than that required for maximum torque; a mixture strength corresponding approximately to the most economical mixture strength. With dual-fuel operation, the hydrogen flow was set at 0.0695 g/sec to maintain the engine at idle (850 rpm, no load) with a fully open throttle. The petrol flow rate was then altered to give the maximum torque at the set engine speed. Then, with the hydrogen flow rate maintained at its constant value, the petrol flow rate was progressively reduced to take the engine throughout its load range. The specific fuel consumption is compared at different engine speeds in figures 8.5-9. In all comparisions of fuel consumption, the petrol energy equivalent to the hydrogen has been used. This is defined as

$$PH_2 = \dot{m}\, H_2 \times 2.746$$

where 2.746 is the ratio of the mass heating values, and PH_2 is the energy equivalent of the mass flow rate of hydrogen $\dot{m}H_2$. At all

times ignition timing was set to the minimum advance required for best torque (M.B.T.). The brake thermal efficiencies at the given engine speeds are also compared in figures 8.10-14.

Figures 8.15 and 8.16 are curves of energy balance against load for petrol and for the dual-fuel mixture respectively. Figure 8.17 shows the effect of changing the ratio of specific heats on engine efficiency. Details of the calculations used in determining these parameters are given in appendix(iii).

The effect of a much greater flow rate of hydrogen was also investigated. In this instance, the flow of hydrogen was increased to such an extent that a given engine speed was maintained with no load using hydrogen alone at a wide open throttle setting. The flow rate of petrol was then increased to take the engine throughout its load range. These results are shown in Figure 8.18.

8.3 EXHAUST EMISSIONS

The exhaust emissions were monitored by non-dispersive infra-red instruments, discussed in Appendix (ii). These were measured in conjunction with the torque consumption curves, initially using petrol only, and then with a hydrogen petrol mixture at wide open throttle. The instruments used gave the emission level of carbon dioxide, carbon monoxide, hydrocarbons (as hexane) and nitrogen oxides (as NO), all as concentrations. To obtain meaningful information, these were then converted to grams per brake horsepower hour for comparison, using the method

discussed in appendix (vi). A listing of the conversion program is also given.

The emissions of carbon monoxide at engine speeds of 1500 rpm and 3000 rpm are plotted in figures 8.19 and 8.20 respectively. Similarly, the emissions of hexane at engine speeds of 1500 rpm and 3000 rpm are plotted in figures 8.21 and 8.22. The emissions of nitric oxide, again at engine speeds of 1500 rpm and 3000 rpm are plotted against torque and equivalence ratio in figures 8.23 and 8.24.

8.4 DIRECT INJECTION INTO CYLINDER

In order to reduce the flow of hydrogen still further, a system was designed whereby the hydrogen could be injected directly into the cylinder through the spark plug, as illustrated in figure 8.25. Since the spark plug is recessed slightly, a hydrogen rich pocket will exist in the vicinity of the electrode. The firing of this mixture should ignite the weak petrol-air charge in the remainder of the cylinder.

When this system of injection was operated, combustion was audibly very rough, and this was attributed to poor mixing. Other workers have also noted incomplete fuel-air charge mixing in the cylinder resulting in incomplete combustion when direct injection techniques were used[72]. They also encountered great difficulty in devising an injector that could deliver the required amount of hydrogen in the time available at speeds above 3000 rpm using a low (30 psi) hydrogen pressure. However, if direct cylinder injection through the spark plug was used for dual-fuel operation, high hydrogen flow rates would not be required, and such a system may well prove viable.

Figure 8.1 Brake Power vs. Engine Speed at Different Throttle Settings

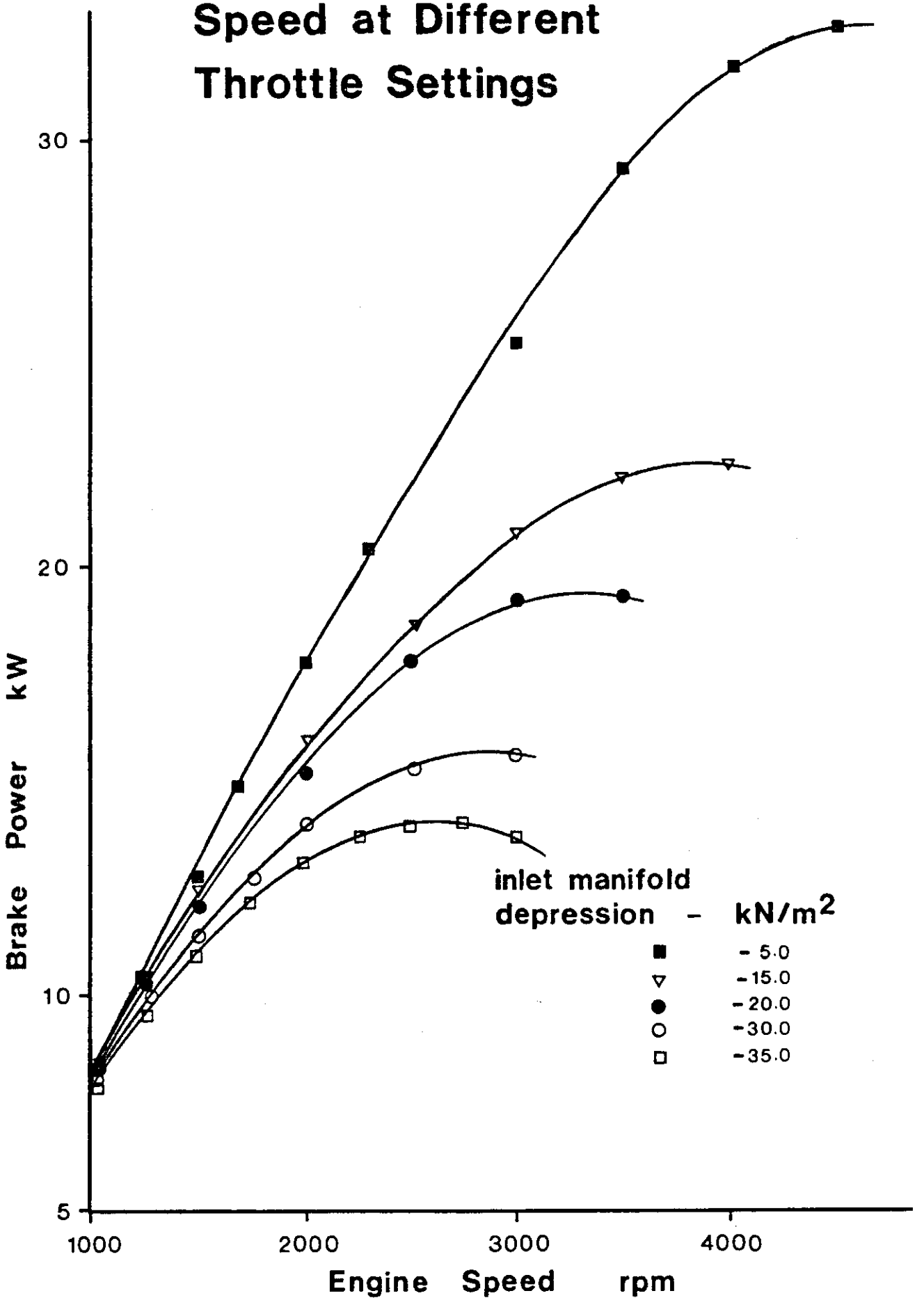

Figure 8.2 B.M.E.P vs. Engine Speed at Different Throttle Settings

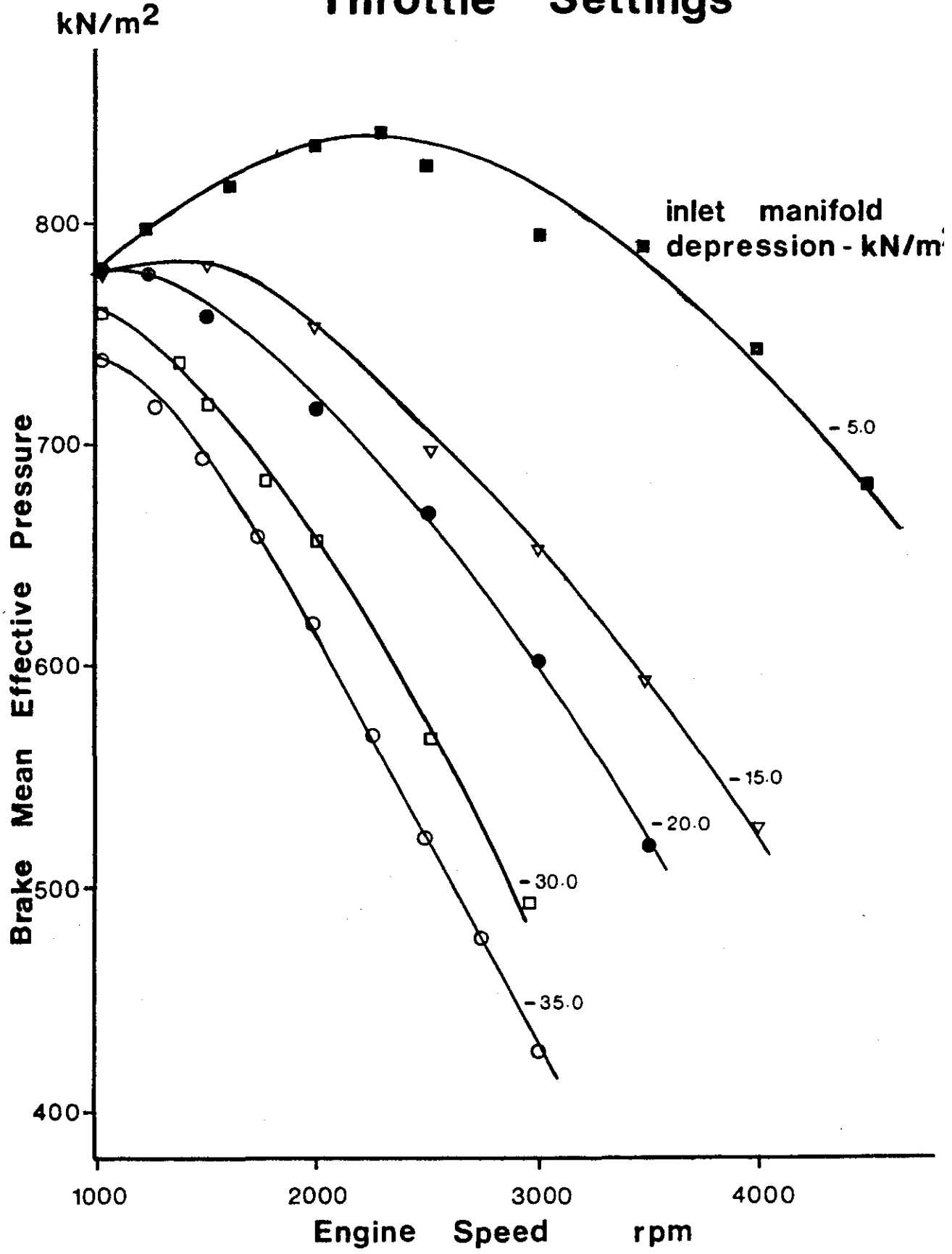

Specific Fuel Consumption vs Engine Speed

Petrol Only

Figure 8.3

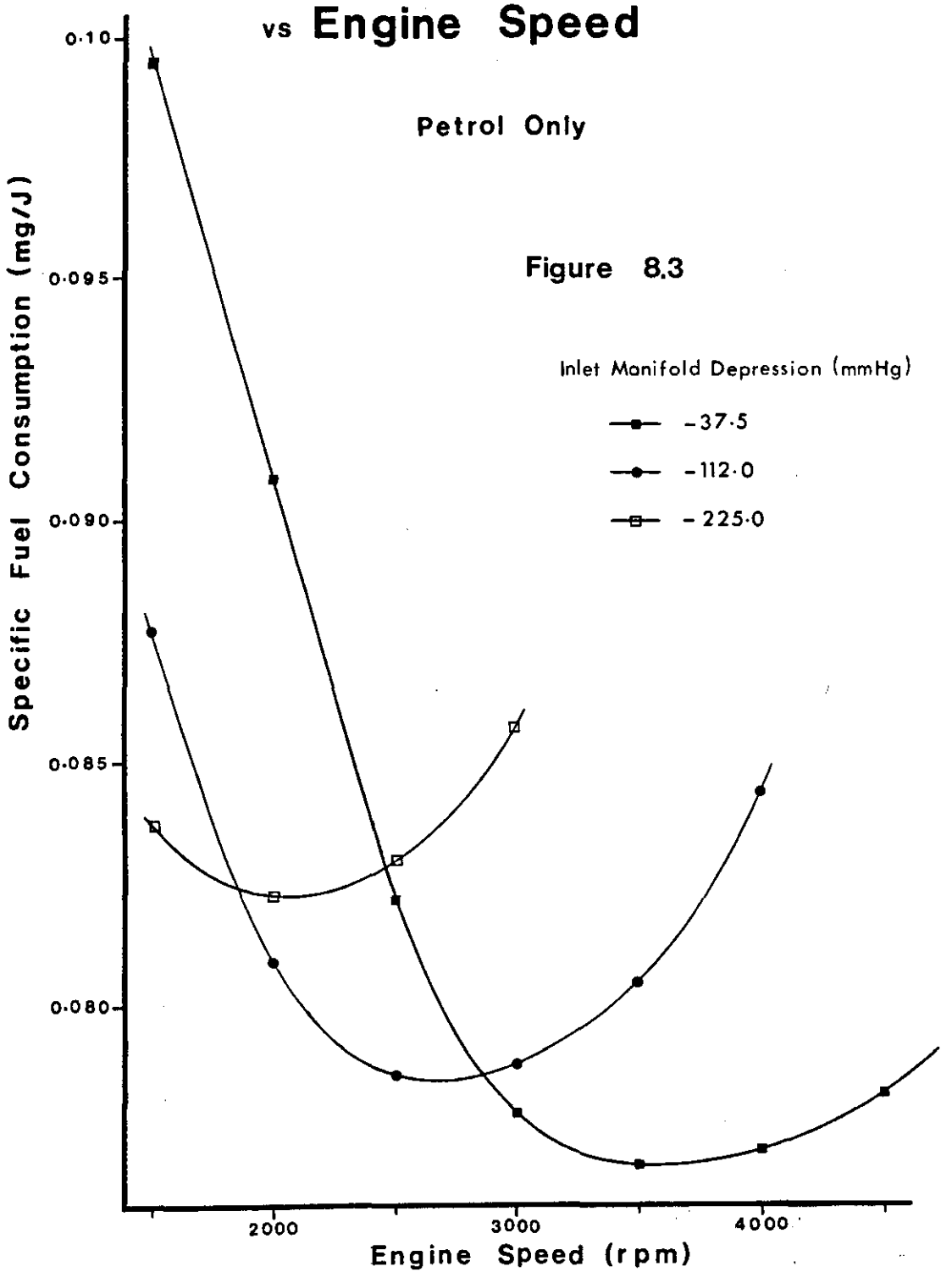

Figure 8.4

Dual - Fuel Engine

M.B.T. Ignition Advance Curves

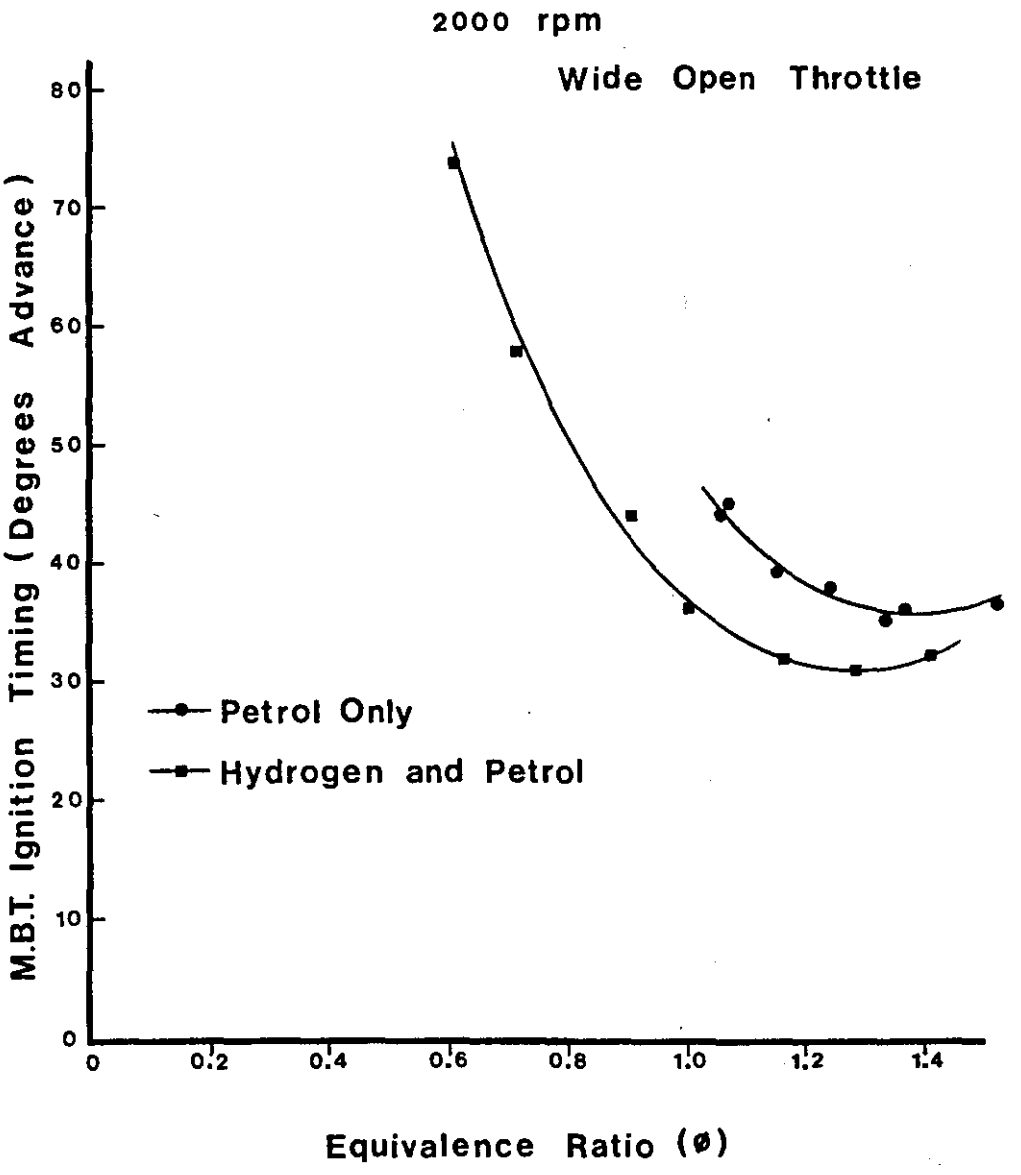

Effect of Hydrogen Supplementation on Specific Fuel Consumption

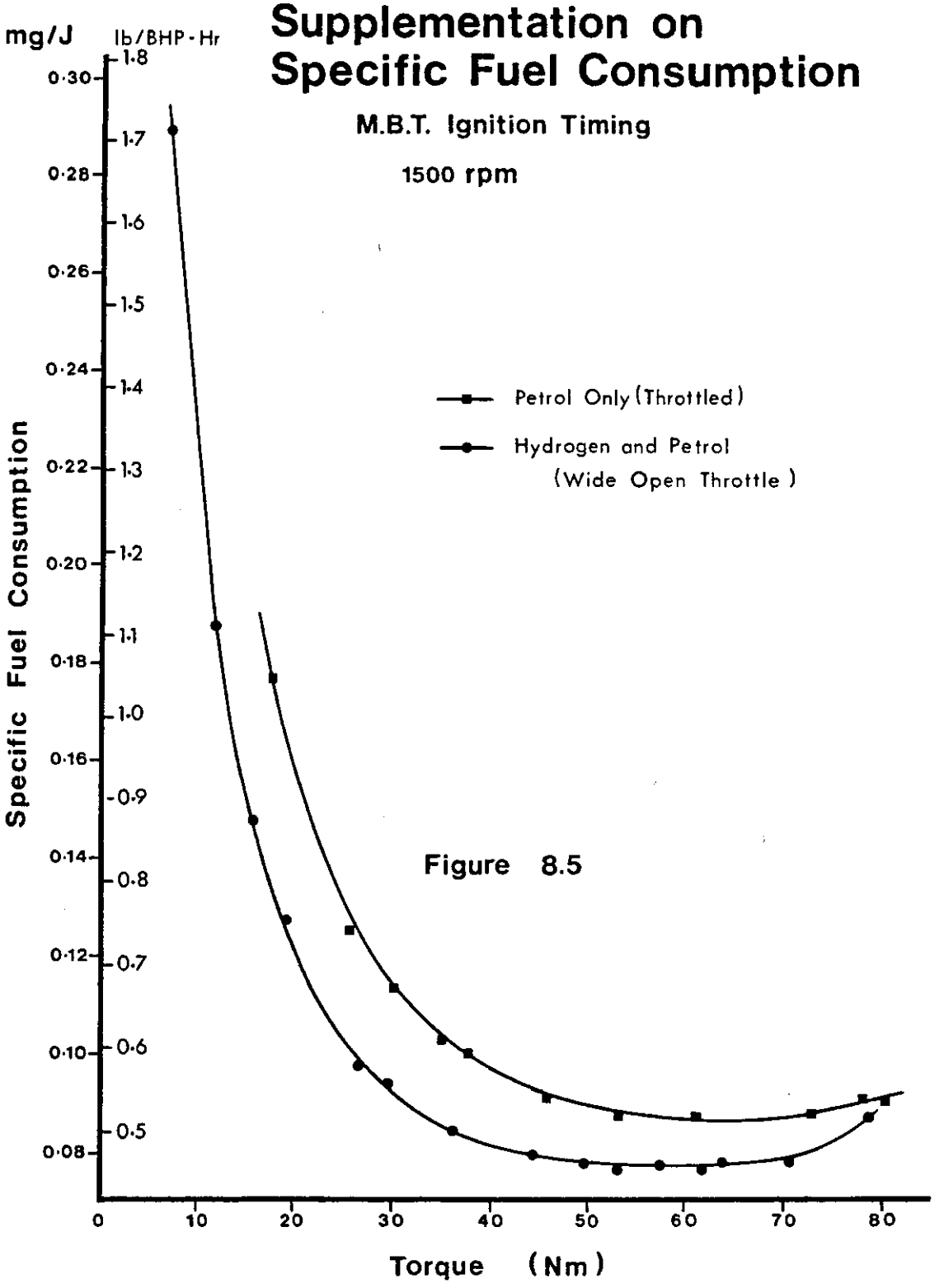

Figure 8.5

Effect of Hydrogen Supplementation on Specific Fuel Consumption

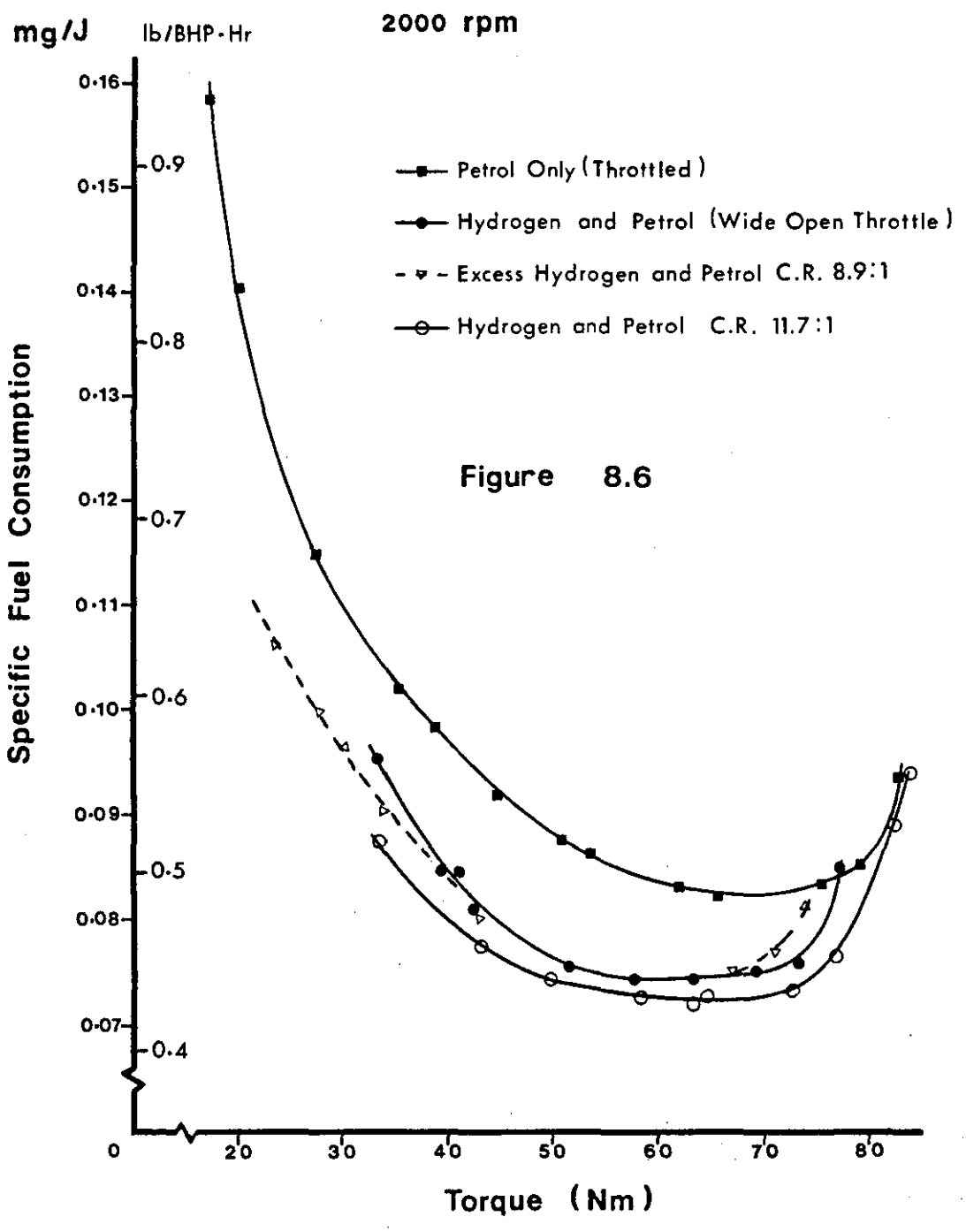

Figure 8.6

Figure 8.7

Effect of Hydrogen Supplementation on Specific Fuel Consumption

M.B.T. Ignition Timing

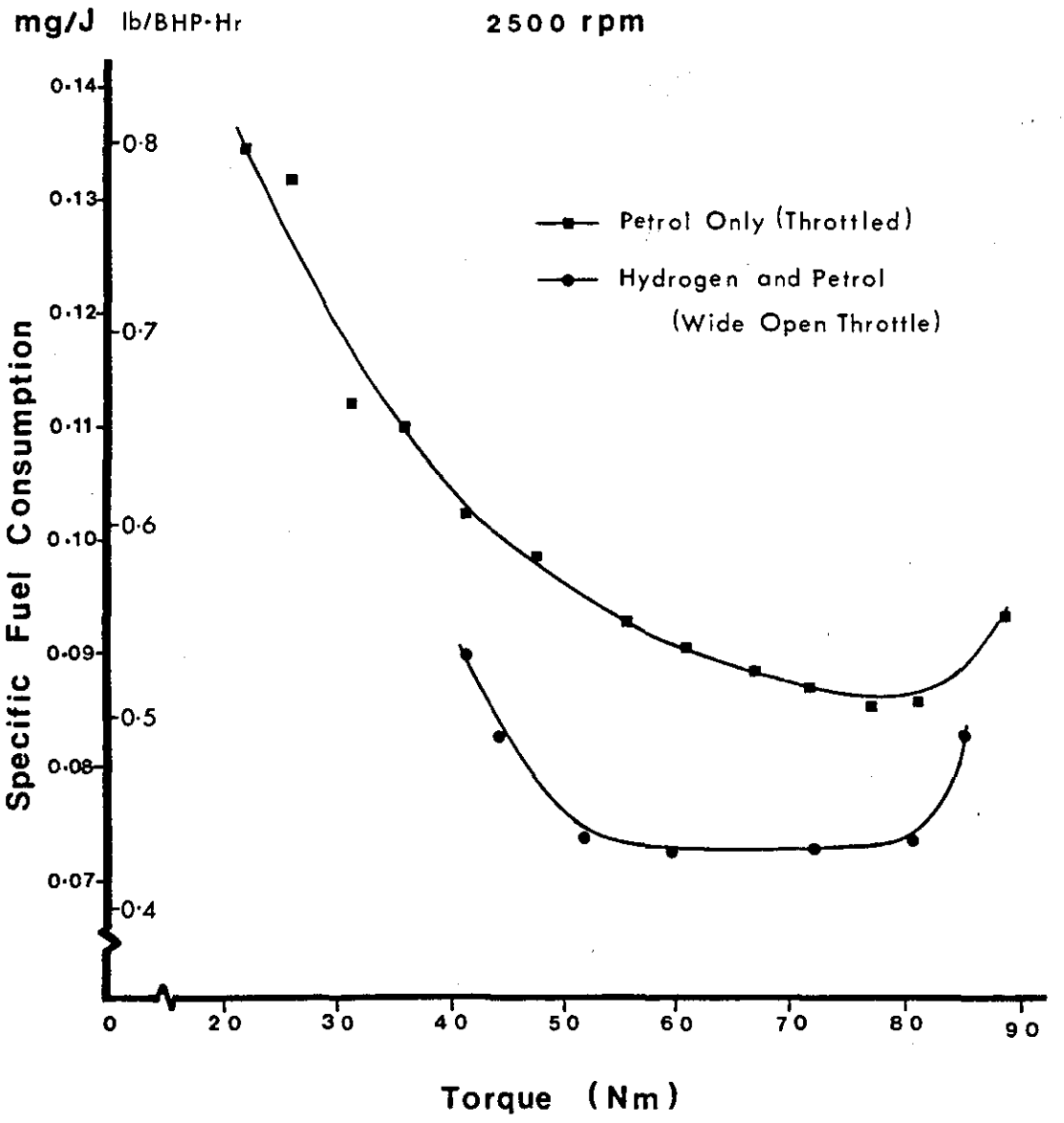

Figure 8.8

Effect of Hydrogen Supplementation on Specific Fuel Consumption

M.B.T. Ignition Timing

3000 rpm

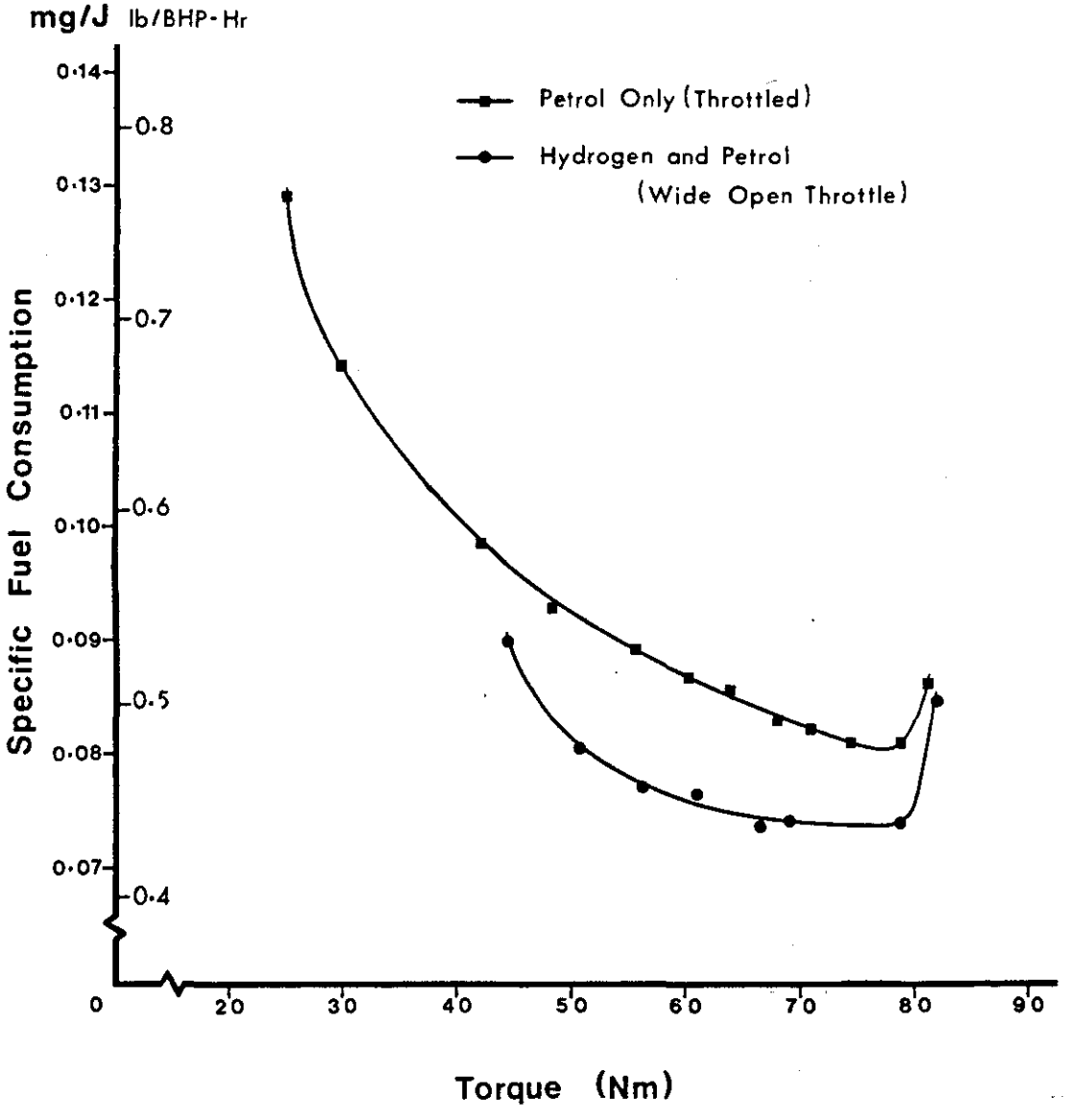

Effect of Hydrogen Supplementation on Specific Fuel Consumption

M.B.T. Ignition Timing

3500 rpm

Figure 8.9

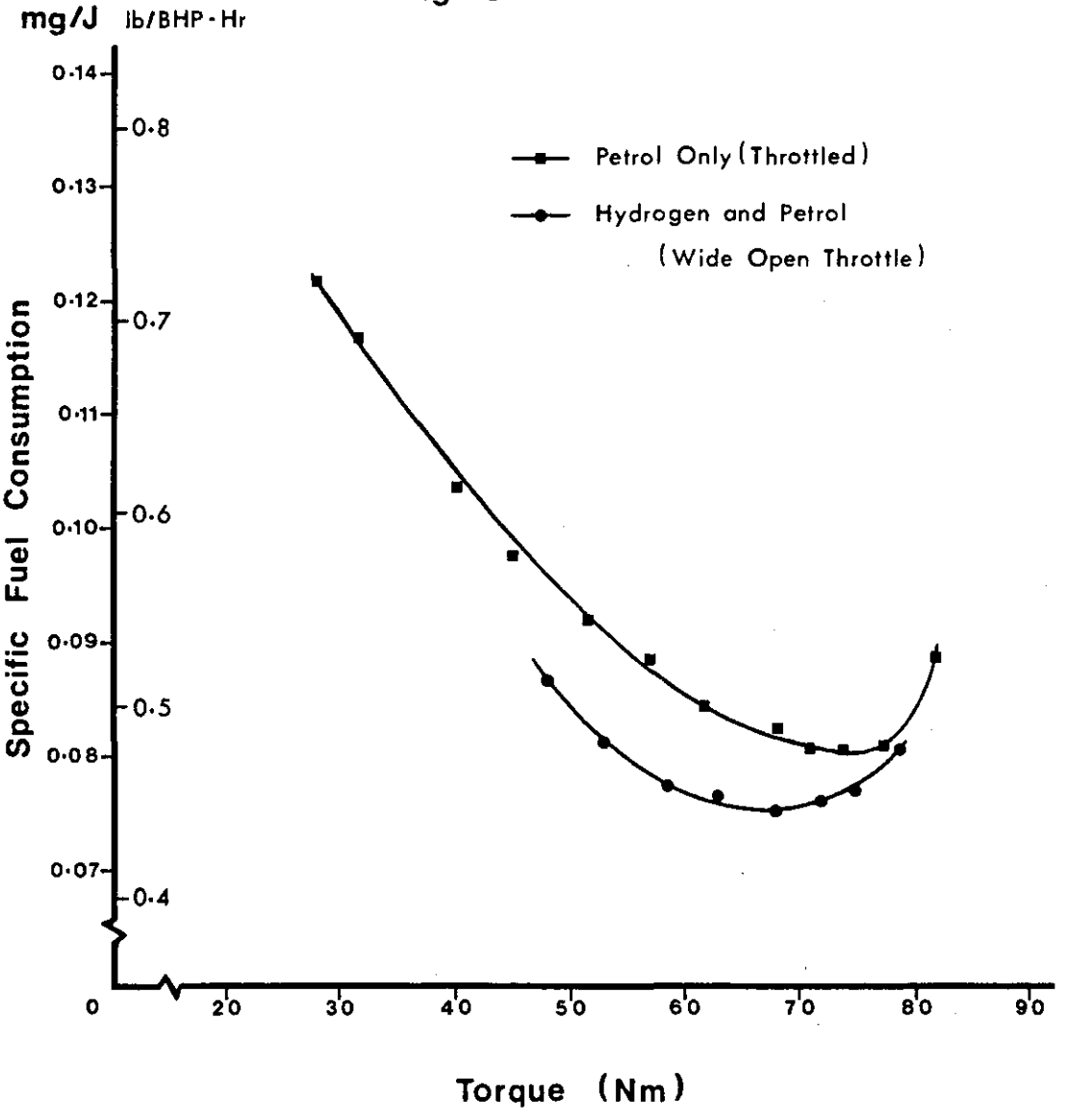

Figure 8.10 **Effect of Hydrogen Supplementation on Thermal Efficiency**

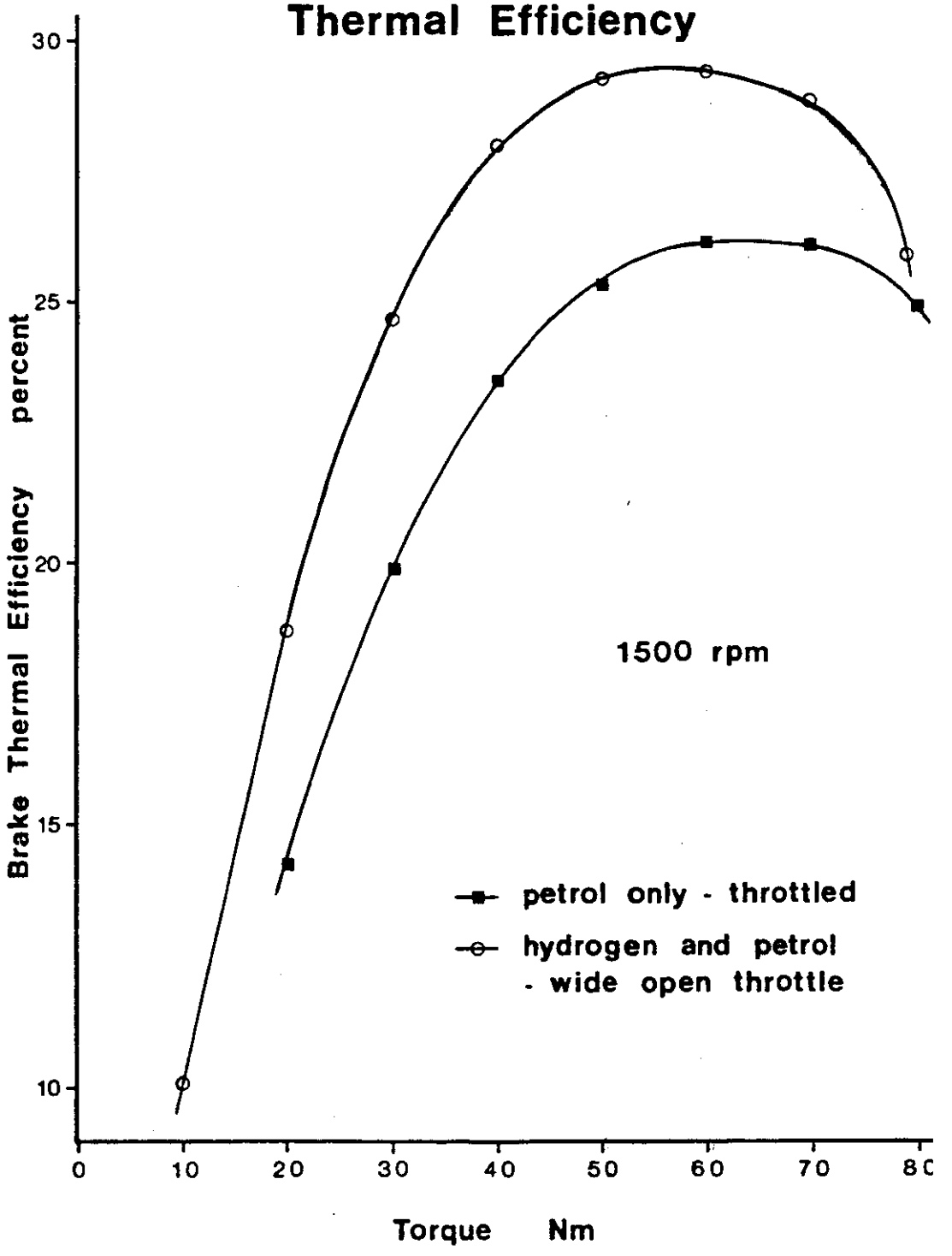

Figure 8.11 **Effect of Hydrogen Supplementation on Thermal Efficiency**

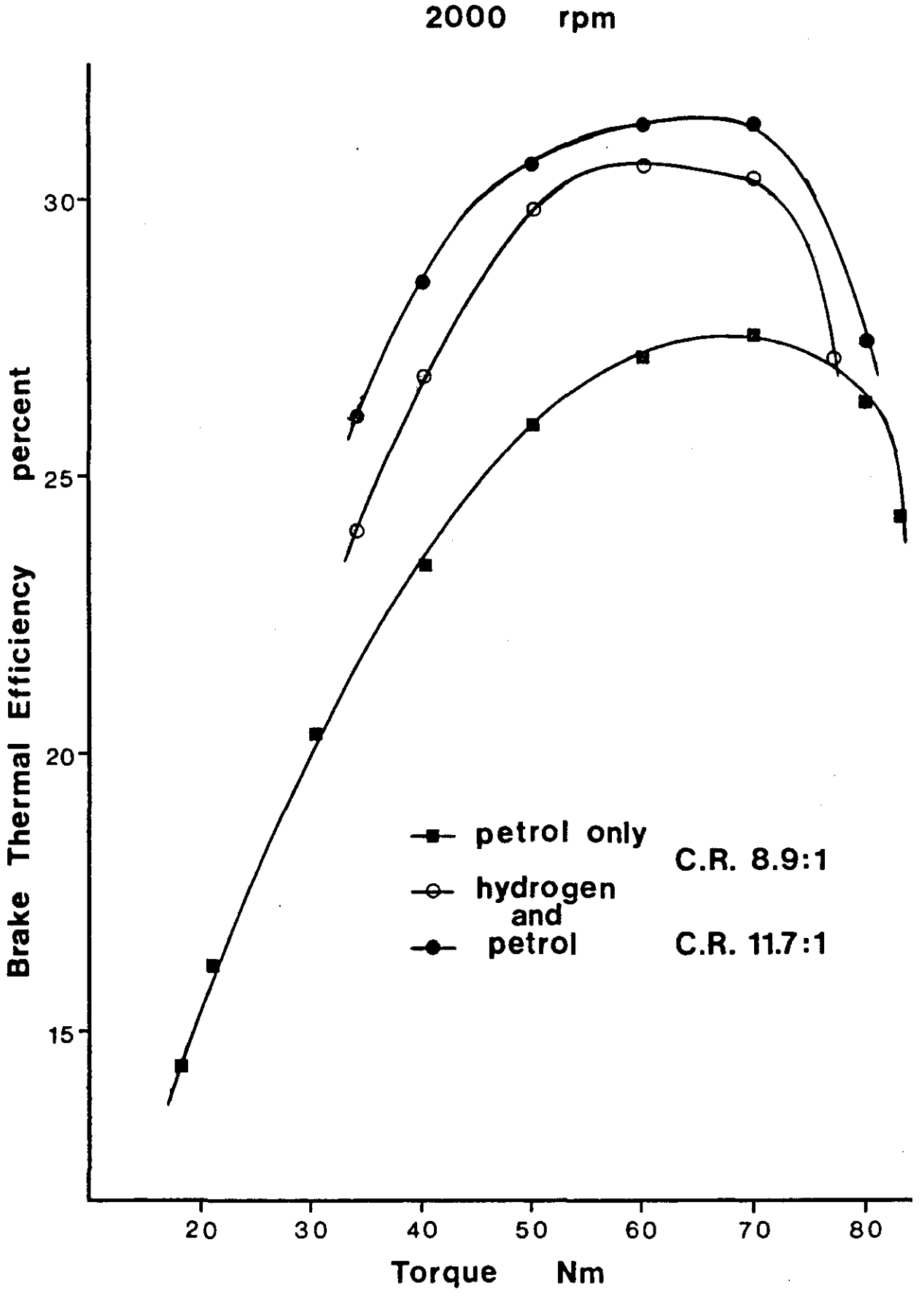

Figure 8.12 **Effect of Hydrogen Supplementation on Thermal Efficiency**

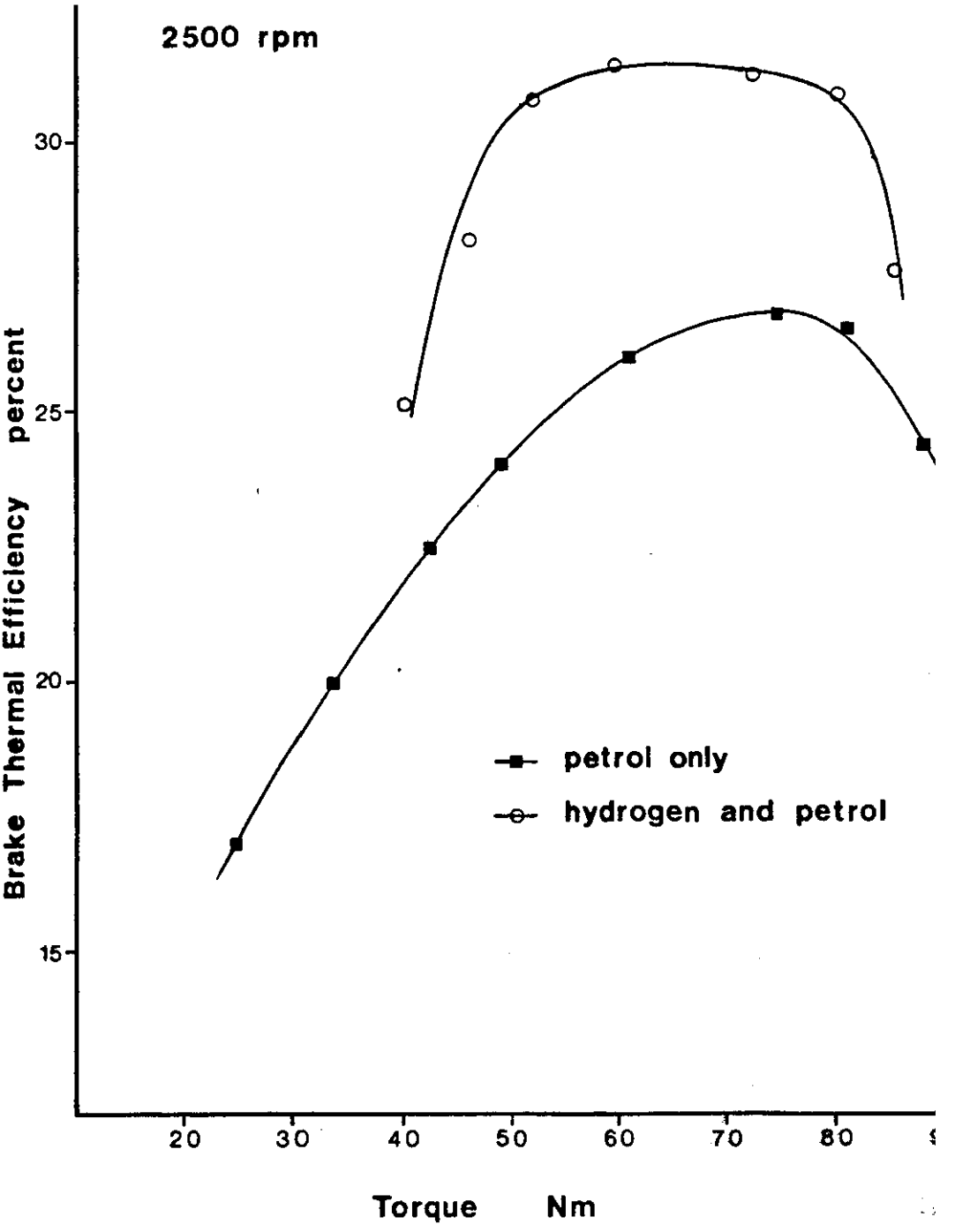

Figure 8.13 **Effect of Hydrogen Supplementation on Thermal Efficiency**

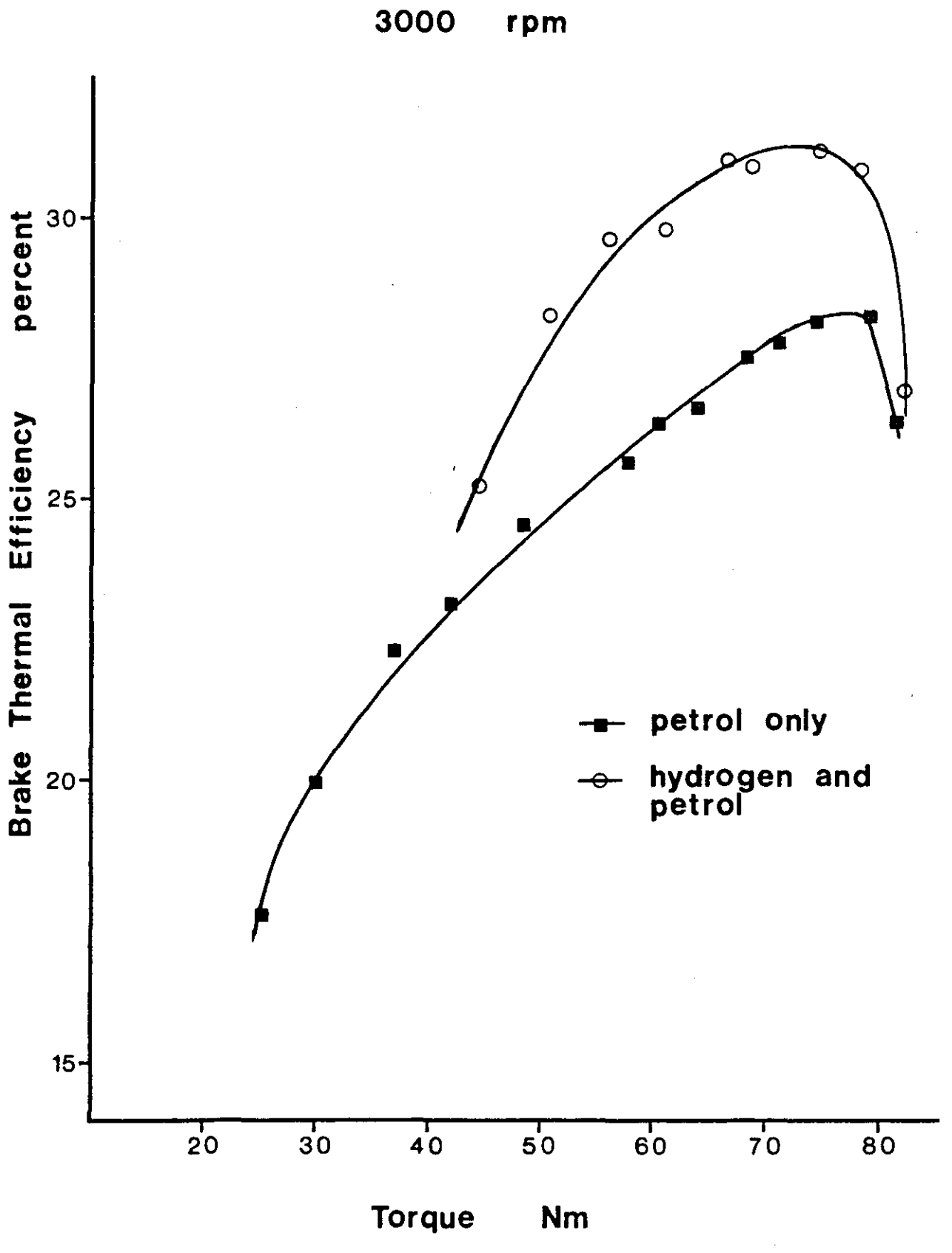

Figure 8.14 **Effect of Hydrogen Supplementation on Thermal Efficiency**

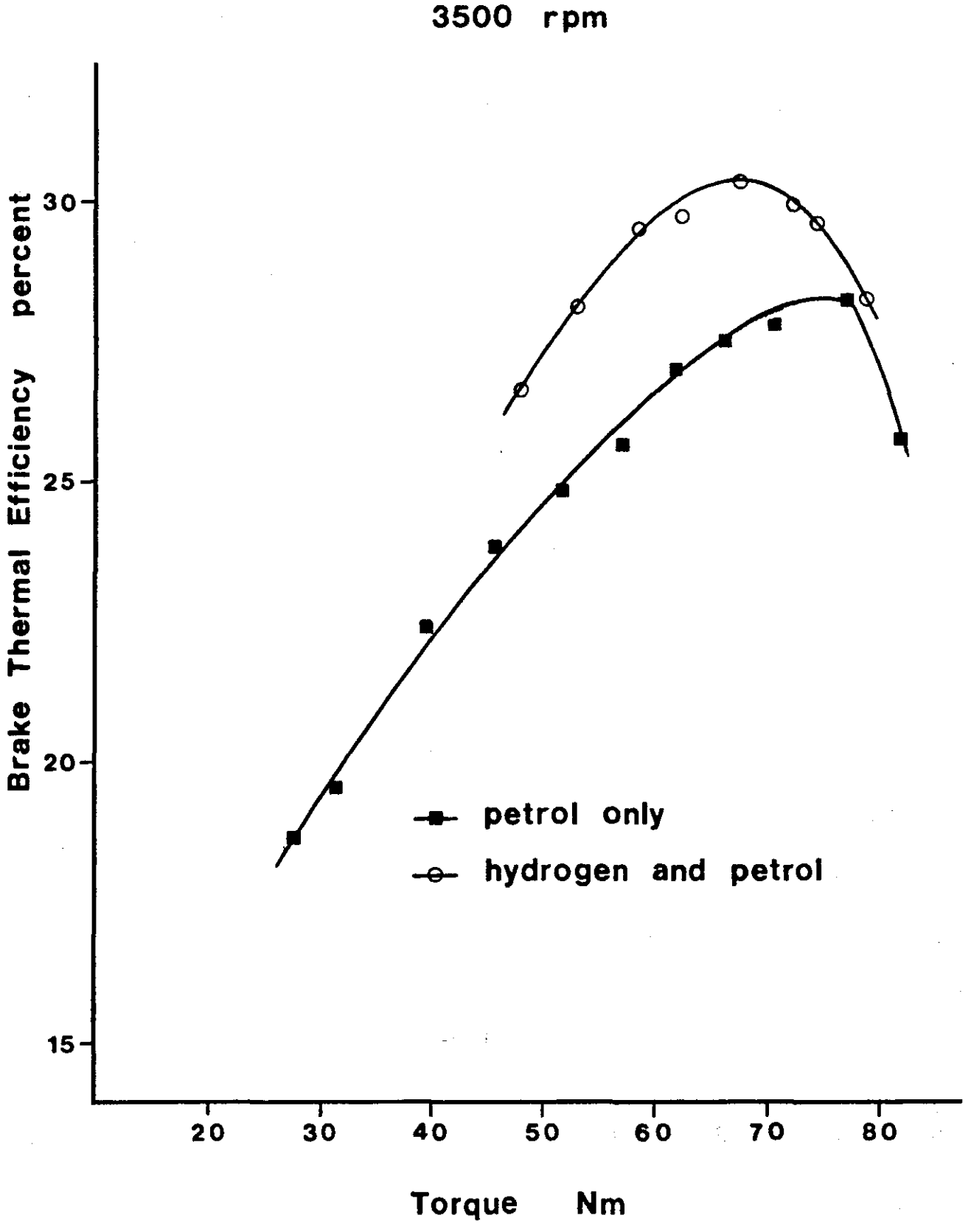

Figure 8.15 **Energy Balance Results**

2500 rpm

Petrol Only - Throttled Operation

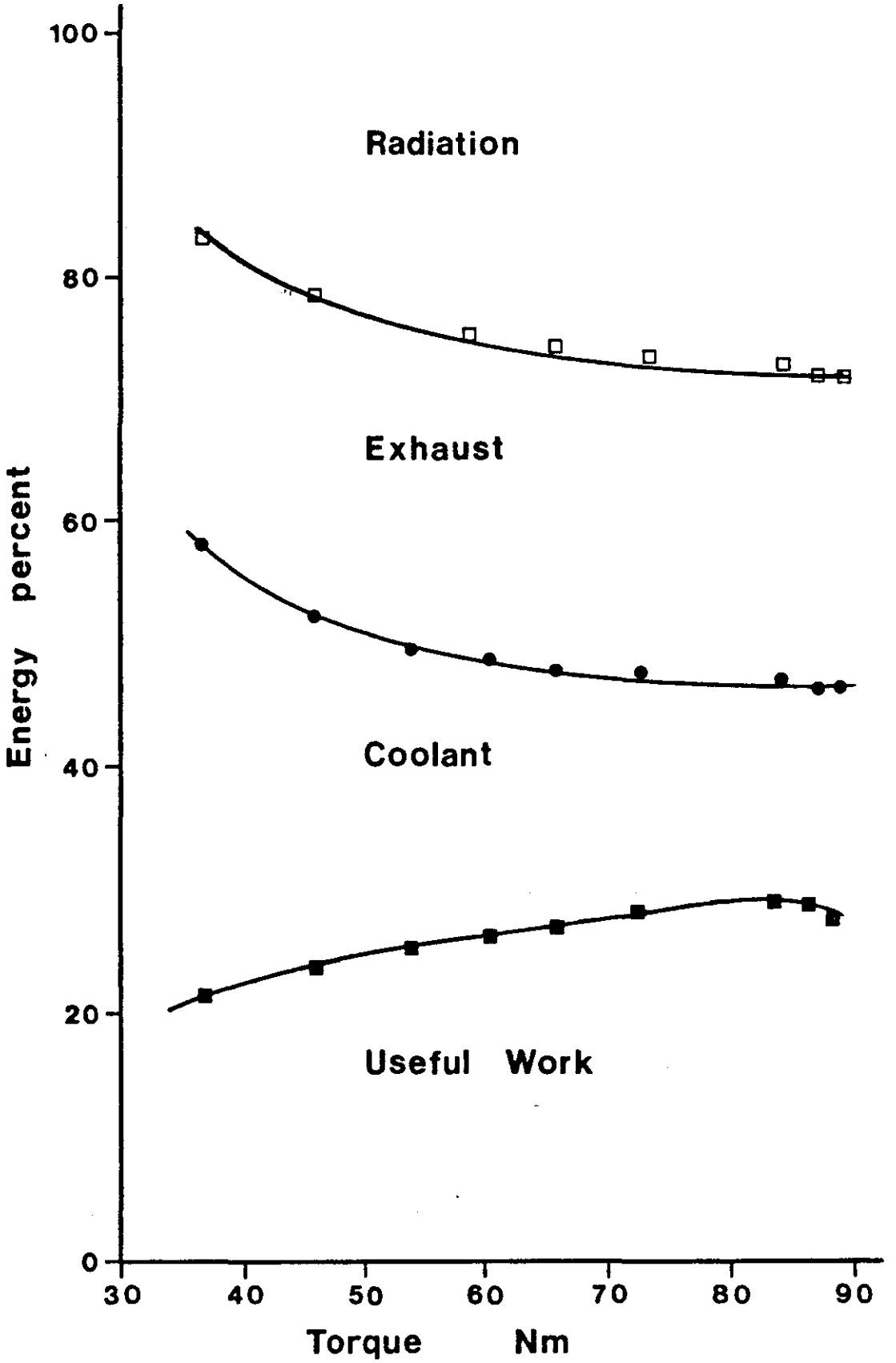

Figure 8.16 **Energy Balance Results**

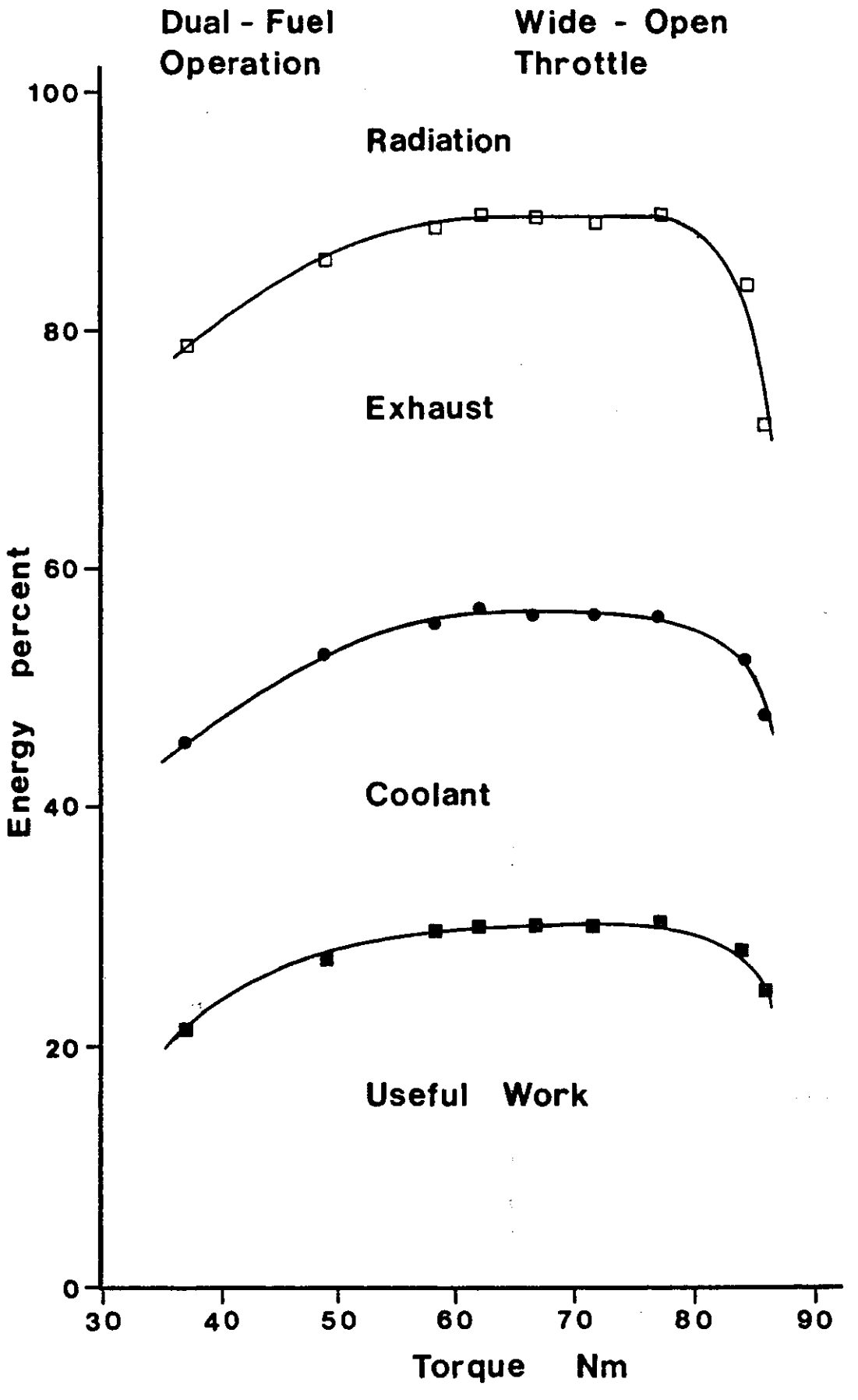

Figure 8.17 **Effect of Changing the Ratio of Specific Heats on Ideal Engine Efficiency**

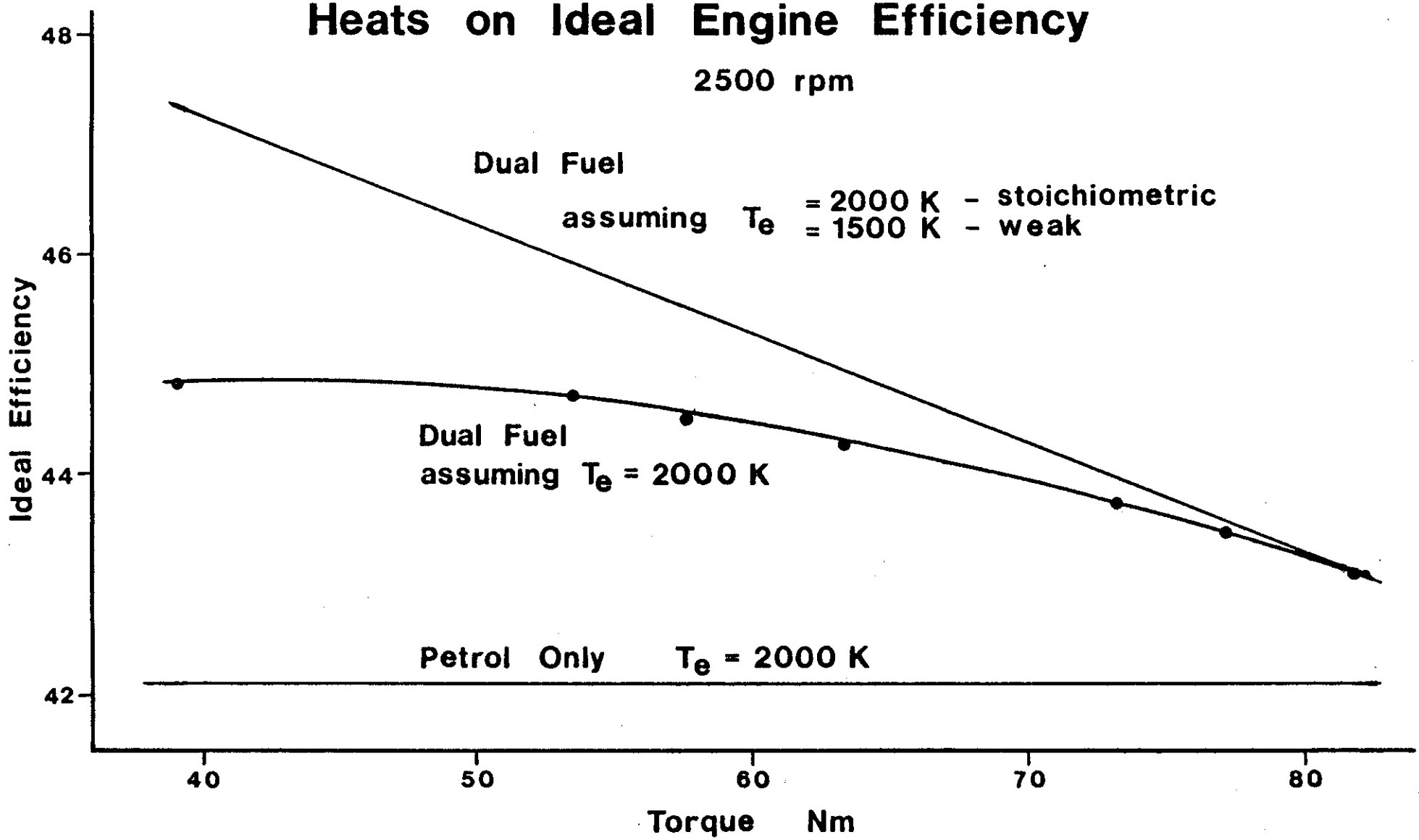

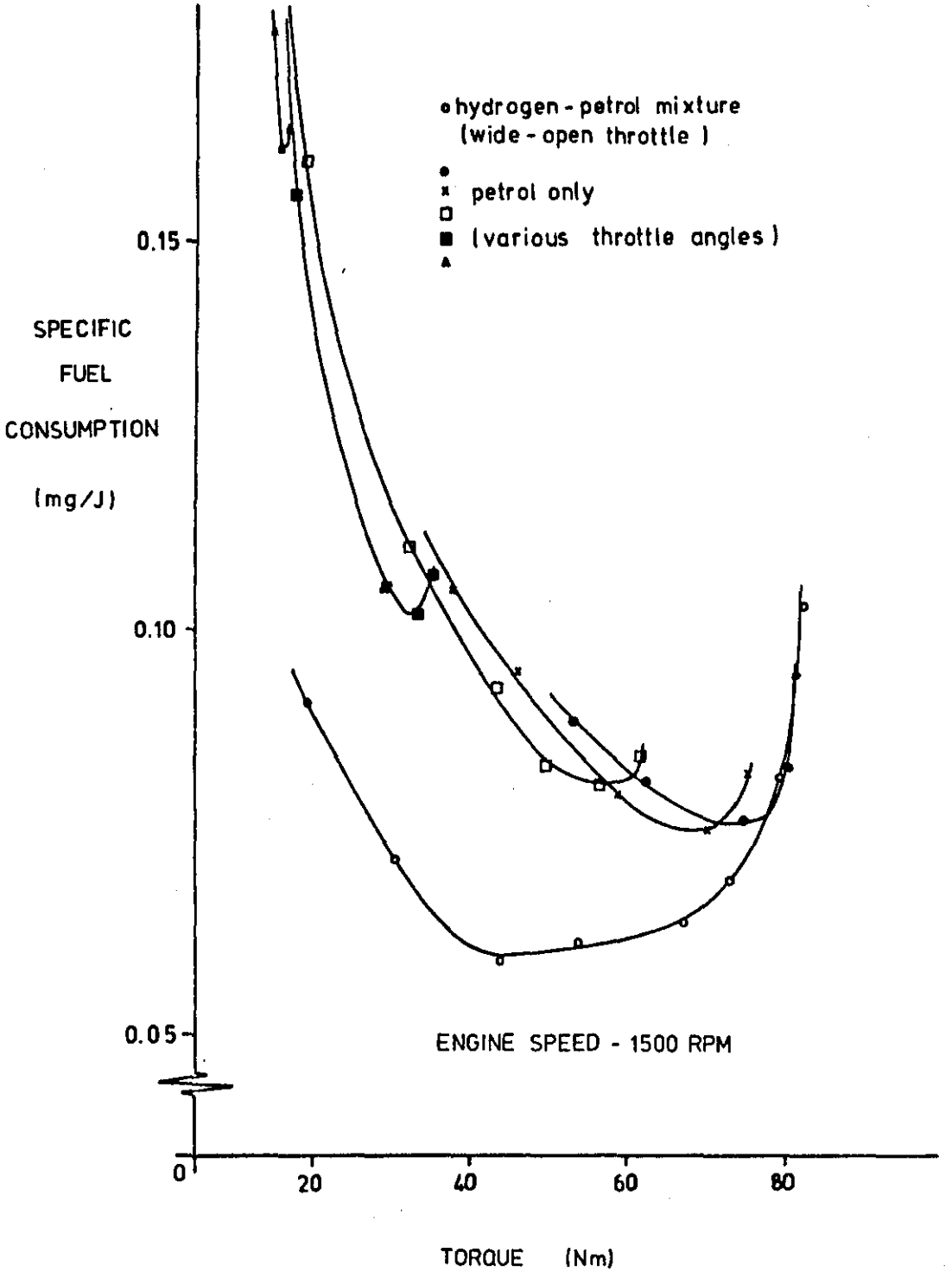

Figure 8.18 Specific Fuel Consumption

Figure 8.19

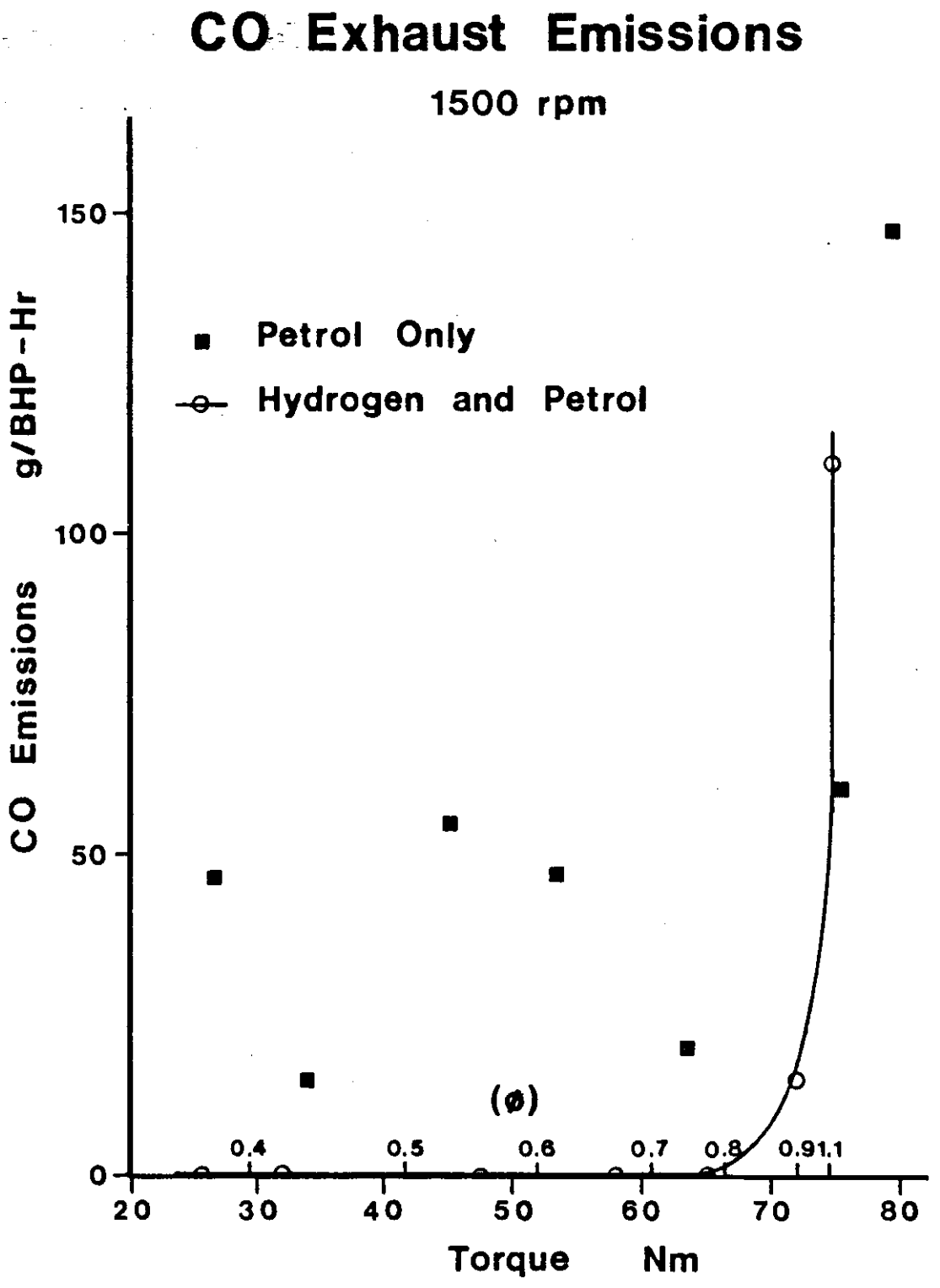
CO Exhaust Emissions
1500 rpm
CO Emissions g/BHP-Hr
150
100
50
0
Petrol Only
Hydrogen and Petrol
(ø)
0.4
0.5
0.6
0.7
0.8
0.9
1.1
20
30
40
50
60
70
80
Torque Nm

Figure 8.20

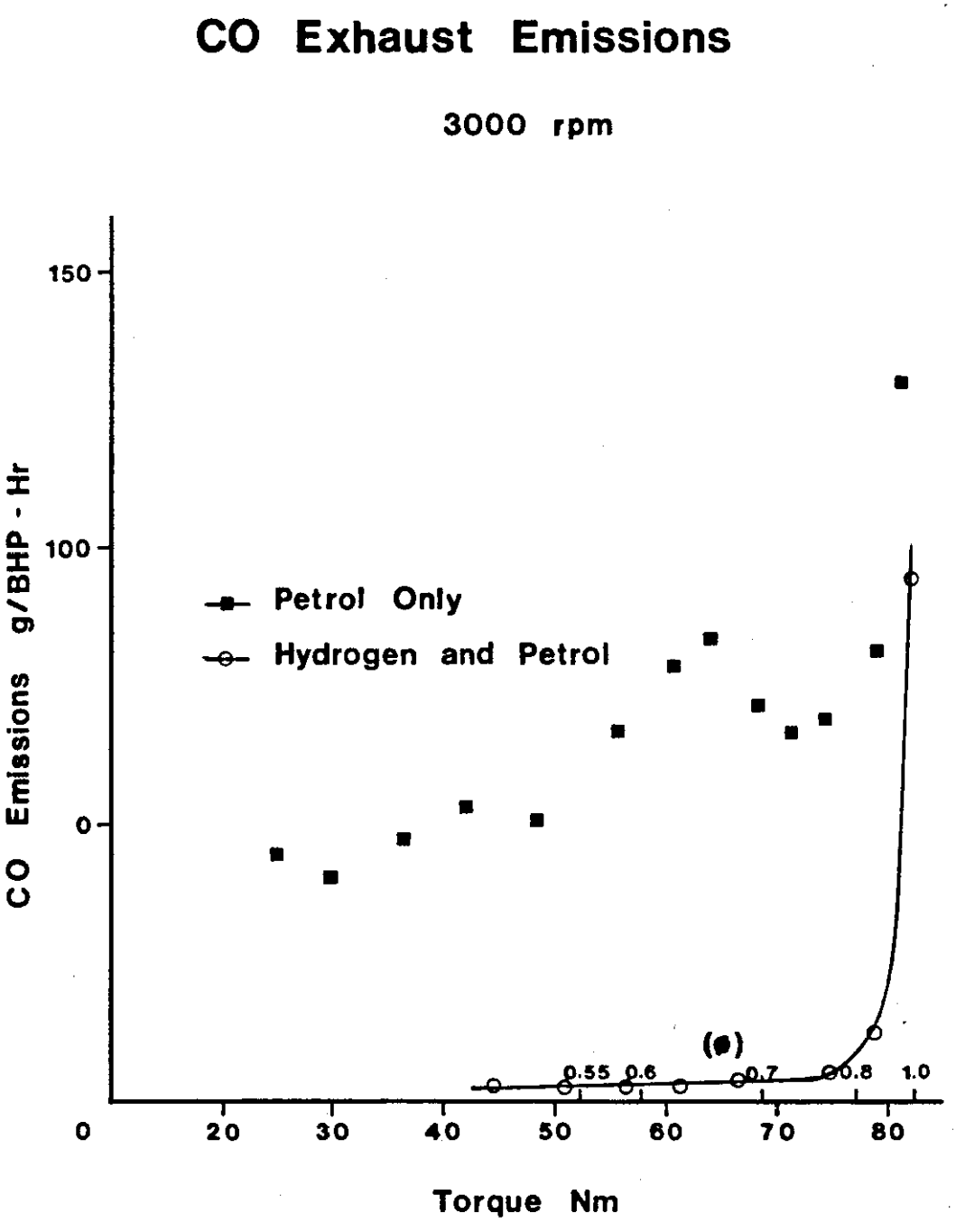
CO Exhaust Emissions
3000 rpm
CO Emissions g/BHP - Hr
150
100
0
Petrol Only
Hydrogen and Petrol
(ϕ)
0.55
0.6
0.7
0.8
1.0
0
20
30
40
50
60
70
80
Torque Nm

Figure 8.21

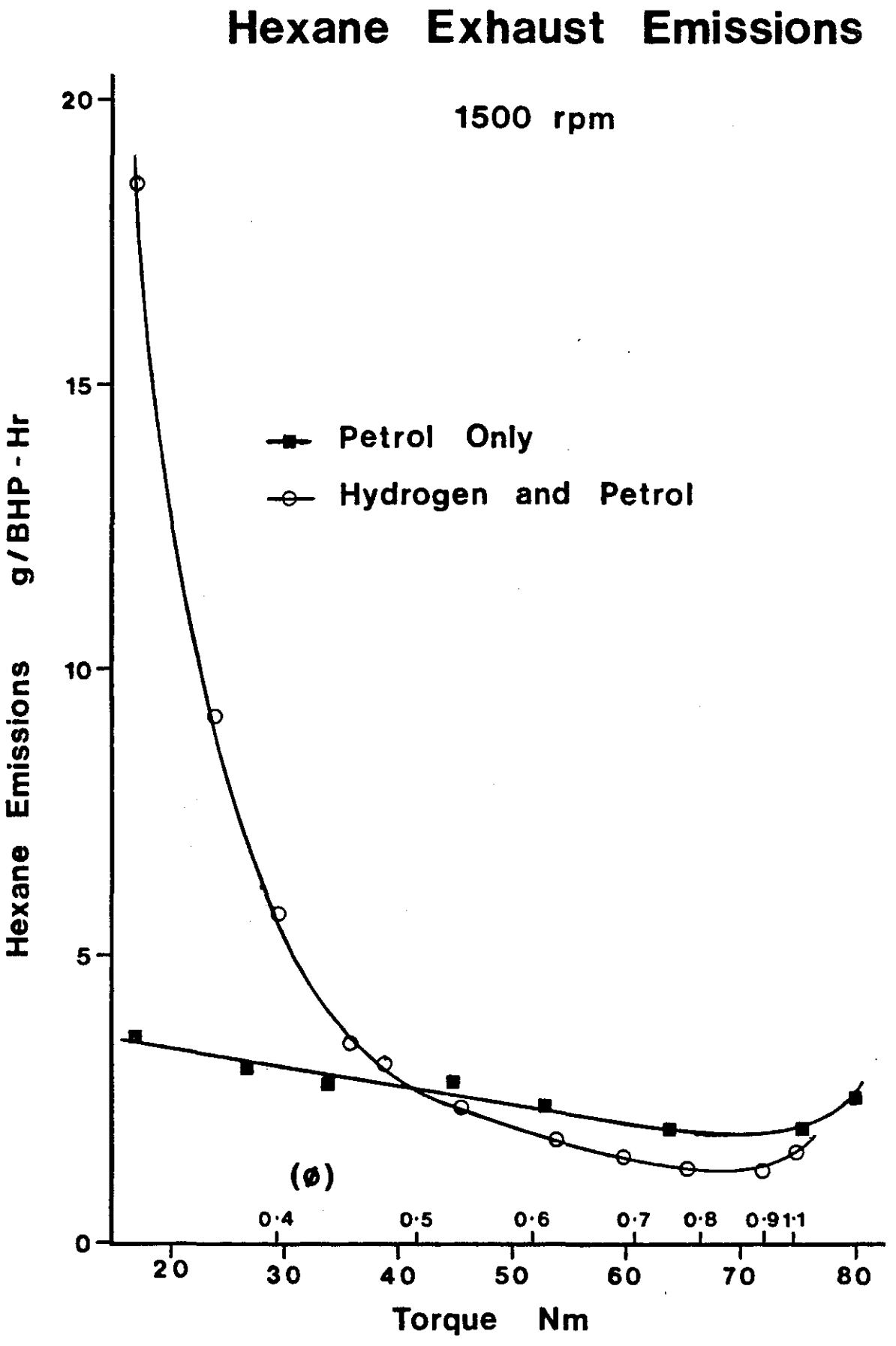
Hexane Exhaust Emissions
1500 rpm
Petrol Only
Hydrogen and Petrol
Hexane Emissions g/BHP-Hr
20
15
10
5
0
(ø)
0·4
0·5
0·6
0·7
0·8
0·9
1·1
20
30
40
50
60
70
80
Torque Nm

Figure 8.22

Hexane Exhaust Emissions

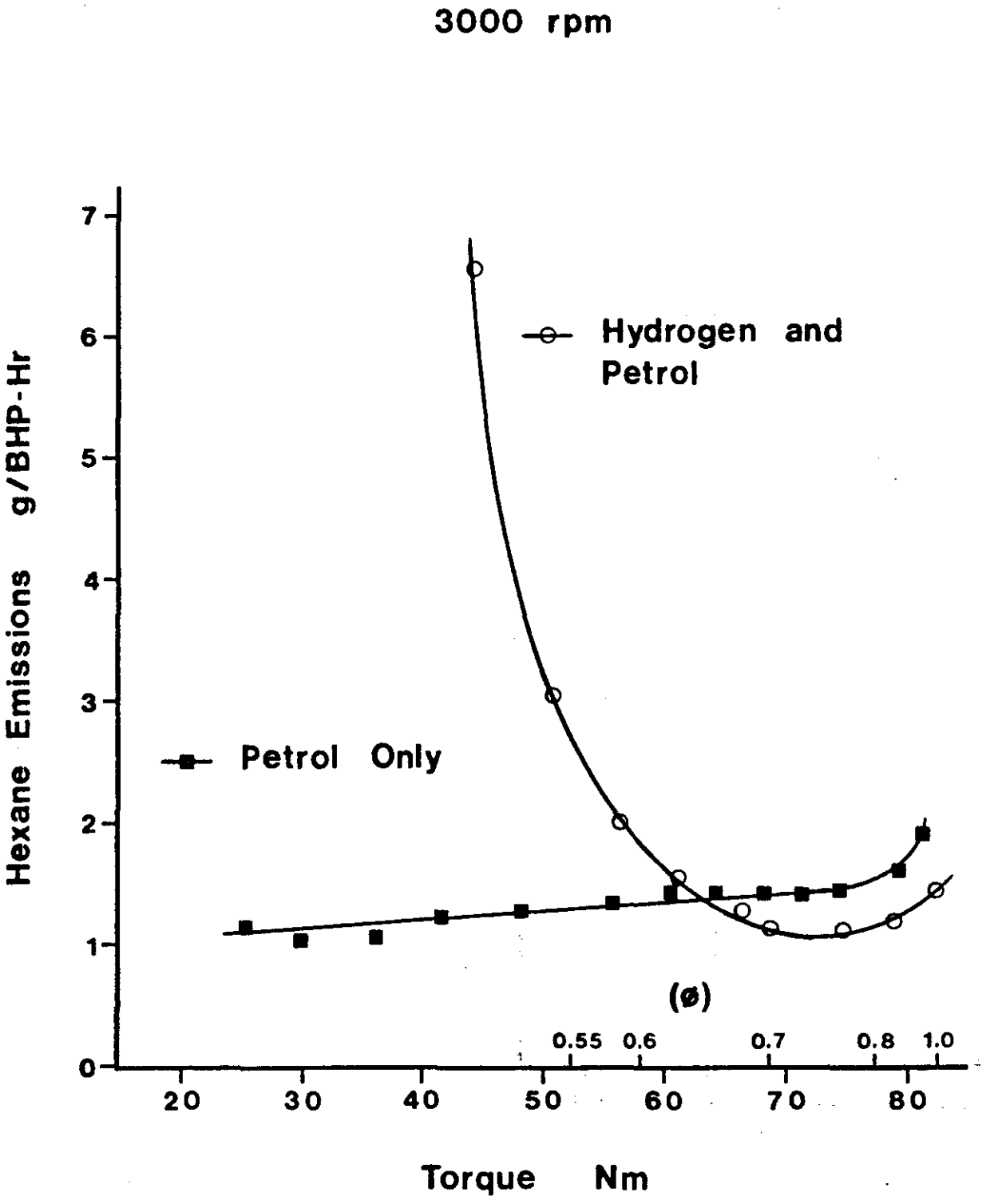

Figure 8.23 **NO Exhaust Emissions**

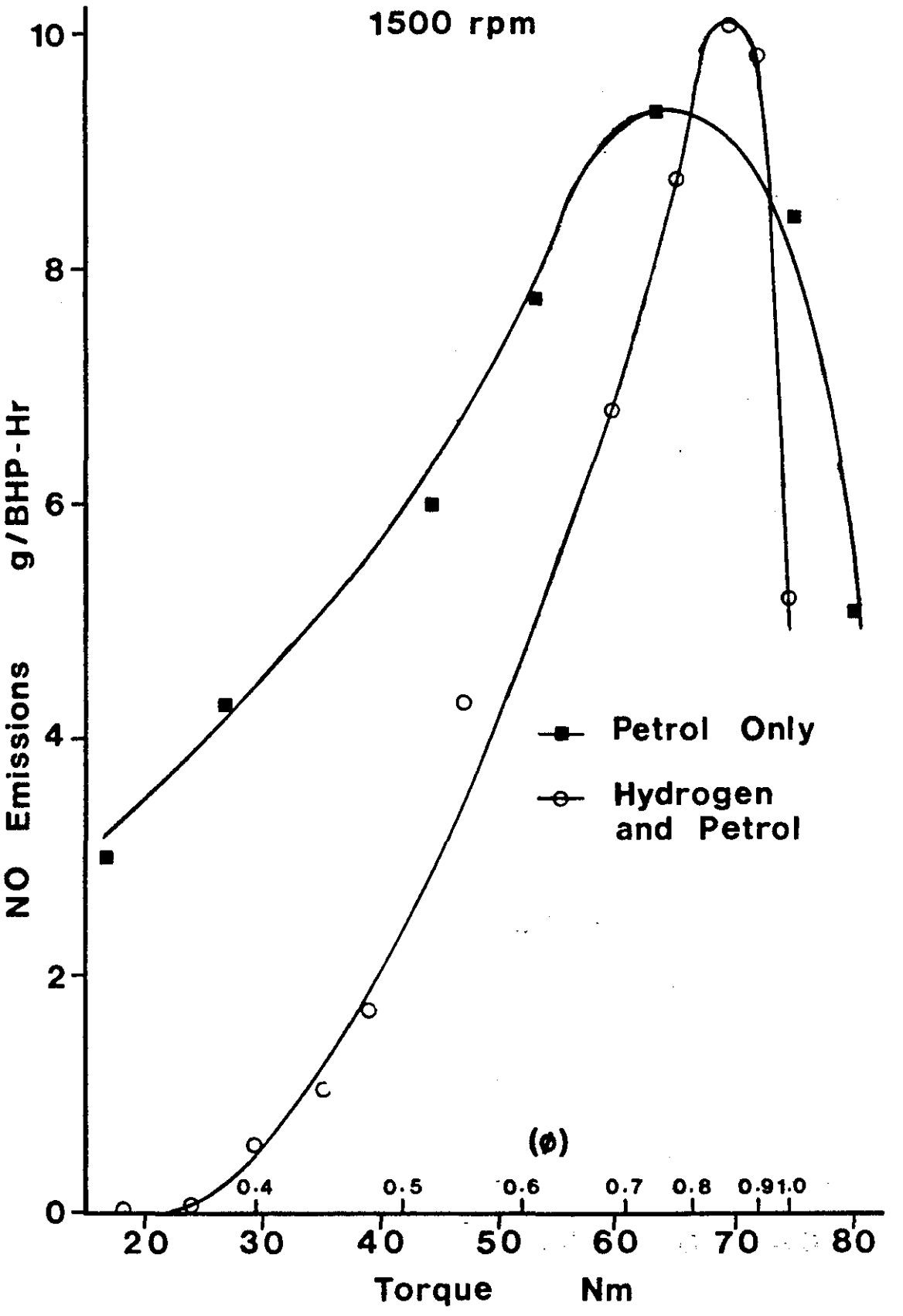

Figure 8.24 **NO Exhaust Emissions**

3000 rpm

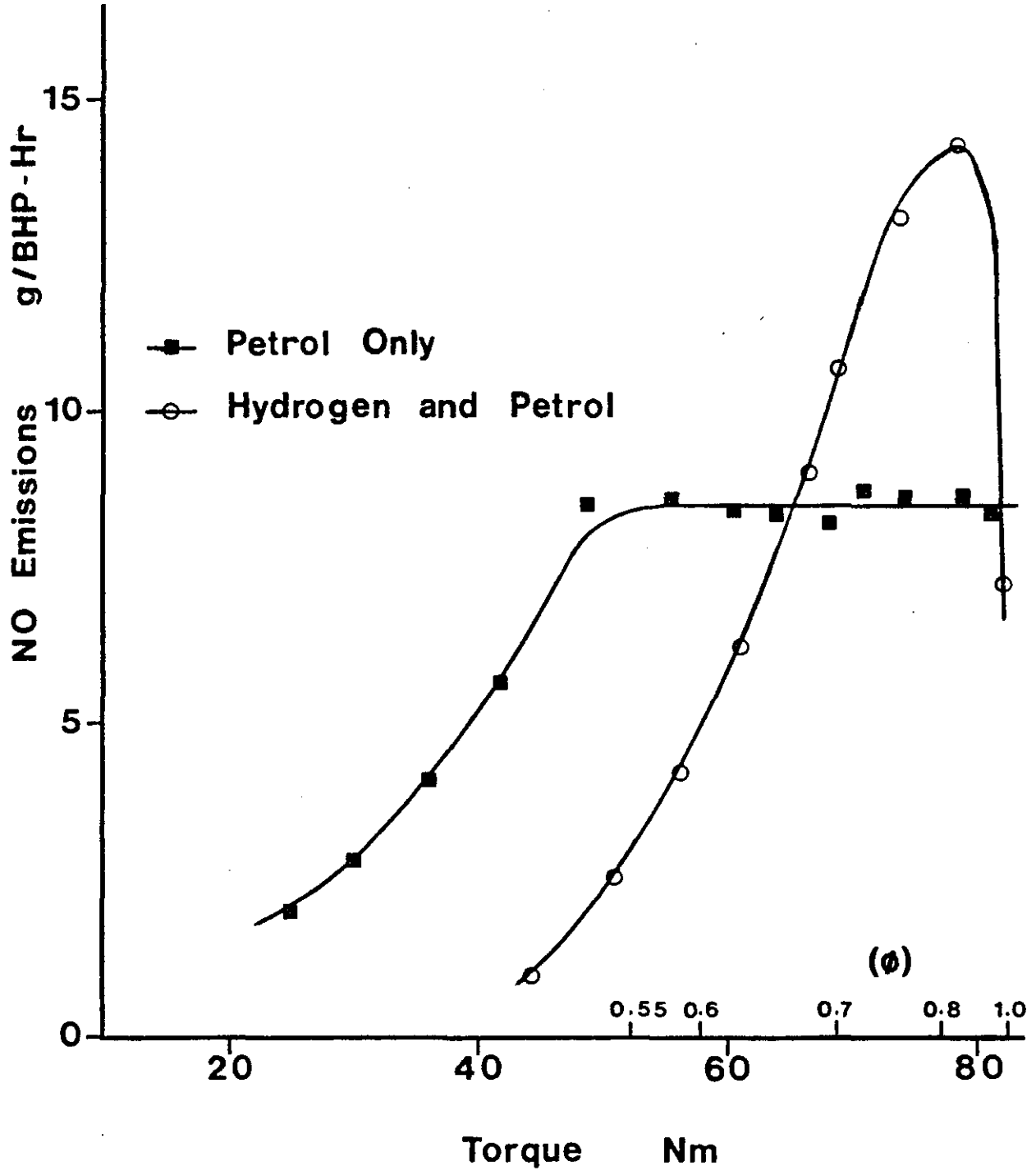

Figure 8.25

Injection Through Spark Plug

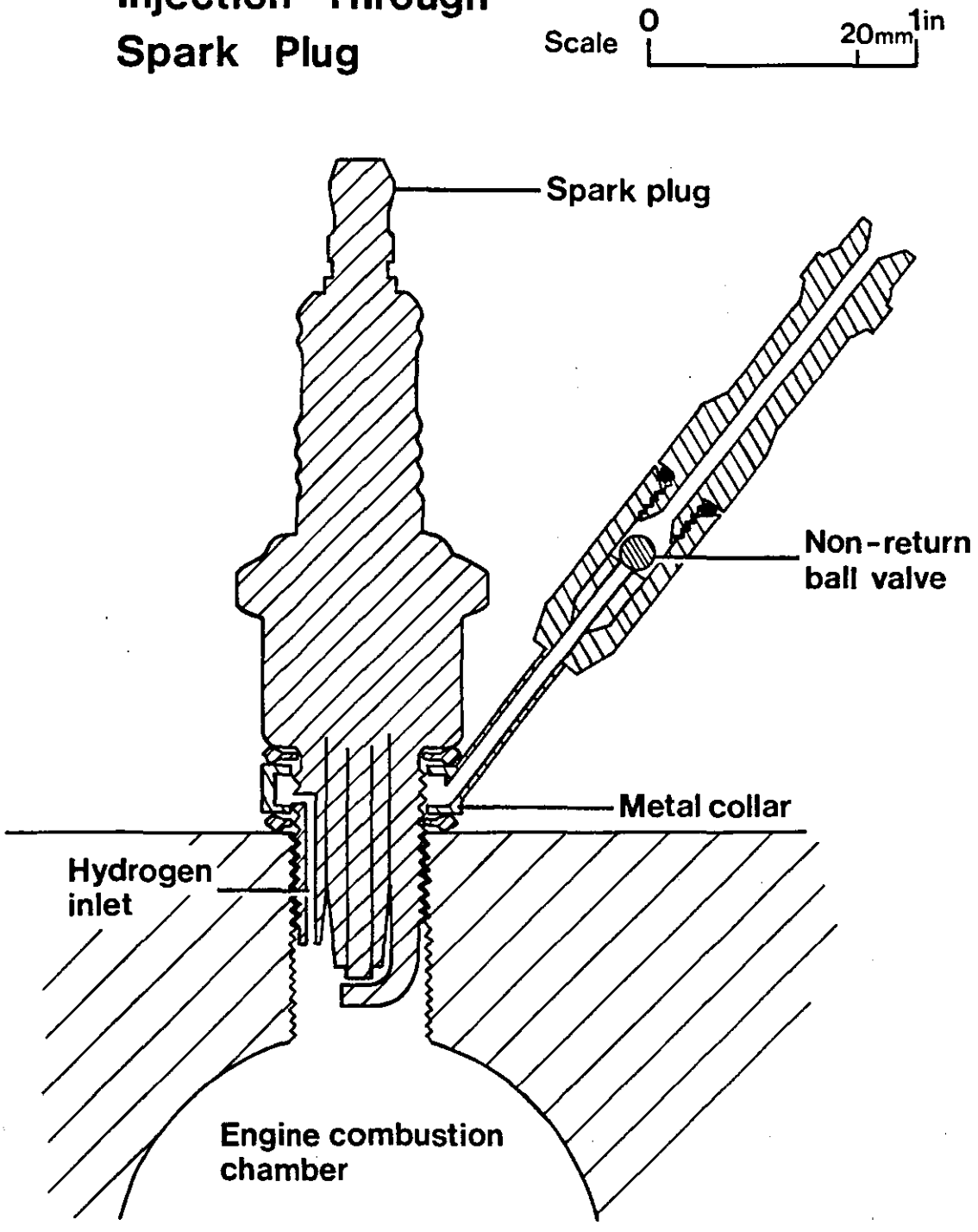

CHAPTER 9

DISCUSSION OF ENGINE TEST-BED RESULTS

CHAPTER 9

The major result illustrated by this investigation is the increase in engine efficiency at part-load when dual-fuel mixtures are used. This is shown by the decrease in specific fuel consumption when hydrogen/petrol mixtures are used (figures 8.5-9), or conversely by the increase in brake thermal efficiency shown in figures 8.10-14.

Increased engine efficiency is due to the use of much leaner mixtures, as well as a higher flame speed for the dual-fuel mixture. Under normal petrol operation with the carburettor, the mixture strength is very close to stoichiometric, resulting in maximum combustion temperatures throughout the load range. Thus heat loss to coolant will be substantially the same at low loads as at high loads, resulting in a significantly greater fraction of the fuel energy being lost to coolant at low loads. However, with dual-fuel operation at wide open throttle, the mixture strength is much leaner at low loads resulting in lower combustion temperatures. Hence the heat loss to coolant is lower and the thermal efficiency higher for hydrogen-petrol mixtures compared to carburetted petrol operation. The lower combustion temperatures would also result in a lower energy loss to exhaust, indicated by a lower exhaust temperature, but for an increase in air flow rate. These are indicated in the energy balance curves shown in figures 8.15 and 8.16.

It has also been indicated[93] that lean mixture operation will result in an increase in efficiency due to a change in the ratio of specific heat. The reduced cycle temperatures lead to much higher values of γ, the ratio of specific heats.

The increase in air/fuel ratio due to lean mixture operation also results in higher values for the ratio of specific heats.[94] Since the air standard efficiency for the Otto cycle is defined by

$$\text{Efficiency} = 1 - \frac{1}{r_v^{\gamma-1}}$$, where r_v is the compression ratio,

an increase in γ leads to an increase in efficiency. Figure 8.17 indicates the increase in efficiency at part load resulting from the change in the ratio of specific heats. The effect of the increase in air/fuel ratio, and the lower cycle temperature are both indicated.

The maximum power output of the engine is slightly lower (1-2%) when running on dual-fuel mixtures, due to the displacement of some of the incoming air by hydrogen. At stoichiometric mixtures, the petrol vapour occupies approximately two percent of the chamber volume, whereas hydrogen occupies nearly thirty percent of the volume.

As can be seen in figures 8.5-9, there is a marked increase in specific fuel consumption at equivalence ratios less than $\emptyset = 0.5$ corresponding to low load operation. An engine will run satisfactorily on pure hydrogen at equivalence ratios as low as $\emptyset = 0.3$, but as the petrol fraction is increased, so the lean extinction limit also increases. Two methods were used to operate the engine at low loads. The first was to increase the hydrogen flow rate slightly to 0.089 g/sec, resulting in a lower lean extinction limit. Thus the specific fuel consumption is less at low loads than when using a smaller hydrogen flow rate, as illustrated in figure 8.6. However,

the maximum torque at any given speed is reduced still further, again due to displacement of the intake air by the increased flow of hydrogen. The second method of operating at low loads was to slightly close the throttle. Again this resulted in a reduction in maximum power output, but the improved combustion at low loads resulted in an improvement in specific fuel consumption compared to wide open throttle operation. In practice, better specific fuel consumption is achieved with a partially closed throttle at low engine speeds (corresponding to low road load), than with a wide open throttle, as illustrated in figure 8.3. It is to be emphasised that the throttle opening at a given load setting is much greater when running on dual-fuel mixtures than with standard carburettor operation using petrol only.

The substantial improvement in thermal efficiency can be seen in figures 8.10-14, and reductions in specific fuel consumption of up to thirty percent are illustrated in figures 8.5-9. As all these results are comparing equivalent fuel energies, any comparison of specific fuel consumption on a mass basis will indicate an even greater fuel saving.

Figure 8.18 shows the effect of greatly increasing the hydrogen flow rate. Operation throughout the load range using a dual-fuel mixture was possible at a wide open throttle setting. The torque consumption loops at various throttle angles, using petrol only, are also shown for comparison. These were obtained by altering the petrol flow rate at each throttle setting, going from a very rich mixture to one so weak the engine was on the verge of stalling.

Another means of improving the performance of the engine by utilizing hydrogen's combustion properties was to increase the compression ratio from the standard 8.9:1 up to 11.7:1, using different pistons. As the flame speed of hydrogen is greater than that of petrol, this could be done without encountering the problem of knock. However, for hydrogen petrol mixtures, occasional "pinking" did occur, depending on ignition timing. The improvements in specific fuel consumption and thermal efficiency when the higher compression ratio was used are shown in figures 8.6 & 8.11 respectively. Using the higher compression ratio, one had the additional advantage of no decrease in maximum power output at full load. The use of a higher compression ratio also resulted in increasing the air standard efficiency of the engine. The combination of these factors resulted in brake thermal efficiencies of up to thirty-one percent, compared with approximately twenty-seven percent when a lower compression ratio was used with petrol alone.

Another significant advantage observed when dual-fuel mixtures were used is that of reduced noxious exhaust emissions during part-load operation. Other workers[95][96] have also shown mixtures of hydrogen and petrol produce significantly less noxious gases. However, these mixtures have been those produced from the parent fuel on board, or the hydrogen petrol mixture has been throttled to take the engine through its load range. Consequently, the exhaust emissions were monitored in this study to determine if wide open throttle operation also resulted in a decrease in emissions.

Figures 8.19 & 8.20 show the carbon monoxide emissions of petrol compared with those of the dual-fuel mixture at engine speeds of 1500 rpm and 3000 rpm. In both cases the level of output is considerably less, when dual-fuel mixtures are used, the main reason being the mixture strength is much weaker since a wide open throttle is being used at all times. This results in almost complete oxidation of any carbon monoxide produced during combustion by the large excess of oxygen present.

The hydrocarbon output, measured as hexane, is plotted in figures 8.21 & 8.22. There is no significant difference in hexane level between dual-fuel and petrol operation throughout most of the load range. However, at low loads the hydrocarbon level is much greater when hydrogen petrol mixtures are used, due to the lean extinction limit of the mixture having been approached, resulting in some engine misfire occurring. It is also possible that as the combustion temperatures are lower, a greater quench layer will exist inside the chamber, thus contributing to increased hydrocarbon emissions. As the exhaust temperature is lower with dual-fuel operation, there will be less after-burning of hydrocarbons in the exhaust. This is undoubtedly also a contributing factor to the hydrocarbon increase.

Figure 8.23 & 8.24 show the nitric oxide emissions, again at engine speeds of 1500 rpm and 3000 rpm. In both cases the peak of the nitrogen oxide curve occurs slightly on the lean side of the stoichiometric mixture, corresponding to the maximum combustion temperature. However, the combustion temperature of the dual-fuel mixture is much cooler away from this peak than the corresponding load setting with throttled operation using petrol. This results in much lower values of nitric oxide at part-load operation with hydrogen and petrol. The slight increase in peak NO_x emissions

when dual-fuel mixtures are used is due to the increase in maximum cycle temperature, possibly enhanced by a faster combustion rate.

The emission levels of hydrogen petrol mixtures were also measured with the engine at a compression ratio of 11.7:1. These results were almost identical to those at the lower compression ratio, with the exception of a reduced nitrogen oxide peak. The reason for this is a lower combustion temperature caused by a smaller ignition advance. If the ignition timing was set to the minimum advance required for best torque, slight pinking was observed, so a somewhat retarded setting was used, resulting in reduced cycle temperatures.

CHAPTER 10

MODIFICATIONS TO VEHICLE TO RUN IN DUAL-FUEL MODE

CHAPTER 10

The test-vehicle, illustrated in the frontespiece, was designed to be operated either in the dual-fuel hydrogen-petrol mode, or on petrol only using the carburettor as normal. As a consequence, many design changes were made which would not be necessary on a vehicle operating solely on a dual-fuel basis. Only those changes required for dual-fuel operation will be discussed here.

10.1 HYDROGEN STORAGE SYSTEMS

For all initial work, hydrogen was stored as a compressed gas in a cylinder in the rear of the vehicle. The cylinder contained 7221 litres or 627 grams of hydrogen, at a pressure of 17 MPa (2500 psi). For reasons of safety, and for rapid replacement, the cylinder was secured in a specially manufactured rack, securely bolted to the floor of the vehicle. The hydrogen was fed through a standard pressure regulator, capable of withstanding pressures up to 27.2 MPa (4000 psi) and then through a flame trap and a cut-off solenoid. The flame-trap isolates the cylinder should a sudden pressure-pulse be detected. This would be the case if a hydrogen flame was travelling in the line. The cut-off solenoid operates in a normally closed position, and is only opened if a pulse is received from the engine. Details of the circuit are given in figure 10.1. Thus, the solenoid will only allow hydrogen to flow if the engine is running. In practice, at speeds above 80 rpm hydrogen begins to flow, which allows the starter motor to draw hydrogen through to the engine.

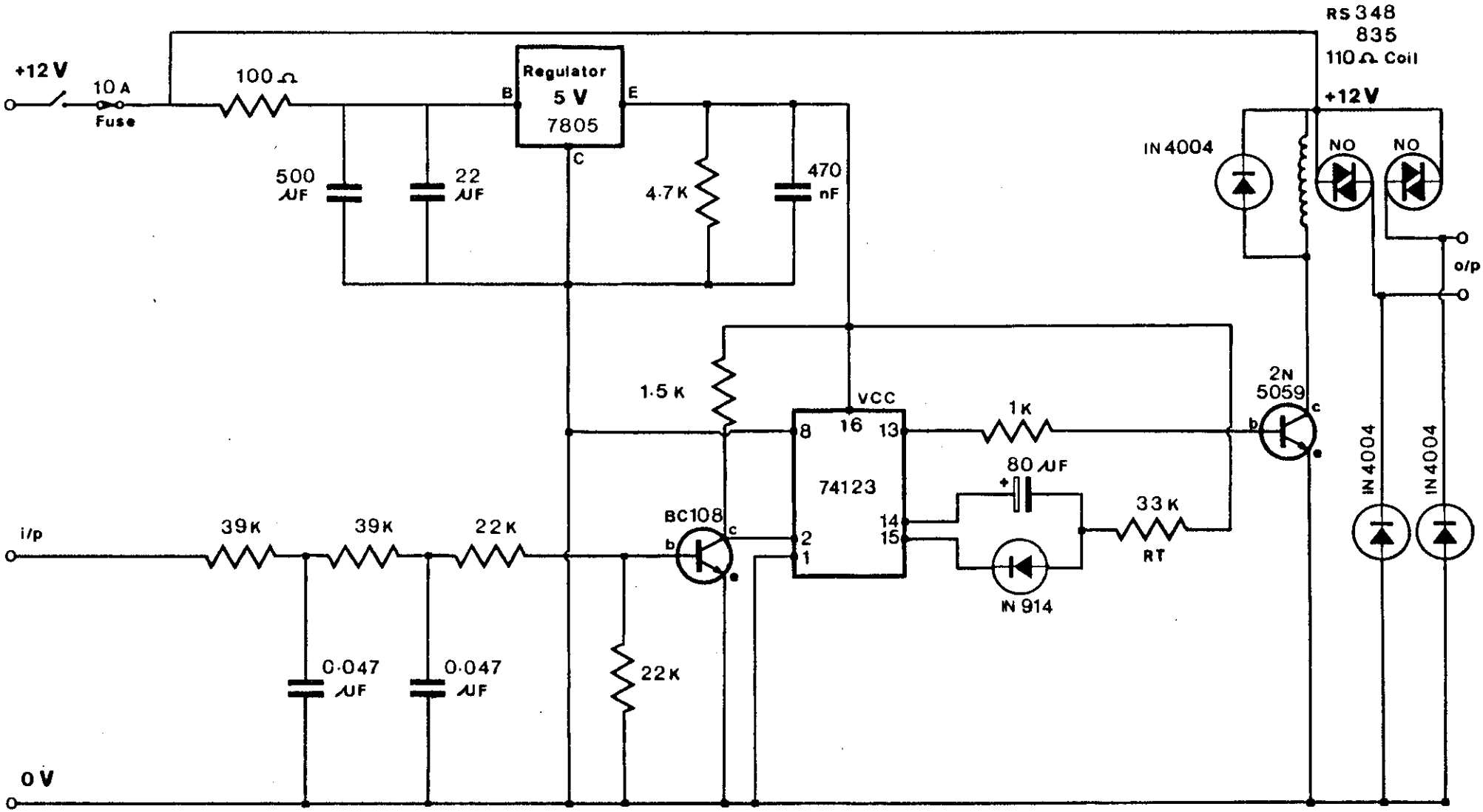

Figure 10.1 Fuel Cut Out Circuit

A similar safety system is intended for use with hydrogen stored in mischmetal-nickel hydride beds. An example of the hydride beds used is illustrated in figure 10.2. A heat exchange unit was manufactured to utilize cooling water from the engine to heat the hydride up to a temperature of approximately 50°C. This corresponds to a dissocation pressure of 0.46 MPa (66 psi) which can then be reduced to a convenient working pressure using a regulator. Figure 10.3 shows the hydride bed installed in the vehicle.

The hydrogen was fed into the engine at a constant rate through a brass adaptor fitted into the intake tract immediately downstream from the carburettor. The adaptor had six inlet holes drilled circumferentially to allow a uniform stream of hydrogen from all directions into the air tract.

The hydrogen pressure in the bed could be controlled by a thermostat valve in the coolant line. Thus the bed could be regulated at a particular temperature, corresponding to a particular dehydriding pressure for the hydride.

10.2 DUAL-FUEL OPERATION

Due to the difficulties involved with controlling petrol flow rates using a needle valve on a moving vehicle, an electronically controlled injector was used for this purpose. As there is a much greater air-flow rate at all engine speeds, a normal carburettor was not satisfactory for controlling petrol consumption, especially so as the petrol flow rate is related to engine load as well as engine speed when the vehicle is operating in a dual-fuel mode. Similarly,

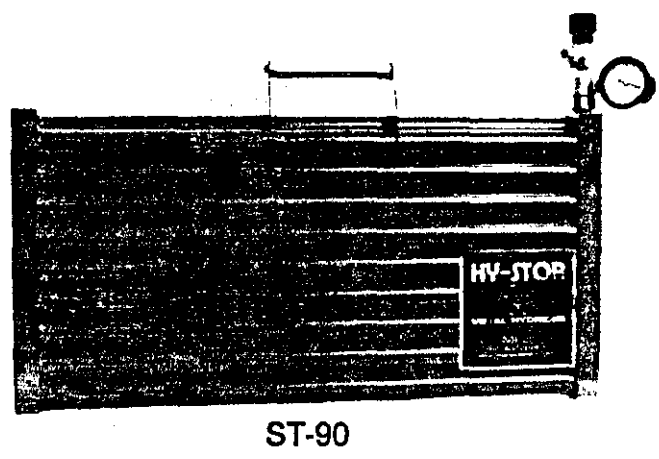

FIGURE 10.2

ST-90 Hydrogen Storage Unit

Ref: Ergenics (88)

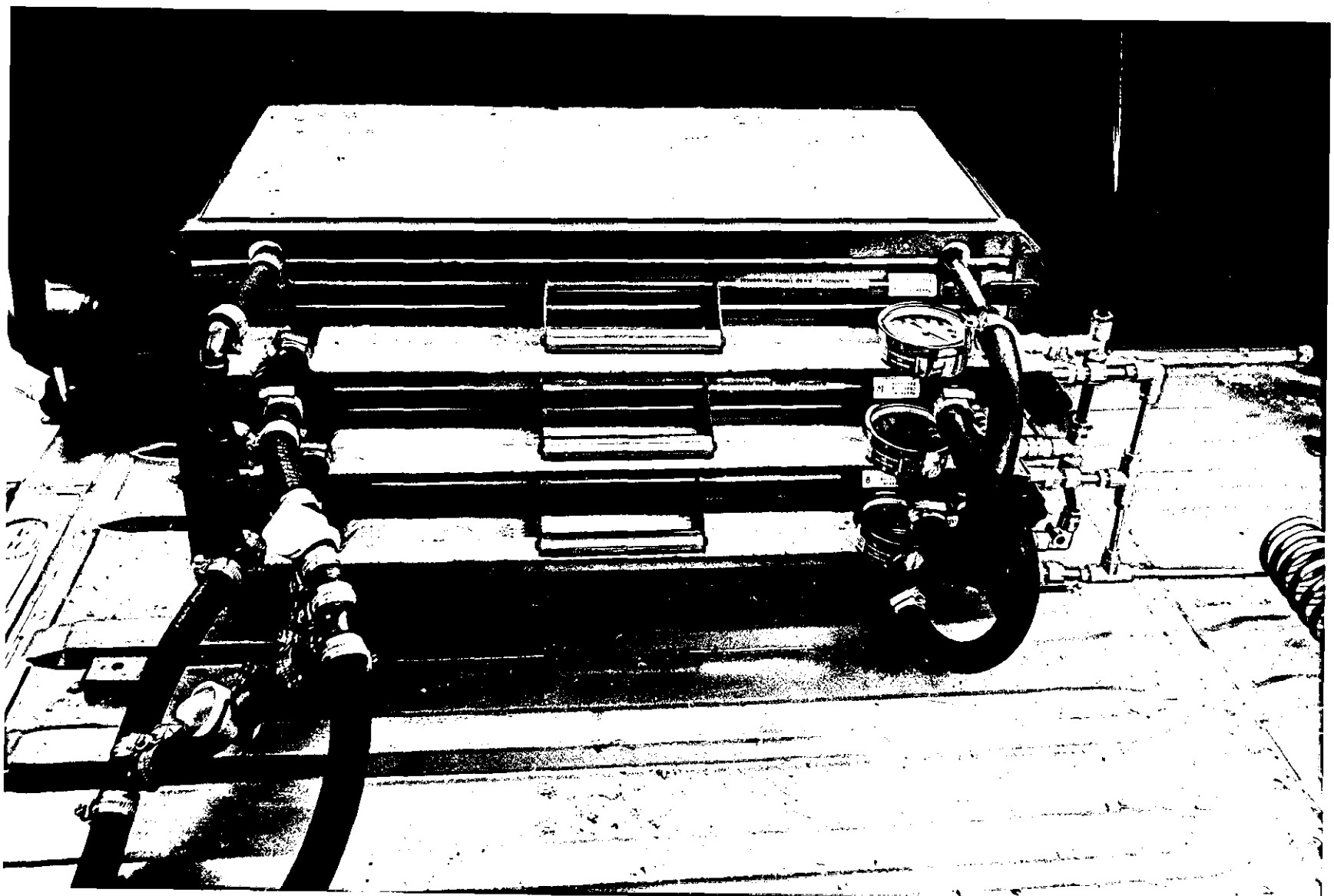

Figure 10.3 Installed Hydride Bed

a needle valve controlled by accelerator pedal position would deliver too much petrol under high load operation at low engine speeds.

The electronic control system used was designed to give an increasing petrol flow rate with increasing engine speed and with increasing load, but the maximum amount of petrol at any given speed was governed to allow a maximum mixture strength of $\emptyset = 1.2$. The amount of petrol admitted at any engine speed had previously been measured at wide-open throttle conditions throughout the speed range with petrol only operation using an identical engine on a test-bed. The control unit for the injector was then designed to allow no more than the maximum petrol flow rate at each engine speed. This was achieved by using an electronic pulse from the engine to open the injector. Thus, it opened twice as frequently at 4000 rpm than at 2000 rpm. The injector opening time was controlled by a variable potentiometer. This in turn was operated by the accelerator pedal. Hence at any given engine speed the petrol flow rate could be varied from zero to a pre-set maximum. This maximum could also be varied by another potentiometer, fixed to the vehicle's instrument panel, should the mixture be too rich or too weak. A circuit diagram for the control system is given in figure 10.4.

10.2.1 Circuit Description of Injector Control Unit

The pulse generation and control section of the circuit produces a negative going pulse on arrival of each positive going pulse from the contact breaker points via the limiting circuit. The duration of this negative pulse (and hence injector opening time) is controlled

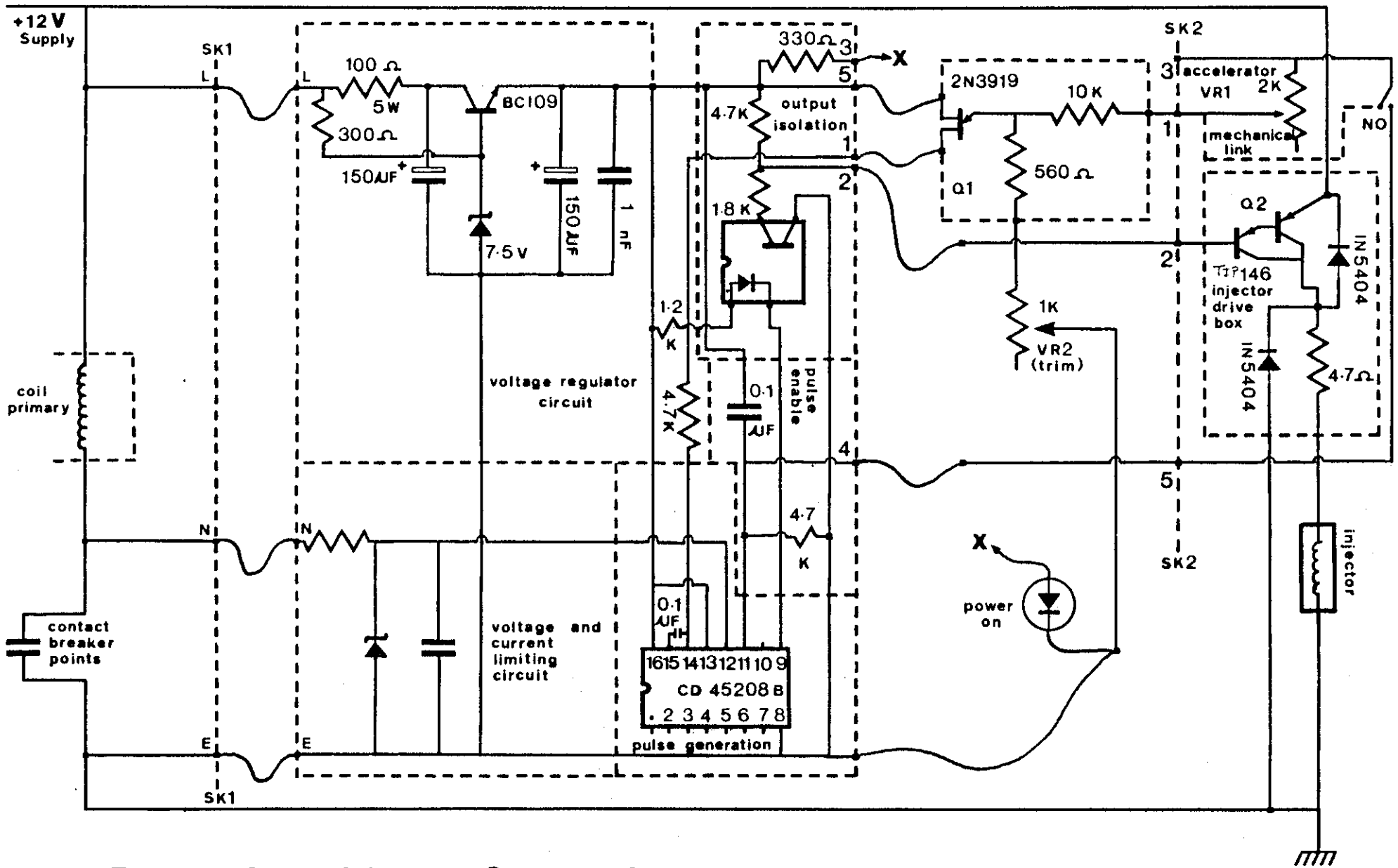

Figure 10.4 Injector Control Circuit

by "accelarator" and "trim" controls via Q_1, a field emitting transistor, shown in figure 10.4.

The pulse enable circuit incorporates a micro-switch attached to the accelerator potentiometer, to ensure the injector does not deliver any petrol (by keeping the injector closed) when the accelerator petrol is not depressed. This circuit also has components to supress spurious triggering during operation of the switch, and to stop interference pick-up on the open switch contact.

The function of the output isolation part of the circuit is to enable the pulse from the pulse generator to be passed to the injector drive circuit (which is attached directly to the engine battery supply) without picking up interference.

The drive box circuit takes the negative going pulse from the output isolation circuit and converts it to a positive going pulse appearing at the injector. The current requirements of the injector are high (approximately 1.5 amps on opening) and a Darlington pair device is employed as Q_2.

The diodes across the injector and Q_2 are to prevent the appearance of reverse voltages when the injector closes. A ballast resistor is also incorporated in the circuit to limit the surge current when the injector is turned on.

The voltage regulator part of the circuit provides a steady voltage supply of approximately 6.8 volts regardless of the engine battery condition, provided that this does not fall below 9.0 volts.

This circuit also inhibits the transmission of interference voltages, from other devices, picked up on the engine supply rails to the remainder of the circuits. The "power on" LED indicates that the regulated supply is present.

The voltage and current limiting section of the circuit is required since the voltages occurring at the secondary of the engine coil are far in excess of those that could be supplied directly to the controlling circuitry. The components in this section of the circuit are arranged to limit the signals appearing at the trigger input of the pulse controller, and also to inhibit spurious triggering from interference.

10.2.2 Petrol Supply

Since much of the operating regime of the vehicle is with a wide-open throttle, a vacuum pump was required to operate the servo-assist mechanism of the brake-boost due to a lack of inlet manifold depression. The installation of an engine-driven vacuum pump necessitated the removal of the petrol pump. This was replaced with a high pressure electric pump, similar to that mentioned in chapter seven. A high pressure petrol pump (up to 40 psi) was also required for the petrol injector to provide an adequate vapour spray. A pressure regulator and a petrol filter were also incorporated in series with the petrol pump.

At low loads, the hydrogen/petrol flow was too low to maintain good combustion using a wide-open throttle. Thus a system was devised whereby the throttle opened progressively at load loads, and was fully

open at approximately one quarter full load. This concept is discussed in detail in the previous chapter.

The petrol injector was mounted in the base of the inlet manifold so petrol was sprayed up into the inlet tract in a direction opposite to that of air flow. It was then found that this mode of operation was not as efficient as the original carburettor, as can be seen from figure 10.5. This shows the specific fuel consumption throughout the load range of the engine at a constant speed of 2500 rpm. One curve is with petrol only using the conventional carburettor, and the other is that obtained with the injector in the manifold. As can be seen, this is approximately thirty percent less efficient.

The reason for this decrease in efficiency is believed to be due to the strong spray of petrol from the injector condensing on the walls of the air intake tract, thus leading to poor petrol distribution between cylinders, and a variation in petrol flow from cycle to cycle. Suggested improvements are given in Chapter twelve.

10.3 VEHICLE OPERATION

Due to lack of access to a chassis dynamometer, preliminary measurements of fuel consumption were carried out at 30 $\pm$ 2 indicated miles per hour in both directions along an apparently flat stretch of road. The total distance of the test was 3.13 miles. Before modification

(i.e. when the vehicle was operated using petrol only through the carburettor, although fitted with the hydrogen storage system), the engine used 0.284 kg petrol during the test.When operating in the dual-fuel mode, the engine consumed 0.288 kg petrol, plus 0.0263 kg hydrogen. This correspondends to an increase of 26.7% in total fuel energy used. This disappointing result is attributed to the characteristics of the single injector petrol injection system used.

Long distance tests were performed to estimate the total range of the hydride bed. For satisfactorily smooth operation at idle, the hydrogen flow rate was set to 0.07g/s. This flow rate also ensured smooth operation during urban driving (at speeds $\leqslant$ 30 m.p.h.), whereas a reduced flow rate, although enabling the engine to idle, caused the engine to falter, and in extreme cases, stall. Thus, when the flow of hydrogen from the hydride pack fell below 0.07g/s, the storage system was deemed to be empty. The total time of operation using the three hydride units shown in figure 10.3 was approximately 2 3/4 hours, indicating a total hydrogen storage capacity of approximately 0.7 kg.

It was noted during operation that the equilibrium dissociation pressure of the hydride rose to 240 p.s.i. gauge, indicating a dehydriding temperature of 72°C. It is not appropriate to use the model developed in chapter 4 to predict the maximum flow rate from the vehicle's hydride bed because its properties are different from those assumed in the model. However, use of the model predicts a maximum

rate of hydrogen evolution of some ten times that required by the vehicle, and the higher reaction temperature on the vehicle indicates the actual on-board hydrogen generation rate will be greater still - i.e. more than adequate for dual-fuel operation.

The most significant drawback with regard to "drive-ability" of the vehicle was a reduction in the amount of engine braking. After the throttle pedal was released, a delay of 2-3 seconds was observed before the engine speed dropped. However, apart from this effect, the vehicle performed in a similar manner when operated in a dual-fuel mode as it had when operated on petrol as the sole fuel.

Thus, although the vehicle used significantly more fuel when running on a hydrogen/petrol mixture, it has been shown that a vehicle can be operated using such a dual-fuel mixture, with the hydrogen stored in a metal hydride. It is hoped that in the near future, the use of a multi-injector fuel injection system will enable significant savings in total fuel consumed to be made.

Figure 10.5 **Comparison of Specific Fuel Consumption Using a Carburettor and Petrol Injector**

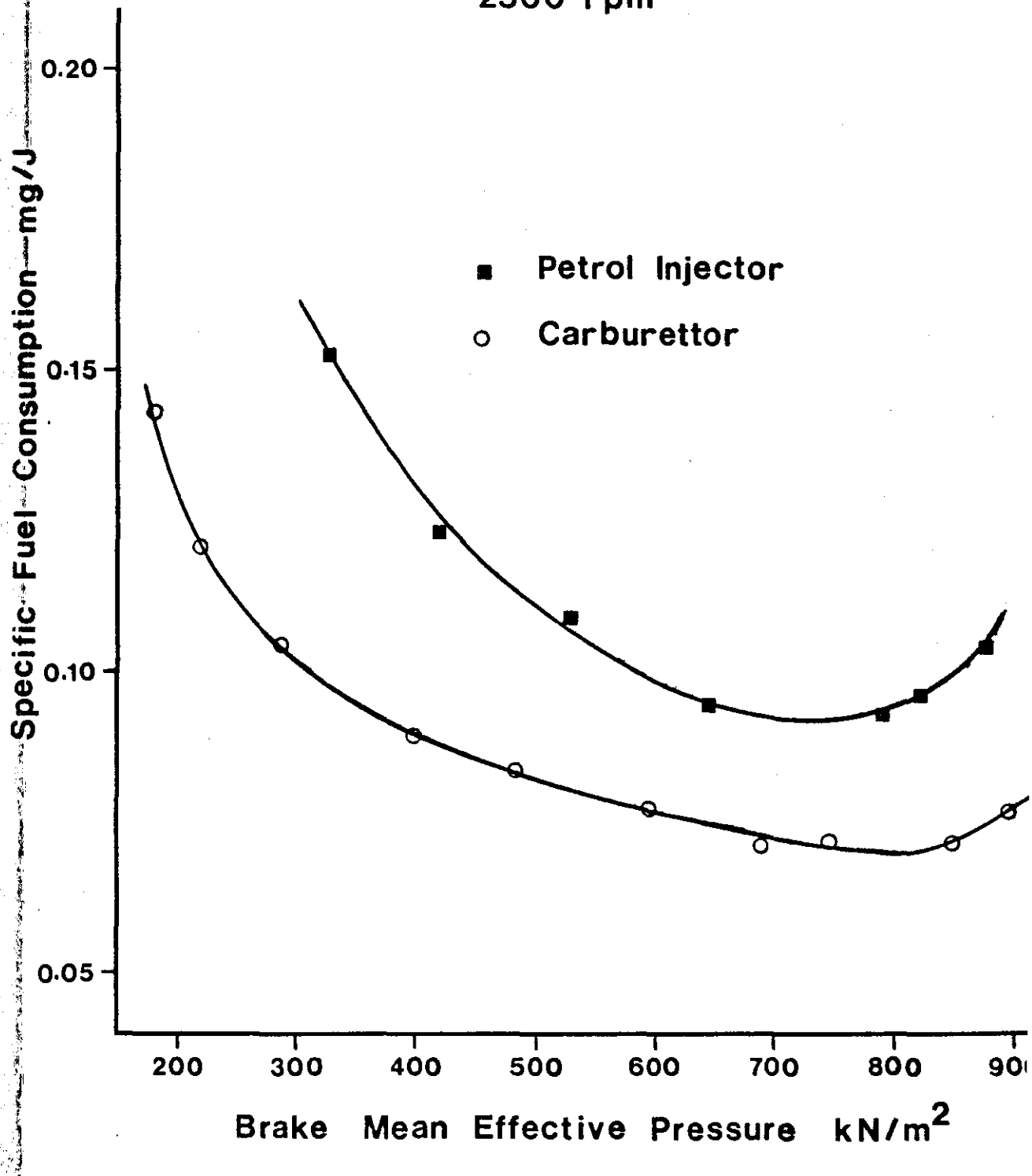

CHAPTER 11

CONCLUSION

CHAPTER 11

CONCLUSIONS

(1) Saline hydrides are not suitable as hydrogen storage media for automotive applications due to the expense and difficulties involved in reprocessing. However, for certain applications (eg - military) they would provide a very compact storage system for generating relatively small amounts (< twenty litres) of hydrogen.

(2) The best practical method of on-board storage of hydrogen is by using metal hydrides which undergo thermal decomposition. These offer the greatest volumetric density of hydrogen stored, and are safer than other storage systems.

(3) The mathematical model developed | indicates | dehydriding (ie - hydrogen desorption) rates for metal hydrides, and can be used to compare desorption rates of different hydrides. It can also be used to predict the effect of differing hydride container dimensions, and to give an indication of the rate of hydrogen absorption (ie - hydriding times). However, the heat requirements predicted for various hydrides will only be accurate if the waste heat recoverable from the engine exceeds the heat of reaction of the hydride. For dual-fuel operation, where hydrogen consumption rates are lower than those for hydrogen only operation, cylinder dimensions could be larger without incurring any penalty to the rate of hydrogen production. These would

result in greater hydride/container weight ratios thus giving more compact, lighter hydrogen storage units. Of the low temperature hydrides (those which have hydrogen desorption pressures of one atmosphere at temperatures below 25^{o}C) for which thermal conduction data are available, the best, regarding hydrogen reaction kinetics, are those of the $RENi_5$ - H type, where RE is lanthanum or a combination of rare earth metals. These hydrides are also less susceptible to poisoning by impurities in the hydrogen gas.

(4) Dual-fuel operation using both hydrogen and petrol offers a means of avoiding the problem of flash-back into the intake manifold, and reducing the problem of on-board storage of hydrogen. Dual-fuel operation also results in greater part-load thermal efficiencies due to wide-open throttle operation being possible throughout the load range, and a reduction in carbon monoxide and nitric oxide exhaust emissions at part-load.

(5) A vehicle can be operated satisfactorily in the dual-fuel mode, with suitable modifications to the intake system, using a metal hydride as the hydrogen storage medium.

CHAPTER 12

FUTURE WORK

CHAPTER 12

FUTURE WORK

(1) Hydrogen absorption and desorption rates should be measured for a variety of selected hydrides, with particular regard to measuring thermal conduction properties.

(2) Hydrogen injection directly into the cylinder should be investigated further to determine if satisfactory operation of the injector system is possible over a long term.

(3) A detailed study of the combustion process using hydrogen/petrol mixtures should be carried out. This would involve the measurement of flame speeds and maximum cycle pressures and temperatures under varying operating conditions.

(4) A microprocessor controlled ignition system should be developed to ensure optimum spark timing for varying hydrogen/petrol mixtures at differing loads and engine speeds.

(5) The petrol injection control system should be optimized to give better fuel consumption. This would involve measuring the air flow, engine speed, and driver requirements to ensure the ideal petrol flow rate. The actual injector system should also be modified to have four injectors, one for each cylinder, thus avoiding the problem of petrol condensation in the intake tract, and uneven distribution of fuel to different cylinders.

REFERENCES

1 E E WIGG and R S LUNT
Methanol as a Gasoline-Extender - Fuel Economy, Emissions, and High Temperature Driveability.
SAE Paper 741008, 1974.

2 D S ADAMS
Electric Road Vehicles - Their Short and Long Term Future.
Transport and Road Research Laboratory Symposium on Energy and Road Transport, April 1978.

3 H M SPIERS
Technical Data on Fuels.
British National Committee World Power Conference, 6th ed, p 260, 1961.

4 H BUCHNER and R POVEL
The Daimler-Benz Hydride Vehicle Project.
International Journal of Hydrogen Energy, Vol 7, No 3, pp 259-266, 1982.

5 K M MACKAY
The Element Hydrogen.
Comprehensive Inorganic Chemistry, Vol 1, Chapter 1, p 3.
Pub Pergamon Press, Oxford, 1973.

6 A P FICKETT and F R KALHAMMER
Water Electrolysis.
Hydrogen: Its Technology and Implications Vol 1: Production Technology Chapter 1.
Published CRC Press, Inc 1979.

7 A MENTH and S STUCKI
Present State and Outlook of the Electrolytic H_2-Production Route.
Hydrogen Energy System: Proceedings of the 2nd World Hydrogen Energy Conference, Zurich, 1978.
Edited: T N Veziroglu and W Seifritz, Published Pergamon Press, 1979.

8 J N MURRAY and M R YAFFE
High Efficiency Alkaline Electrolysis Technology.
14th Intersociety Energy Conversion Engineering Conference, Boston, Massachusetts, Paper 799155, 1979.

9 G KISSEL, P W T LU, M H MILES and S SRINIVASAN
Hydrogen Production by Water Electrolysis - Methods for Approaching Ideal Efficiencies.
10th Intersociety Energy Conversion Enineering Conference, 1975.

10 L J NUTTALL
Development Status of the General Electric Solid Polymer Electrolyte Water Electrolysis Technology.
16th Intersociety Energy Conversion Engineering Conference, Paper 819625, 1981.

11 L J NUTTALL and J H RUSSEL
Solid Polymer Electrolyte Water Electrolysis - Development Status.
International Journal of Hydrogen Energy, Vol 5, No 1, pp 75-84, 1980.

12 R I KERMODE
Hydrogen from Fossil Fuels
Hydrogen: Its Technology and Implications, Vol 1: Production Technology Chapter 3.
Published CRC Press, Inc 1979.

13 J E FUNK
Thermochemical Water Decomposition
Hydrogen: Its Technology and Implications, Vol 1: Production Technology Chapter 2.
Published CRC Press, Inc 1979.

14 J E FUNK and R M REINSTROM
Energy Depot Electrolysis Systems Study - System Study of Hydrogen Generation by Thermal Energy.
EDR 3714 United States Atomic Energy Commission 1964.

15 G E BEGHI
Review of Thermochemical Hydrogen Production.
International Journal of Hydrogen Energy, Vol 6, No 6, pp 555-566, 1981.

16 W J GASIONOWSKI, D G JOHNSON, and J B PANGBORN
Suitability of Gas Distribution Equipment in Hydrogen Service.
14th Intersociety Energy Conversion Engineering Conference, Boston, Massachusetts, Paper 799159, 1979.
Published American Chemical Society.

17 G G LEETH
Transmission of Gaseous Hydrogen.
Hydrogen: Its Technology and Implications, Vol 2, Transmission and Storage, Chapter 1.
Published CRC Press, Inc 1979.

18 D P GREGORY ET AL
Prospects for Pipeline Delivery of Hydrogen as a Fuel and as a Chemical Feedstock.
American Gas Association Monthly, Vol 58, November 1976, pp 24-31.

19 F J EDESKUTY and K D WILLIAMSON
Liquid Hydrogen Storage and Transmission.
Hydrogen: Its Technology and Implications, Vol 2: Transmission and Storage, Chapter 3.
Published CRC Press, Inc 1979.

20 W F STEWART and W J D ESCHER
Liquid - Hydrogen Automotive Onboard Storage and Servicing System Project: A Progress Report.
SAE Paper 810351, 1981.

21 W F STEWART and F J EDESKUTY
Liquid Hydrogen as a Vehicular Fuel: An Evaluation.
Mechanical Engineering Vol 103, No 5, May 1981.

22 G D BREWER
The Prospects for Liquid Hydrogen Fuelled Aircraft.
International Journal of Hydrogen Energy, Vol 7, No 1, pp 21-41, 1982.

23 D FRAENKEL and J SHABTAI
Encapsulation of Hydrogen in Molecular Sieve Zeolites.
Journal of the American Chemical Society, Vol 99, No 21, p 7074, 1977.

24 D FRAENKEL and J SHABTAI
The Potential of Zeolite Molecular Sieves as Hydrogen Storage Media.
Alternative Energy Sources - Proceedings Miami International Conference, 1977.

25 F A KUIJPERS and H H van MAL
Sorption Hysteresis in the $LaNi_5$-H and $SmCo_5$-H Systems.
Journal of the Less-Common Metals, Vol 23, pp 395-398, 1971.

26 K C HOFFMAN ET AL
Metal Hydrides as a Source of Fuel For Vehicular Propulsion.
SAE Paper 690232, 1969.

27 J F STAMPFER, C E HOLLEY and J F SUTTLE
The Magnesium-Hydrogen System.
Journal of the American Chemical Society, Vol 82, p 3504, 1960.

28 J J REILLY and R H WISWALL
The Reaction of Hydrogen with Alloys of Magnesium and Nickel and the Formation of Mg_2NiH_4
Inorganic Chemistry, Vol 7, No 11, p 2254, 1968.

29 J J REILLY
Metal Hydrides as Hydrogen Storage Media and Their Applications.
Hydrogen: Its Technology and Implications, Vol 2, Transmission and Storage Chapter 2.
Published CRC Press Inc 1979

30 H C ANGUS
Rechargeable Metallic Hydrides for Hydrogen Storage.
Physics Technology, pp 245-250, 257, Vol 12, 1981.

31 J J REILLY and R H WISWALL
The Reaction of Hydrogen with Alloys of Magnesium and Copper.
Inorganic Chemistry Vol 6, No 12, p 2220, 1967.

32 J J REILLY
Synthesis and Properties of Useful Metal Hydrides.
Brookhaven National Laboratory Report, BNL23047, 1977.

33 DR O BERNAUER
Daimler Benz - Private Communication, 1982.

34 DR H BUCHNER
The Hydrogen/Hydride Energy Concept.
International Journal of Hydrogen Energy, Vol 3, No 4, pp 385-406, 1978.

35 C E LUNDIN
Hydrogen Storage Properties and Characteristics of Rare Earth Compounds.
Journal de Physique, Colloque C5, Supplement au No 5, Tome 40, Mai 1979.

36 J H N van VUCHT, F A KUIJPERS and H C A M BRUNING
Reversible Room-Temperature Absorption of Large Quantities of Hydrogen by Intermetallic Compounds.
Philips Research Report, Vol 25, pp 133-140, 1970.

37 C E LUNDIN and F E LYNCH
Solid State Hydrogen Storage Materials for Application to Energy Needs.
Final Technical Report AFOSR Contract No F44620-C-0020, Aug 1976.

38 J J REILLY and R H WISWALL
The Higher Hydrides of Vanadium and Niobium.
Inorganic Chemistry Vol 9, No 7, p 1678, 1970.

39 G D SANDROCK
A Survey of the Hydrogen Storage Properties of Nickel-Copper-Mischmetal-Calcium Alloys.
Alternative Energy Sources - International Conference Proceedings, 1977.

40 G D SANDROCK
A New Family of Hydrogen Storage Alloys Based on the System Nickel-Mischmetal-Calcium.
12th Intersociety Energy Conversion Engineering Conference, Paper 779146, 1977.

41 W E GARNER and E W HAYCOCK
The Thermal Decomposition of Lithium Aluminium Hydride.
Proceedings of the Royal Society Series A, Vol 211, No 1106, 1952.

42 E C ASHBY, G J BRENDEL, and H E REDMAN
Direct Synthesis of Complex Metal Hydrides.
Inorganic Chemistry, Vol 2, No 3, p 499, 1963.

43 A KARTY, J GRUNZWEIG-GENOSSAR, and P S RUDMAN
Hydriding and Dehydriding Kinetics of Mg in a Mg/Mg_2Cu Eutectic Alloy: Pressure Sweep Method.
Journal of Applied Physics, Vol 50, 1979.

44 J TOPLER, E LEBSANFT, and R SCHATZLER
Determination of the Hydrogen Diffusion Coefficient in Ti_2Ni by Means of Quasielastic Neutron Scattering.
Journal of Physics F: Metal Physics, Vol 8, 1978.

45 J S RAICHLEN and H DOREMUS
Kinetics of Hydriding and Allotropic Transformation in $SmCo_5$.
Journal of Applied Physics Vol 42, 1971.

46 D G WESTLAKE, C B SATTERTHWAITE, and J H WEAVER
Hydrogen in Metals.
Physics Today, November 1978.

47 E LEBSANFT ET AL
Hydrogen in Iron-Titanium: Experimental Investigations of Structure, Heat of Solution, Diffusion, and Hydriding Kinetics,
2nd World Hydrogen Energy Conference, 1978.

48 R C BOWMAN ET AL
2nd International Congress of Hydrogen in Metals, 1977.

49 K NOMURA, E AKIBA, and S ONO
Kinetics of the Reaction Between Mg_2Ni and Hydrogen.
International Journal of Hydrogen Energy, Vol 6, No 3, pp 295-303, 1981.

50 P S RUDMAN
Hydrogen-Diffusion-Rate-Limited Hydriding and Dehydriding Kinetics.
Journal of Applied Physics, Vol 50, 1979.

51 D L CUMMINGS and G J POWERS
The Storage of Hydrogen as Metal Hydrides.
Industrial Engineering Chemistry: Process Design and Development, Vol 13, No 2, pp 182-192, 1974.

52 W S YU, E SUUBERG, and C WAIDE
Modelling Studies of Fixed-Bed Metal-Hydride Storage Systems.
Brookhaven National Laboratory Report, BNL-18720, 1974.

53 P W FISHER and J S WATSON
Modelling and Evaluation of Designs for Solid Hydrogen Storage Beds.
3rd World Hydrogen Energy Conference, Tokyo, 1980.

54 P W FISHER, and J S WATSON
Modelling Solid Hydrogen Storage Beds.
Oak Ridge National Laboratory Report ORNL/TM-7561, 1981.

55 W D MURRAY and F LANDIS
Transactions of ASME Series C, Vol 81, Part 2, p 106, 1959.

56 G G LUCAS and W L RICHARDS
Mathematical Modelling of Hydrogen Storage Systems.
4th World Hydrogen Energy Conference, Pasadena, Los Angeles, 1982.

57 J R P GIBB and C E MESSER
A Survey Report on Lithium Hydride.
United States Atomic Energy Commission Report NYO-3957, Medford, Massachusetts, 1954.

58 C E LUNDIN and F E LYNCH
Safety Characterisitcs of FeTi Hydride.
10th Intersociety Energy Conversion Engineering Conference, Published Institute of Electrical and Electronic Engineers, New York, 1975.

59 M S NEWKIRK and J L ABEL
The Boston Reformed Fuel Car.
SAE Paper 720670, 1972.

60 J HOUSEMAN and D J CERINI
On-Board Hydrogen Generation for a Partial Hydrogen Injection Internal Combustion Engine.
SAE Paper 740600, 1974.

61 J HOUSEMAN and G E VOECKS
Hydrogen Engines Based on Liquid Fuels, a Review.
3rd World Hydrogen Energy Conference, Tokyo, 1980.

62 H R RICARDO
Further Note on Fuel Research.
Proceedings of the Institution of Automobile Engineers, Vol XVIII part 1, pp 327-341, 1924.

63 R O KING, W A WALLACE and B MAHAPATRA
The Hydrogen Engine and the Nuclear Theory of Ignition.
Canadian Journal of Research, Section F, Vol 26, pp 264-276, 1948.

64 R O KING and M RAND
The Hydrogen Engine.
Canadian Journal of Technology, Vol 33, pp 445-469, 1955.

65 G G LUCAS and L E MORRIS
The Backfire Problem of the Hydrogen Engine,
UNICEG Symposium, London, 1980.

66 R E BILLINGS ET AL
Ignition Parameters of the Hydrogen Engine.
9th Intersociety Energy Conversion and Engineering Conference, 1974.

67 F E LYNCH
Backfire Control Techniques for Hydrogen Fuelled Internal Combustion Engines.
The Hydrogen Economy Miami Energy Conference, Pub Plenum Press, New York, 1974.

68 H C WATSON
Examination of Some of the Engine Design and Fuel Storage Interactions for the Hydrogen Fuelled Car.
Passenger Car Power Plant of the Future Conference, Institute of Mechanical Engineers, London, October 1979.

69 H C WATSON and E E MILKINS
Some Problems and Benefits from the Hydrogen Fuelled Spark Ignition Engine.
SAE Paper 789212, 1978.

70 M R SWAIN and R R ADT
The Hydrogen-Air Fuelled Automobile.
7th Intersociety Energy Conversion and Engineering Conference, Paper 729217, 1972.

71 C A MacCARLEY
A Study of Factors Influencing Thermally Induced Backfiring in Hydrogen Fuelled Engines, and Methods for Backfire Control.
16th Intersociety Energy Conversion Engineering Conference, Paper 819632, Pub American Society of Mechanical Engineers, New York, 1981.

72 C A MacCARLEY and W D VAN VORST
Electronic Fuel Injection Techniques for Hydrogen Powered I C Engines.
International Journal of Hydrogen Energy, Vol 5, No 2, pp 179-203, 1980.

73 J G FINEGOLD ET AL
The UCLA Hydrogen Car: Design, Construction, and Performance.
SAE Paper 730507, 1973.

74 J G FINEGOLD and W D VAN VORST
Hydrogen Engine Performance.
Proceedings of 2nd National Conference on Energy and Environment, 1974, Pub 1975.

75 R L WOOLLEY and D L HENRIKSEN
Water Induction in Hydrogen-Powered I C Engines.
International Journal of Hydrogen Energy, Vol 1, pp 401-412, 1977.

76 M R SWAIN ET AL
Hydrogen-Fuelled Automotive Engine: Experimental Testing to Provide an Initial Design-Data Base.
SAE Paper 810350, 1981.

77 J B FINEGOLD and W D VAN VORST
Engine Performance with Gasoline and Hydrogen: A Comparative Study.
The Hydrogen Economy Miami Engineering Conference, Pub Plenum Press, New York, 1974.

78 G G LUCAS and W L RICHARDS
A Hydrogen-Petrol Dual Fuel Engine.
SITEV Symposium (Institute of Mechanical Engineers), Geneva, May 1980.

79 G G LUCAS and W L RICHARDS
The Hydrogen/Petrol Engine - The Means to Give Good Part-Load Thermal Efficiency.
SAE Paper 820315, 1982.

80 A N PODGORNY and A I MISHCHENKO
Hydrogen Application to Gasoline Automotive Engines.
3rd World Hydrogen Energy Conference, Tokyo, 1980.

81 I L VARSHAVSKII, A I MISHCHENKO, and V YU STEPANOV
Low-Pollutant Automobile.
Zashch Vozdushn Basseina Zagnyaz Toksichnymi: Vybrosami Transp Sredstv, Dokl, Vses Nauchn Konf 1977.

82 R F STEBAR and F B PARKS
Emission Control with Lean Operation Using Hydrogen-Supplemented Fuel.
SAE Paper 740187, 1974.

83 J S MACDONALD
Evaluation of the Hydrogen-Supplemented Fuel Concept with an Experimental Multicylinder Engine.
SAE Paper 760101, 1976.

84 K S VARDE
Combustion Characteristics of Small Spark Ignition Engines Using Hydrogen Supplemented Fuel Mixtures.
SAE Paper 810921, 1981.

85 H BUCHNER and R POVEL
The Daimler-Benz Hydride Vehicle Project.
International Journal of Hydrogen Energy, Vol 7, No 3, pp 259-266, 1982.

86 J S CHATTERJEE and P SOM
An Alternative Fuel for Cars.
Electronics and Power, pp 528-529, August 1976.

87 W G TASCHEK
Miniature Hydrogen Generator.
U S Patent 4,155,712, May 1979.

88 Ergenics Division
ST90-B Hydrogen Storage Unit Instruction Manual.
MPD Technology Corporation, 1981.

89 F E LYNCH
Operating Characteristics of High Performance Commercial Metal Hydride Heat Exchangers.
Journal of the Less-Common Metals, Vol 74, pp 411-418, 1980.

90 P D GOODELL
Thermal Conductivity of Hydriding Alloy Powders and Comparisons of Reactor Systems.
Journal of the Less-Common Metals, Vol 74, pp 175-184, (1980).

91 Handbook of Chemistry and Physics.
Pub CRC Press, Cleveland, Ohio.

92 A B GREENE and G G LUCAS
The Testing of Internal Combustion Engines.
EUP, 1969.

93 J H WEAVING and W J CORKHILL
British Leyland Experimental Stratfied Charge Engines.
Institute of Mechanical Engineers Conference on Stratfied Charge Engines, November 1976.

94 G G LUCAS
Thermodynamic Properties of Exhaust Gas - Gas Turbines and Multi-Fuel Engines.
Engine Design and Applications, December 1965.

95 K SJOSTROM, S ERIKSSON, and G LANDQUIST
On-Board Hydrogen Generation for Hydrogen Injection into Internal Combustion Engines.
SAE Paper 810348, 1981.

96 F B PARKS
A Single-Cylinder Engine Study of Hydrogen-Rich Fuels.
SAE Paper 760099, 1976.

97 L E MORRIS
PhD Thesis, Loughborough University, To be Published.

98 G A KARIM and S R KLAT
The Measurement of the Mass Flow Rate of Different Gases Using a Choked Nozzle.
Laboratory Practice, Vol 15, No 2, pp 184-186.

99 The Analytical Development Co Ltd, Salisbury Road, Rye Park, Hoddesden, Hertfordshire.
Instruction Manual for Operation and Service of Infra-Red Gas Analyzer - 200 Series. August 1970.

APPENDIX (i)

THE MEASUREMENT OF HYDROGEN FLOW RATES USING A CHOKED SONIC NOZZLE

To accurately measure the mass flow rate of hydrogen, a series of choked sonic nozzles was used. These had previously been manufactured and calibrated by L E Morris[97]. As any given nozzle is only effective for a given upstream pressure range, three sonic nozzles were constructed to cover the range required. The throat diameters used are 0.005"; 0.020"; and 0.025". The entry profile to the throats is shown schematically in figure 1, and is as near as possible to a quarter circle. The parallel section of the throats was kept to less than the throat diameter, ie

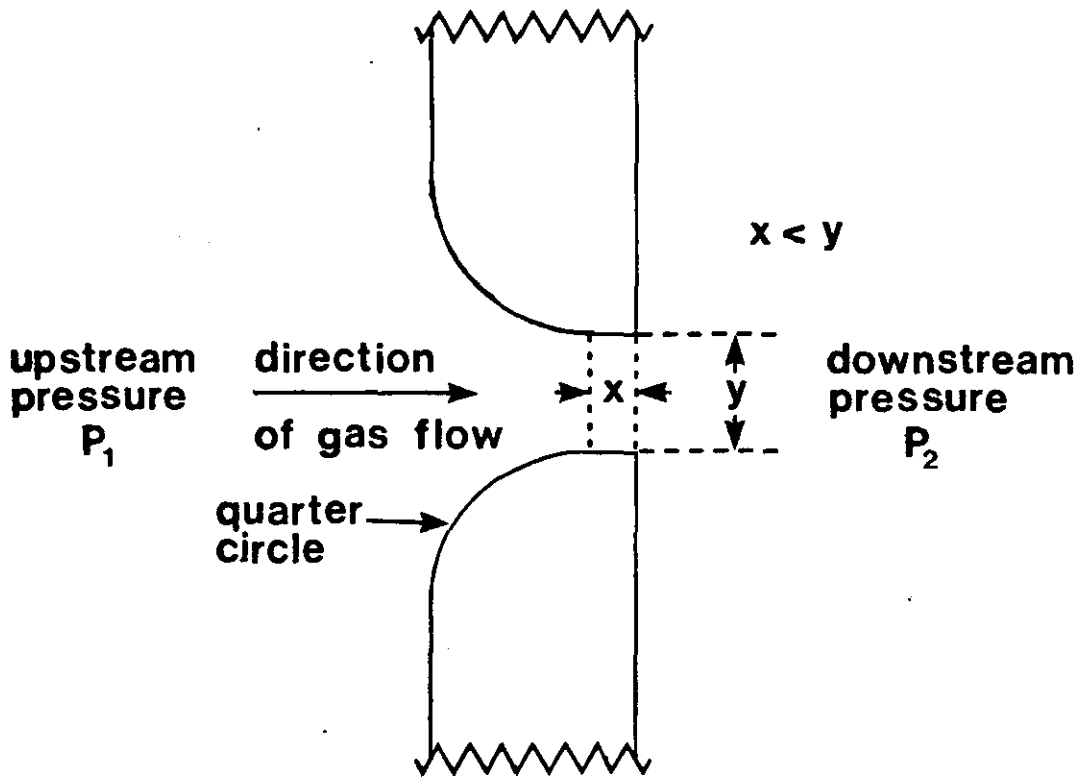

Figure A(i).1 Schematic diagram of nozzle throat

Principle of Operation

When the ratio of the absolute downstream pressure, P_2, to the absolute upstream pressure, P_1, is reduced below a certain critical value (Pc = 0.528 for hydrogen), the velocity of the gas flow through the nozzle is equal to the velocity of sound under the conditions prevailing at the throat.

Further reduction of the downstream pressure, with the upstream pressure fixed, causes no increase in the flow through the nozzle because the pressure at the throat is no longer dependent on the downstream pressure, but is equal to a constant fraction of the upstream pressure. The nozzle is then said to be choked.

Thus when $P_2/P_1 < Pc$ (the critical pressure ratio), the mass flow rate of the gas is a function of the upstream temperature and pressure only[98] (this is actually true only for well rounded nozzles).

$$\text{ie -} \qquad \dot{m} = K \frac{Po}{\sqrt{To}}$$

A photograph of the choked sonic nozzle meter is shown in figure 2. The upstream hydrogen pressure is measured in psi using a USG test gauge, and the upstream temperature is measured using a Comark 3501 digital thermometer. As long as the critical pressure ratio is exceeded, the following constants apply:-

Sonic nozzle no 1 = 1.175×10^{-5} (hole size 0.020")

Sonic nozzle no 2 = 2.186×10^{-5} (hole size 0.025")

Sonic nozzle no 3 = 0.402×10^{-5} (hole size 0.005").

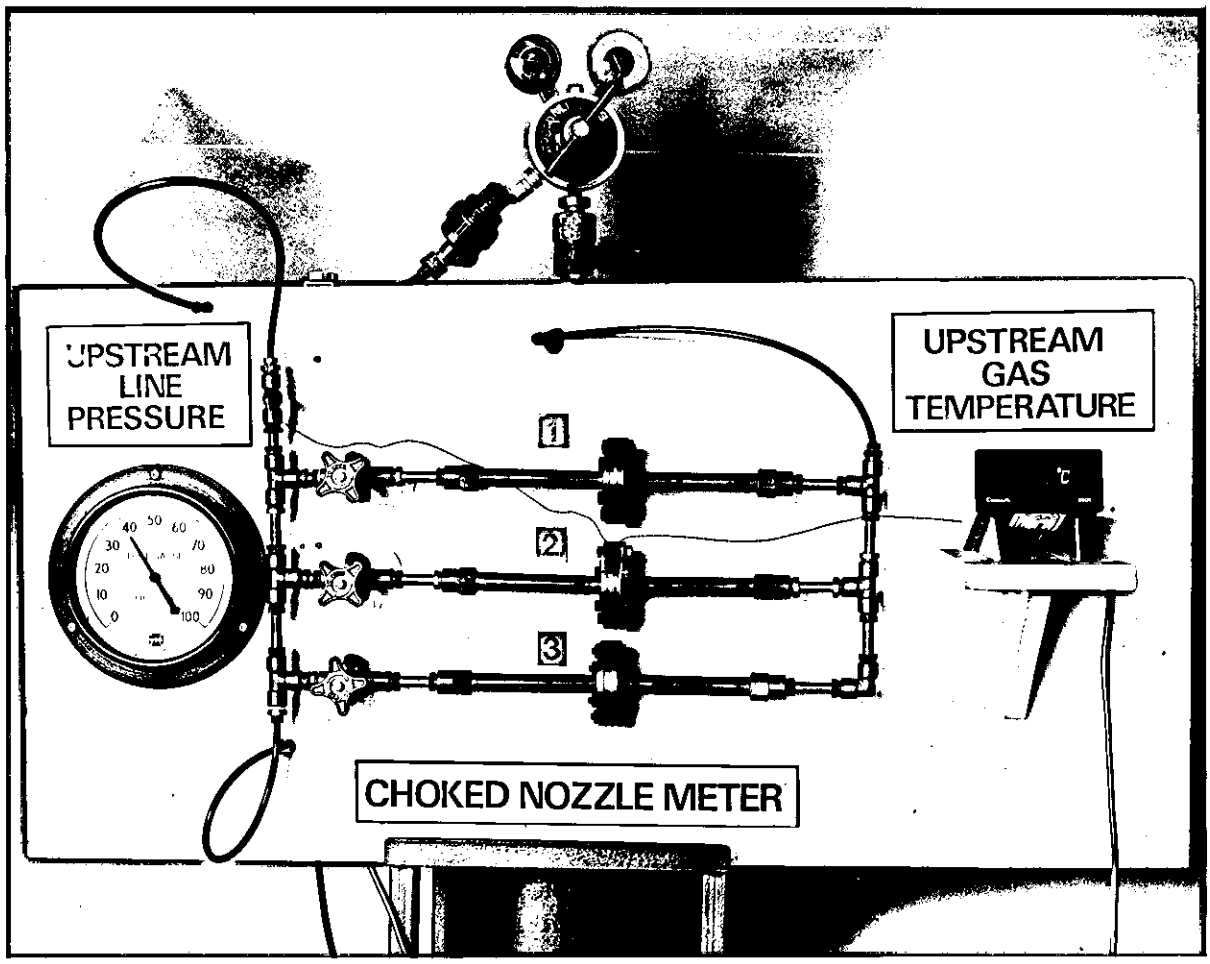

Figure 2 Choked Sonic Nozzle Meter

These values for the constants give a mass flow of hydrogen in kg/s when the absolute upstream pressure ($P_o = P_{gauge} + P_{ambient}$) is in pounds per square inch, and the absolute upstream temperature (To) is in degrees Kelvin.

The engine reduction program listed in appendix(v) uses these constants, and the only inputs required are the nozzle number (or combination of nozzles), the upstream gauge pressure in psi, and the upstream gauge temperature in degrees Celsius. Since the downstream pressure, P_2, is essentially atmospheric (14.7 psi absolute), then, to maintain choking conditions, the minimum value of the upstream pressure, P_1, is 27.8 psi absolute, or ≈ 13 psi gauge pressure.

$$\text{ie} \quad \frac{P_2}{P_1} < Pc$$

$$\Rightarrow \quad \frac{14.7}{P_1} < 0.528$$

$$\Rightarrow \quad P_1 \geq 27.8 \text{ psi absolute}$$

Advantages of Choked Sonic Nozzles

There are several advantages to be found using choked sonic nozzles, quite apart from their high accuracy. They are not affected by pressure pulsations downstream from the meter (due to pressure pulsations in the inlet manifold) so no damping capacity is required, as opposed to the situation if pressure difference devices are used. Variable orifice meters are also affected by pressure pulsations, and

no allowance can be made for changes in ambient conditions.

Since the flow velocity through the sonic nozzle is fixed at the local velocity of sound, the sonic nozzle is an effective flame trap, as the flame speed of hydrogen-air mixtures is much less than the velocity of sound. As an added safety precaution, a flame trap is positioned immediately downstream from the hydrogen cylinder. This unit isolates the cylinder if a sudden pressure pulse is detected in the hydrogen line, as is mentioned in Chapter ten.

Sonic nozzles also have the advantage of being extremely cheap and very robust. Their only disadvantage lies in the small size of the orifice which means any accumulated dirt in the line can block the nozzle.

APPENDIX (ii)

EXHAUST GAS ANALYSIS EQUIPMENT

The non-dispersive infra-red analyzers used are discussed in some detail in the instruction manuals produced by the Analytical Development Co Ltd[99]. The analyzer output is calibrated in terms of gas concentration (by volume), but the calibration is not absolute. This is established by standardizing with a known gas mixture at one point on the calibrated scale. The detector responds to low energy infra-red radiation. However, since it is filled with a pure sample of the type of gas to be measured, it can only respond to energy in that region of the infra-red spectrum corresponding to the absorption band peculiar to that gas. When the gas to be measured enters the analyzer, it passes through a cell in the path between the radiation source and the detector, and, according to the concentration present, absorbs some radiation and thus reduces the level of energy reaching the detector. Since water vapour and nitric oxide absorb infra-red radiation at similar frequencies, it is essential that all water vapour is removed from the exhaust gas before it enters the analyzers. The detector is symmetrical about its centre line, being divided by a pressure sensitive diaphragm into two chambers. Infra-red energy reaching the gas in the cells is absorbed by molecular vibration at the frequencies characteristic of that gas, and then converted to translational energy which heats the gas. Since the chambers are sealed, the heat causes the gas pressure to rise and act upon the diaphragm. Insulated electrodes forming capacitors on either side of the diaphragm are connected to an electronic bridge circuit to detect diaphragm movement and hence the difference in energy received between the detector cells.

APPENDIX (iii)

CALCULATION OF THE EFFECT OF CHANGING THE RATIO OF SPECIFIC HEATS ON IDEAL ENGINE EFFICIENCY

Determination of Ideal Engine Efficiency

The expression used for calculating the specific heat of the different exhaust constituent gases was that given by Lucas[94]:

$$C_p = 1 + mT + \frac{n}{T^2}$$

Although sixth order polynomials can also be used to determine C_p, the above expression was deemed sufficiently accurate to illustrate the principle of greater engine efficiency at lean mixture strengths due to a change in the ratio of specific heats. As this derivation is covered in detail by Lucas, essential calculations only will be dealt with here.

Given that 1 kg of the fuel (petrol only, or hydrogen/petrol mixture) contains A kg of carbon and B kg of hydrogen, and that a is the air/fuel ratio by weight, the above expression becomes

$$C_{pe} = \frac{(C + 0.2392a) + (D + 0.00003193a)\ T_e - \frac{(E + 620a)}{T^2}}{(1 + a)} \text{ Chu/lb}^{\circ}\text{K}$$

where T is the temperature of the exhaust gas stream in degrees Kelvin, and the coefficients

$$C = 0.2842A + 1.860B$$

$$D = 0.00009167A + 0.000980B$$

$$E = 13833A - 10000B$$

The gas constant of the exhaust gases is given by

$$R = \frac{2780}{(1+a)} \left(\frac{B}{4} + 0.03467a\right)$$

from which the specific heat at constant volume of the exhaust gas stream is

$$C_{ve} = \left(C_{pe} - \frac{R}{1400}\right) \quad \text{Chu/lbK}$$

and the ratio of specific heats is given by

$$\gamma = \frac{C_{pe}}{C_{ve}} = \frac{C_{pe}}{C_{pe} - \frac{R}{1400}}$$

Since the carbon/hydrogen ratio of petrol is constant, and the air/fuel ratio is nearly constant at all loads, a value for γ of 1.249 at 2000^{o}K was calculated. Applying this to the formula

$$\text{Ideal Efficiency} = \left(1 - \frac{1}{r^{\gamma-1}}\right) \times 100$$

where r is the compression ratio of the engine (8.9:1), a value of 42.0% is obtained for the ideal efficiency of the engine using petrol. By inserting the appropriate values for γ in this expression, the

ideal efficiency can similarly be found for the dual-fuel mixture. The values of the various constants for the dual-fuel mixture throughout the load range at 2500 rpm are tabulated in table 1, and illustrated in figure 8.17. The effect of temperature on the ratio of specific heats is also illustrated.

LOAD	AIR FLOW	PETROL FLOW	HYDROGEN FLOW	AIR/FUEL RATIO	CARBON CONTENT	HYDROGEN CONTENT OF FUEL	FRACTION OF C IN FUEL	FRACTION OF H IN FUEL				GAS CONSTANT	C_{pe}	C_{ve}	γ	ENGINE EFFIC-IENCY
Nm	kg/s	kg/s	kg/s	a	kg/s	kg/s	A	B	C	D	E	R	Chu/lbK	Chu/lbK		%
81.66	0.0302	1.52×10^{-3}	6.92×10^{-5}	19.00	1.30×10^{-3}	2.88×10^{-4}	0.819	0.181	0.569	0.000252	9519.2	97.85	0.341	0.271	1.258	43.1
77.19	0.0303	1.35×10^{-3}	6.92×10^{-5}	21.35	1.15×10^{-3}	2.64×10^{-4}	0.813	0.187	0.579	0.000258	9376.2	97.89	0.338	0.268	1.261	43.5
73.07	0.0304	1.25×10^{-3}	6.92×10^{-5}	23.04	1.07×10^{-3}	2.49×10^{-4}	0.811	0.189	0.582	0.000260	9328.6	97.84	0.336	0.266	1.263	43.7
66.99	0.0311	1.14×10^{-3}	6.92×10^{-5}	25.72	9.76×10^{-4}	2.34×10^{-4}	0.807	0.193	0.588	0.000263	9233.2	97.80	0.333	0.263	1.266	44.1
63.23	0.0312	1.06×10^{-3}	6.92×10^{-5}	27.63	9.07×10^{-4}	2.22×10^{-4}	0.803	0.197	0.595	0.000267	9137.9	97.80	0.332	0.262	1.267	44.2
57.68	0.0315	0.976×10^{-3}	6.92×10^{-5}	30.14	8.35×10^{-4}	2.10×10^{-4}	0.799	0.201	0.601	0.000270	9042.6	97.77	0.330	0.260	1.269	44.5
53.56	0.0318	0.918×10^{-3}	6.92×10^{-5}	32.21	7.86×10^{-4}	2.02×10^{-4}	0.796	0.204	0.606	0.000273	8971.1	97.75	0.328	0.258	1.271	44.7
39.05	0.0323	0.828×10^{-3}	6.92×10^{-5}	36.00	7.07×10^{-4}	1.89×10^{-4}	0.789	0.211	0.617	0.000279	8804.2	97.74	0.327	0.257	1.272	44.8

TABLE 1 - CALCULATIONS FOR DETERMINATION OF SPECIFIC HEAT OF EXHAUST AND IDEAL ENGINE EFFICIENCY

APPENDIX (iv)

ENERGY BALANCE RESULTS

The determination of energy utilization is based on the method given by Greene and Lucas[92]. The total energy output in an engine is given by

$$\dot{E}_{fuel} = \text{Brake Power} + \dot{E}_{coolant} + \dot{E}_{exhaust} + \dot{E}_{radiation} \text{ etc}$$

The fuel rate of energy input $\dot{E}_{fuel}$ is given by the mass flow rate of the fuel multiplied by its lower calorific value. For petrol this is 43681 kJ/kg and for hydrogen 119960 kJ/kg.

The rate of energy flow to coolant is given by the expression

$$\dot{E}_{coolant} = \dot{M}_c \times C_{p_c} \times (T_{c_{out}} - T_{c_{in}}) \text{ kW}$$

where $\dot{M}_c$ is the coolant mass flow rate (kg/s), C_{p_c} is the specific heat of the coolant (4.19 kJ/kg K for water), $T_{c_{out}}$ is the outlet temperature of the coolant (K), and $T_{c_{in}}$ is the inlet temperature of the coolant (K).

The rate of energy flow to the exhaust is given by

$$\dot{E}_{exhaust} = (\dot{M}_{air} + \dot{M}_{petrol} + \dot{M}_{hydrogen}) \times C_{p_{exhaust}} \times T_{exhaust} - \dot{M}_{air} \times C_{p_{air}} \times T_{air} - \dot{M}_{petrol} \times C_{p_{petrol}} \times T_{petrol} - \dot{M}_{hydrogen} \times C_{p_{hydrogen}} \times T_{hydrogen}$$

where $T_{exhaust}$, T_{air}, T_{petrol}, and $T_{hydrogen}$ are the temperatures of the respective constituents, and C_p are their respective specific heats. The specific heat of air is 1.00 kJ/kg K, that of petrol is 2.240 kJ/kg K, and that of hydrogen is 14.24 kJ/kg K. The specific heat of the exhaust gases is a function of fuel composition, air/fuel ratio, and exhaust temperature. Details of its determination are given in appendix (iii).

Table (iv.1) gives the various energy losses for the case of both dual-fuel operation and petrol operation at 2500 rpm.

TABLE (iv.1) - RESULTS OF ENERGY BALANCE TEST

Engine Speed 2500 rpm

Hydrogen/Petrol (WOT Operation)

Torque Nm	Fuel Energy Rate kJ/sec	Brake Thermal Efficiency %	Rate of Energy Loss to Coolant %	Rate of Energy Loss to Exhaust %	Rate of Energy Loss to Radiation etc %
85.82	90.91	24.64	20.6	26.72	28.04
84.22	77.80	28.26	24.1	31.21	16.43
77.09	66.45	30.33	25.7	33.64	10.33
71.75	62.07	30.16	25.8	32.98	11.06
66.77	58.13	29.98	26.1	33.41	10.51
62.32	54.20	30.03	26.5	33.14	10.33
58.23	51.32	29.58	25.8	32.93	11.69
48.97	47.30	27.01	25.7	33.06	14.23
36.87	44.59	21.56	24.1	33.03	21.31

Petrol Only (Throttled Operation)

Torque Nm	Fuel Energy Rate kJ/sec	Brake Thermal Efficiency %	Rate of Energy Loss to Coolant %	Rate of Energy Loss to Exhaust %	Rate of Energy Loss to Radiation etc %
87.97	100.47	22.85	17.8	22.47	36.88
87.96	82.99	27.67	23.1	29.59	19.64
83.66	76.88	28.35	24.4	30.67	16.58
75.26	71.64	27.46	21.8	29.26	21.48
65.62	65.96	25.97	23.5	26.90	23.63
58.49	59.84	25.32	24.4	26.12	24.16
45.49	50.67	23.53	30.4	24.59	21.48
36.41	41.45	22.97	35.1	24.97	16.96

APPENDIX (v)

COMPUTER PROGRAM FOR REDUCTION OF ENGINE RESULTS

A program was developed to obtain useful data from various engine performance parameters, and a listing is given later in this appendix. The program is specifically for four cylinder spark ignition engines, and is designed for the fuel to be petrol or hydrogen, or both. Input parameters are in two sets, the first designating ambient conditions and engine volume. Also included are an air-flow calibration factor, and a dynamometer constant. This constant is given by the manufacturer such that

$$\text{Brake Power} = \frac{\text{Load (lb)} \times \text{Speed (rad/s)}}{C} \quad \text{kW}$$

where C is the dynamometer constant.

The second set of input parameters are those for the engine's operating conditions. These are engine speed; load; time for consumption of 50 ml of petrol, depression in the viscous air-flow meter, hydrogen gauge pressure, hydrogen inlet temperature, and a constant depending on the combination of sonic nozzles used. There is also the facility for the input of two dummy variables, which are not operated on in the program.

The output parameters are engine speed, volumetric efficiency, brake power, torque, specific fuel consumption, brake thermal efficiency, mass flow rate of air, brake mean effective pressure, mass flow rate

of petrol, mass flow rate of hydrogen, the absolute pressure and temperature of hydrogen upstream from the sonic nozzle, and the equivalence ratio. In all cases, corrected values are given, taking into account ambient conditions.

The specific fuel consumption of hydrogen is converted to its equivalent specific petrol consumption, since the calorific value of hydrogen is 2.746 times that of petrol.

```
LISTING OF WLREN  14:00  09 JUL 82

      INTEGER*2 ITEN(10),OFIL(10)
$INSERT SYSCOM)A$KEYS
$INSERT SYSCOM)KEYS.F
      CALL RNAM$A('ENTER INPUT FILE NAME',21,A$FUPP,ITEN,10)
      CALL SRCH$$(K$READ,ITEN,10,1,TYPE,IC)
      CALL ERRPR$(K$NRTN,0,0,0,0,0,0)
      CALL RNAM$A('ENTER OUTPUT FILE NAME',22,A$FUPP,OFIL,10)
      CALL SRCH$$(K$WRIT,OFIL,10,2,TYPE,CODE)
      CALL ERRPR$(K$NRTN,0,0,0,0,0)
C THIS PROGRAM GIVES ANALYSIS OF S.I. ENGINE DATA USING HYDROGEN
C AND PETROL AS FUEL.  TO BE USED FOR FOUR CYLINDER ENGINES ONLY.
      READ (5,*) ITIT
202   FORMAT ('                    BL ENGINE  RUN NO. ',I4)
      WRITE (6,202) ITIT
      WRITE (6,203)
203   FORMAT (1HO//)
      N24 = 4
C N24 IS THE STROKE NUMBER OF THE ENGINE
      READ (5,*) PA,TA,SV,C,A
C PA IS THE AMBIENT PRESSURE IN MILLIBARS
C TA IS THE AMBIENT TEMPERATURE IN DEGREES CELSIUS
C SV IS THE SWEPT VOLUME IN LITRES
C A IS THE AIR FLOWMETER CALIBRATION FACTOR
      WRITE (6,205) C
205   FORMAT (5X,'DYNAMOMETER CONSTANT (S.I.) = ',F10.4)
      PA = PA / 1.33324
C PA IS NOW IN MM OF HG
      WRITE (6,206) PA,TA,SV
206   FORMAT (5X,'AMBIENT PRESSURE (MM HG) =',F9.2/5X,'AMBIENT TEMPER',
     1'ATURE (DEG C) =',F7.2/5X,'SWEPT VOLUME (LITRE) =',F9.4///)
      WRITE (6,207)
207   FORMAT (30X,21HSPARK IGNITION ENGINE)
      WRITE (6,208)
208   FORMAT (1HO//)
      WRITE (6,209) A
209   FORMAT (4X,40HVISCOUS FLOWMETER - CALIBRATION FACTOR =,F10.4//)
      WRITE (6,208)
      RHO = PA * 0.1333224 / 0.287 / (TA + 273.15)
C RHO IS THE DENSITY OF AIR (KG./CU.M)
      WRITE (6,210)
210   FORMAT (119H SPEED  VOL.EFF    BP    TORQUE      SFC    B.TH.E.    AIR
     1      BMEP      MPET         MH2          IMP  IGN     PABS    TABS  EQR)
      WRITE (6,211)
211   FORMAT (115H  RPM    PERCENT    KW      NM     MILLIG/J PERCENT    KG/S
     1    KN/SQM     KG/S         KG/S       MMHG  DBTDC    PSI    DEGK )
      WRITE (6,208)
```

```
      RPM = 3.1415926 / 30
10    READ (5,*) R,W,TF,DPAIR,DEP,CSUCT,PG,TG,INN
C  R IS THE ENGINE SPEED IN RPM
C  W IS THE DYNAMOMETER LOAD IN LBF
C  TF IS THE TIME FOR CONSUMPTION OF 50 ML OF PETROL IN SECONDS
C  DPAIR IS THE PRESSURE DROP ACROSS THE VISCOUS FLOW METER IN MM H20
C  DEP IS THE INLET MANIFOLD DEPRESSION IN MM HG
C  CSUCT IS THE SPARK ADVANCE IN D.B.T.D.C.
C  PG IS THE GAUGE PRESSURE ON THE CHOKED NOZZLE METER
C  TG IS THE UPSTREAM GAS TEMPERATURE OF HYDROGEN
C  INN IS THE NOZZLE COMBINATION NUMBER
      SUM = R + DPAIR + W
      IF (SUM.EQ.0.0) GO TO 2
      R = R * RPM
C  R IS NOW IN RAD/SEC
      F = 760.0 / (PA - DPAIR / 13.6) * SQRT((TA + 273.15)/ 293.15)
      WAIR = A * DPAIR *RHO / 1000.0
C  WAIR IS THE MASS FLOW RATE OF AIR IN KG/SEC
      RHO1 = RHO
      TW = SV * R * RHO1 / N24 /3141.5926
C  TW IS TH. AIR IN KG/S
      VOLE = WAIR / TW * 100.0
C  VOLE IS THE VOLUMETRIC EFFICIENCY OF THE ENGINE IN PERCENT
      RZ = R / RPM
C  RZ IS THE ENGINE SPEED IN REV/MIN
      WAZ = WAIR
      TWZ = TW
      T = W / C * 1000
C  T IS TORQUE
      BP = W * R /C
C  BP IS BRAKE POWER
      BMEP = BP * N24 * 3.1415926 / R / SV * 1000.0
C  BMEP IS THE BRAKE MEAN EFFECTIVE PRESSURE
      BMEPZ = BMEP * F
      BPZ =BP * F
      TZ = T * F
      TABS = 273.15 + TG
      PAM = PA * 1.333224
      PABS = PAM/1013.25 * 14.6959 + PG
      GO TO (51,52,53,54,55,56,57,58),INN
51    SH2 = 1.172/100.0 * PABS/SQRT(TABS)
      GO TO 60
52    SH2 = 2.186/100.0 * PABS/SQRT(TABS)
      GO TO 60
53    SH2 = 0.402/100.0 * PABS/SQRT(TABS)
      GO TO 60
54    SH2 =3.763/100.0 * PABS/SQRT(TABS)
      GO TO 60
55    SH2 = 3.361/100.0 * PABS/SQRT(TABS)
      GO TO 60
56    SH2 = 2.588/100.0 * PABS/SQRT(TABS)
      GO TO 60
57    SH2 = 1.577/100.0 * PABS/SQRT(TABS)
      GO TO 60
58    SH2 = 0.0
      GO TO 60
60    PH2 = SH2 * 2.746
C  PH2 IS THE ENERGY PETROL EQUIVALENT OF THE MASS OF HYDROGEN SH2 (G)
      SFC = (0.74 * 50.0 / TF + PH2)/BP
      BTE = 100000.0/SFC/43850.0
      SFCZ = SFC
      WH2 = SH2 / 1000.0
```

```
      WPET = 0.74/20.0/TF
C  WH2 IS THE MASS OF HYDROGEN IN KG/SEC
C  WPET IS THE MASS FLOW RATE OF PETROL IN KG/SEC
      AH2 = WH2 * 34.1
      APET = WPET * 14.7
      EQR = (AH2 + APET)/WAIR
C  EQR IS THE EQUIVALENCE RATIO (STOIC. MASS OF AIR REQUIRED/MASS AVAILABL
      WRITE (6,212) RZ,VOLE,BPZ,TZ,SFCZ,BTE,WAZ,BMEPZ,WPET,WH2,DEP,CSUCT
     1,PABS,TABS,EQR
212   FORMAT (F7.1,F7.2,F8.2,F7.2,F9.4,F9.2,F8.4,F8.2,2E11.3,1X,F8.1,F6.
     11,2F7.1,F6.2)
      GO TO 10
2     WRITE (6,203)
      CALL SRCH$$(K$CLOS,0,0,1,TYPE,CODE)
      CALL SRCH$$(K$CLOS,0,0,2,TYPE,CODE)
      CALL EXIT
      END
```

APPENDIX (vi)

COMPUTER PROGRAM FOR CONVERSION OF EXHAUST EMISSIONS DATA

This program converts the units in which exhaust emissions are measured (either parts per million or percentages by volume) to grams per brake horsepower hour. This is done using the total mass flow of air, hydrogen, and petrol into the engine, assuming an average molecular weight for air of 28.96 g, and for petrol 110.3 g. This corresponds to a molecular formula for petrol of $C_{7.85}H_{15.76}$.

The basic combustion equation is as follows:

$$m\ C_{7.85}H_{15.76} + n\ H_2 + x\ O_2 + \frac{79}{21}\ x\ N_2 \rightarrow$$

$$7.85\ m\ CO_2 + \{\frac{15.76}{2}\ m + n\}\ H_2O + \frac{79}{21}\ x\ N_2 +$$

$$x - \{\frac{n}{2} + \frac{15.76\ m}{4} + 7.85\ m\}\ O_2$$

From the input mass flows, the amounts of oxygen remaining, nitrogen remaining, and carbon dioxide produced can be calculated. All water produced is absorbed from the exhaust stream before measurement occurs, as discussed in appendix (ii). Thus an approximate total number of moles of dry gas per unit time in the exhaust stream can be calculated. Using the measured concentrations by volume of the exhaust constituents, approxiamte mass concentrations can then be calculated. This process was found to give exhaust gas concentrations correct to within five percent, which is a greater accuracy than the exhaust analysis instruments will measure.

The mass outputs per second are then divided by the power output (in brake horsepower) multiplied by 3600 to give an output in grams per brake horsepower hour.

```
LISTING OF EXHEM  13:47  09 JUL 82

      INTEGER*2 ITEN(10),OFIL(10)
$INSERT SYSCOM)A$KEYS
$INSERT SYSCOM)KEYS.F
      CALL RNAM$A('ENTER INPUT FILE NAME',21,A$FUPP,ITEN,10)
      CALL SRCH$$(K$READ,ITEN,10,1,TYPE,IC)
      CALL ERRPR$(K$NRTN,0,0,0,0,0,0)
      CALL RNAM$A('ENTER OUTPUT FILE NAME',22,A$FUPP,OFIL,10)
      CALL SRCH$$(K$WRIT,OFIL,10,2,TYPE,CODE)
      CALL ERRPR$(K$NRTN,0,0,0,0,0)
C THIS PROGRAM CALCULATES EXHAUST EMISSIONS IN GRAMS PER BRAKE HORSEPOWER
C HOUR FROM GAS ANALYSER FIGURES.
      AMWHEX = 86.18
      AMWPET = 110.3
      AMWCO2 = 44.01
      AMWCO = 28.01
      AMWNIT = 28.0134
      AMWOXY = 31.9988
      AMWNO = 30.01
      AMWHYD = 2.0158
      AMWAIR = 28.964
      WRITE (6,100)
100   FORMAT (1H ,'   HEXANE    CARBON MONOXIDE    CARBON DIOXIDE    N',
     1'ITROGEN OXIDES    BHP          BP          EQR    PCO2    CPCO2')
300   READ (5,*) WAIR,WPET,WH2,PHEX,PCO2,PCO,PNO,BP,EQR
      IF (WAIR.EQ.0.0) GO TO 400
      BHP = BP * 1.341
      AMOAIR = WAIR / AMWAIR
      AMOOXY = 0.21 * AMOAIR
      AMONIT = 0.79 * AMOAIR
      AMOPET = WPET / AMWPET
      AMOHYD = WH2 / AMWHYD
      RMOXY = AMOHYD / 2.0 + (15.76 /4.0 + 7.85) * AMOPET
      REMOX = AMOOXY - RMOXY
      IF (AMOOXY.LT.RMOXY) REMOX = 0.0
      PROCO2 = 7.85 * AMOPET
      REMNIT = AMONIT
      TOTMOL = REMOX + PROCO2 + REMNIT
      ACTHEX = PHEX / 1000000.0 * TOTMOL
      ACTCO = PCO / 100.0 * TOTMOL
      ACTNO = PNO / 1000000.0 * TOTMOL
      ACTCO2 = PROCO2 - ACTCO - 6.0 * ACTHEX
      ACTNIT = REMNIT - 0.5 * ACTNO
      ACTOXY = REMOX - 0.5 * ACTNO
      TMOL = ACTHEX + ACTCO + ACTNO + ACTCO2 + ACTNIT + ACTOXY
      CPCO2 = ACTCO2 / TMOL * 100.0
      GHEX = ACTHEX * AMWHEX / BHP * 3600.0
      GCO = ACTCO * AMWCO / BHP * 3600.0
      GNO = ACTNO * AMWNO2 / BHP * 3600.0
      GCO2 = ACTCO2 * AMWCO2 / BHP * 3600.0
      WRITE (6,200) GHEX,GCO,GCO2,GNO,BHP,BP,EQR,PCO2,CPCO2
200   FORMAT (1X,F8.4,7X,F8.4,12X,F8.4,10X,F8.4,6X,F8.4,3X,F6.2,6X,F4.2,
     13X,F5.2,4X,F5.2)
      GO TO 300
400   CONTINUE
      CALL SRCH$$(K$CLOS,0,0,1,TYPE,CODE)
      CALL SRCH$$(K$CLOS,0,0,2,TYPE,CODE)
      CALL EXIT
      END
```

APPENDIX (vii)

COMPUTER PROGRAM FOR HYDRIDING MODEL

The main purpose of the hydriding/dehydriding computer program (listed later in this appendix) was to develop solutions to the heat transfer equation:

$$T = 2(T_f - T_i) \sum_{n=1}^{\infty} \frac{1}{\lambda_n R} e^{-\lambda_n^2 \alpha t} \frac{J_0(\lambda_n R)\, J_1(\lambda_n R)}{J_0(\lambda_n R)^2 + J_1(\lambda_n R)^2} \qquad (4.12)$$

for differing values of radial position (r) and time (t) for various metal hydrides (corresponding to the values of α). It also takes into account the rate kinetics of hydriding according to the rate equation

$$\frac{dn}{dt} = k' (P - Peq)/t$$

Two slightly different models have been developed, one to represent hydriding, and the other dehydriding. From the model illustrated in figure 4.2, the value of the Biot modulus for the cylinder was determined to be 11. Thus equation 4.7 could be rewritten as

$$\lambda_n R \frac{J_1(\lambda_n R)}{J_0(\lambda_n R)} - 11 = 0$$

and values for $\lambda_n R$ were then found using standard tables. Using an appropriate value for the container radius, a series of λ_n's were calculated. These were used to determine the radial constants:

$$RADF\ (n) = \frac{1}{\lambda_n R} \times \frac{J_1(\lambda_n R)}{J_o^2(\lambda_n R) + J_1^2(\lambda_n R)}$$

where J_o and J_1 are the appropriate Bessel functions. A series of small radii, ranging from 0 (at the centre of the cylinder) up to R_c (the inner radius of the container) were evaluated in increments of $0.1 \times R_c$, and the product of these with the series of λ_n's was calculated, as was the Bessel function J_o of the product, thus giving a series of values for $J_o\ (\lambda_n R)$. The appropriate value for α was calculated from a combination of the values of α for the outside container, the aluminium capsule, and the fraction of metal hydride which had reacted. Hence a value for the time function could be calculated:

$$TF = \exp\ (\lambda_n^2 \alpha t)$$

where t is the total reaction time in seconds. The temperature change during reaction is thus given by

$$T = 2\ (T_f - T_i) \sum_{n=1}^{4} TF \times RADF(n) \times J_o\ (\lambda_n r)$$

This is plotted against time for each radius, as illustrated in figure 4.5. The time taken to reach the reaction temperature (ie - the temperature corresponding to the particular equilibrium pressure) at each radius is then determined, and an appropriate heat transfer rate is then calculated from the fraction of the bed reacted per unit time.

Reaction kinetics and diffusion are also taken into account using the rate expression given by Nomura et al[49]. The equilibrium dissociation pressure is calculated from the van't Hoff equation:

$$PEQ = EXP\ (TCON/TABS + ENCON)$$

where TABS is the absolute temperature of the hydride bed, TCON is a constant depending on the enthalpy change of the hydriding reaction, and ENCON is a constant related to the entropy change. Both are tabulated for various hydrides in table 4.1 . This equilibrium pressure (in atmospheres) is converted to kg/cm^2 to use in the rate expression

$$RDIFF = 0.032\ (EQPKC - PAKGCM) \times 60$$

where RDIFF is the rate of reaction (cm^2/s) taking into account both the reaction kinetics and the rate of diffusion, EQPKC is the equilibrium pressure, and PAKGCM is the ambient pressure in kg/cm^2.

The time taken for heat transfer (through a given area) to occur is added to the time taken for the actual reaction to take place, thus giving a final reaction rate incorporating heat transfer, reaction kinetics, and the diffusion rate. It is this final reaction rate which is used in the comparison with measured hydriding or dehydriding curves.

The inputs to the program for hydriding are: TFLUD, the temperature of the surrounding fluid; TINT, the equilibrium temperature

inside the hydride, corresponding to the recharging hydrogen pressure; XALPH, the value of α for the particular metal hydride; PAMB, the ambient pressure in psi; TCON, the enthalpy constant in the rate expression for the particular hydride; and ENCON, the entropy constant for the hydride.

For dehydriding, the inputs are essentially the same, except TINT is the ambient temperature inside the hydride, before hydrogen is removed, and XALPH is the thermal diffusivity of the metal powder.

```
LISTING OF DEHYDRIDE  14:00  09 JUL 82

C  THIS PROGRAM CALCULATES THE TEMPERATURE AT ANY POINT IN AN
C  INFINITELY LONG CYLINDER HAVING AN OUTER TUBE OF COPPER AND
C  AN INNER SHELL OF ALUMINIUM.
      DOUBLE PRECISION X
      DIMENSION R(5)
      DIMENSION DA(4),RADF(4),XV(4)
      DIMENSION YTEMP(1000),XTIME(1000)
      DIMENSION SR(11)
      DIMENSION YFRACT(11),XTIM(11)
C  RADC = OUTER RADIUS OF COPPER TUBE
C  RADT = INNER RADIUS OF COPPER TUBE / OUTER RADIUS OF ALUMINIUM CAPSULE
C  BRAD = INNER RADIS OF ALUMINIUM CAPSULE / OUTER RADIUS OF HYDRIDE
      BRAD = 0.0100
      RADT = 0.0105
      RADC = 0.0110
      XV(1) = 0.38829
      XV(2) = 3.8519
      XV(3) = 7.0262
      XV(4) = 10.181
      IFAIL = 0
      DA(1) = XV(1)/RADC
      DA(2) = XV(2)/RADC
      DA(3) = XV(3)/RADC
      DA(4) = XV(4)/RADC
C. TFLUD = TEMPERATURE OF SURROUNDING FLUID
C  TINT = AMBIENT TEMPERATURE OF HYDRIDE
C  XALPH = THERMAL DIFFUSIVITY OF METAL
C  PAMB = AMBIENT PRESSURE IN P.S.I.
C  TCON IS TEMPERATURE CONSTANT (A)
C  ENCON IS ENTROPY CONSTANT (C)
      READ (5,203) TFLUD,TINT,XALPH,PAMB,TCON,ENCON

203   FORMAT (6F0.0)
      WRITE (6,211)
211   FORMAT (1H1/////////)
      DO 500 J =1,4
      X = DA(J) * RADC
      VALUE = S17AEF(X,IFAIL)
      VAB1 = S17AFF(X,IFAIL)
      RADF(J) = VAB1 / (VALUE * VALUE + VAB1 *VAB1) / X
      WRITE (6,201) J,RADF(J)
201   FORMAT (1H1,'       RADIAL FUNCTION ( ',I1,' )  = ',F10.7)
500   CONTINUE
      WRITE (6,202)
202   FORMAT (1H1,'            HEAT TRANSFER IN CYLINDER        ')
      RFU = 1.0
```

```
      DO 600 JSR = 1,11
      SR(JSR) = RFU * BRAD
600   RFU = RFU - 0.1
      CALL C1051N
      CALL AXIPLO(0,0.0,0.0,1,1,10,10,0.,1000.,20.,50.,'TIME (SECONDS)',
     *14,'TEMPERATURE',11)
      DO 300 JR = 1,11
      JGRA = 0
      ALPHA1=(RADC*RADC-RADT*RADT)/(RADC*RADC-SR(JR)*SR(JR))*1.092E-4
      ALPHA2=(RADT*RADT-BRAD*BRAD)/(RADC*RADC-SR(JR)*SR(JR))*9.458E-5
      ALPHA3=(BRAD*BRAD-SR(JR)*SR(JR))/(RADC*RADC-SR(JR)*SR(JR))*XALPH
      ALPHA = ALPHA1 + ALPHA2 + ALPHA3
      WRITE (6,204) SR(JR),ALPHA
204   FORMAT (1H0//,20X,'RADIUS = 'F10.7,10X,'ALPHA = ',E12.5)
      DO 200 IME = 1,1000
      TEMPS = 0.0
      DO 100 N = 1,4
      X = DA(N) * SR(JR)
      IFAIL = 0
      VALUE = S17AEF(X,IFAIL)
      RADFNO = RADF(N) * VALUE
      EXPF = -DA(N) * DA(N) * ALPHA * IME
      TF = EXP(EXPF)
      TEMPF = TF * RADFNO
100   TEMPS = TEMPS + TEMPF
      TEMPD = (TFLUD - TINT) * 2.0 * TEMPS
      TEMP = TFLUD - TEMPD
      XTIME(IME) = IME
      YTEMP(IME) = TEMP
      IF (TEMPD.LT.0.005) GO TO 700
      WRITE (6,205) TEMP,IME
205   FORMAT (5X,'TEMPERATURE = ',F6.3,4X,'TIME = ',I4)
700   IF (TEMPD.LT.0.005) GO TO 200
      JGRA = JGRA + 1
      IF (JGRA.EQ.1) NIME = IME
200   CONTINUE
      FRACT = (BRAD * BRAD - SR(JR) * SR(JR)) / (BRAD * BRAD)
      WRITE (6,701) FRACT,NIME
701   FORMAT (1H0//,20X,'FRACTION REACTED = 'F5.3,10X,'TIME TAKEN = ',I
     *5)
      IF (JR.EQ.3) DIF1 = SR(JR) * SR(JR)
      IF (JR.EQ.3) DTIM1 = NIME
      IF (JR.EQ.5) DIF2 = SR(JR) * SR(JR)
      IF (JR.EQ.5) DTIM2 = NIME
      YFRACT(JR) = FRACT
      XTIM(JR) = NIME
      IF (JR.GT.4) GO TO 301
      MPEN = JR
      GO TO 400
301   IF (JR.GT.8) GO TO 302
      MPEN = JR - 4
      GO TO 400
302   MPEN = JR - 8
      GO TO 400
400   CALL PENSEL(MPEN,0.0,0)
      CALL GRAPOL (XTIME,YTEMP,1000)
300   CONTINUE
      CALL DEVEND
      CALL C1051N
      CALL AXIPLO(0,0.0,0.0,1,1,10,10,0.,1000.,0.,1.,'TIME (SECONDS)',14
     *,'FRACTION REACTED',I6)
      CALL GRACUR(XTIM,YFRACT,11)
```

```
      CALL DEVEND
C   RREACT IS RATE OF HEAT TRANSFER
C   PEQ IS EQUILIBRIUM PRESSURE IN ATMOSPHERES
C   EQPKC IS EQUILIBRIUM PRESSURE IN KG/SQCM
C   PAKGCM IS AMBIENT PRESSURE IN KG/SQCM
C   RDIFF IS RATE OF DIFFUSION
      RREACT = (DIF1 -DIF2) * 3.141593 * 10000.0 / (DTIM2 - DTIM1)
      TABS = TFLUD + 273.15
      PEQ = 2.718282 ** (TCON / TABS + ENCON)
      EQPKC = PEQ * 1.033232
      PAKGCM = PAMB * 0.070307
      RDIFF = 0.032 * (EQPKC - PAKGCM) * 60.0
      EXTIM = RREACT / RDIFF
      FRERA = RREACT / (1 + EXTIM)
      WRITE (6,333) RDIFF,RREACT,FRERA
333   FORMAT (1HO////,' DIFFUSION RATE = ',F8.4,2X,'CM/SEC',//,' REACTIO
     *N RATE = ',F8.6,2X,'CM/SEC',//,' FINAL REACTION RATE = ',F8.6,2X,'
     *CM/SEC')
      STOP
      END
```